UNIVERSIDADE FEDERAL DE SANTA CATARINA
PROGRAMA DE PÓS-GRADUAÇÃO EM ENGENHARIA ELÉTRICA

Juliana Camilo Inácio

DESIGN AND ANALYSIS OF FULLY-DIVERSE MULTIDIMENSIONAL CONSTELLATIONS FOR RAYLEIGH FADING CHANNELS

Florianópolis
2018

Juliana Camilo Inácio

DESIGN AND ANALYSIS OF FULLY-DIVERSE MULTIDIMENSIONAL CONSTELLATIONS FOR RAYLEIGH FADING CHANNELS

Tese submetida ao Programa de Pós-Graduação em Engenharia Elétrica da Universidade Federal de Santa Catarina para a obtenção do Grau de Doutora em Engenharia Elétrica.
Orientador: Prof. Dr. Bartolomeu Ferreira Uchôa Filho

Florianópolis
2018

Ficha de identificação da obra elaborada pelo autor,
através do Programa de Geração Automática da Biblioteca Universitária da UFSC.

Inácio, Juliana Camilo
Design and Analysis of Fully-Diverse Multidimensional Constellations for Rayleigh Fading Channels / Juliana Camilo Inácio ; orientador, Bartolomeu Ferreira Uchôa-Filho, 2018.
147 p.

Tese (doutorado) - Universidade Federal de Santa Catarina, Centro Tecnológico, Programa de Pós Graduação em Engenharia Elétrica, Florianópolis, 2018.

Inclui referências.

1. Engenharia Elétrica. 2. Design of fully diverse multidimensional constellations. 3. Signal space diversity. 4. Grouped linear constellation precoding. 5. Subcarrier-index modulation. I. Uchôa Filho, Bartolomeu Ferreira. II. Universidade Federal de Santa Catarina. Programa de Pós-Graduação em Engenharia Elétrica. III. Título.

DESIGN AND ANALYSIS OF FULLY-DIVERSE MULTIDIMENSIONAL CONSTELLATIONS FOR RAYLEIGH FADING CHANNELS

Juliana Camilo Inácio

Esta tese foi julgada adequada para obtenção do Título de "Doutora em Engenharia Elétrica" e aprovada em sua forma final pelo Programa de Pós-Graduação em Engenharia Elétrica.

Florianópolis, 2 de Agosto de 2018.

Prof. Bartolomeu Ferreira Uchôa Filho, Dr.
Coordenador do Programa de Pós-Graduação em Engenharia Elétrica

Banca Examinadora:

Prof. Bartolomeu Ferreira Uchôa Filho, Dr. – UFSC
Orientador

Prof. Didier Le Ruyet, Ph.D. – CNAM (França)

Prof. Mário de Noronha Neto, Dr. – IFSC

Prof. Carlos Aurélio Faria da Rocha, Dr. – UFSC

This work is dedicated to my parents.

ACKNOWLEDGEMENTS

Firstly, I would like to thank my parents, José and Liege, and my brother, Eduardo, and sister-in-law, Alessandra, for all the support, encouragement and understanding during my entire academic journey. I also want to thank my friends and my boyfriend, Gabriel, for the moments of leisure and relaxation and for the votes of success.

I would like to thank my advisor, Bartolomeu, for his excellent guidance and teaching, patience, incentive and understanding throughout the development of this work. I would also like to thank the Professor Didier for his excellent teaching and guidance and for the receptivity and support during my period of sandwich doctorate. I am very grateful for the opportunity to work with two excellent professors.

My thanks also to my laboratory colleagues, Bruno, Márcio, Maria Cláudia, Paulo, Ricardo, Robinson and for all LCS members, for the discussions, suggestions, support and relaxed lunches and breaks. Definitely, these people made the realization of this work more enjoyable.

Finally, I thank to *Coordenação de Aperfeiçoamento de Pessoal de Nível Superior* (CAPES) for the financial support.

My sincere thanks to all mentioned here!

RESUMO

As técnicas de transmissão propostas na literatura, que exploram a diversidade de espaço de sinais (SSD) para canais com desvanecimento, consideram rotação ou precodificação de uma constelação de sinais original. Nesta tese são propostas duas metodologias para o projeto de constelações multidimensionais com máxima diversidade. A primeira considera uma abordagem unificada para multiplexação por divisão de frequência ortogonal (OFDM) com subportadoras agrupadas, a qual engloba os esquemas existentes, tais como modulação por índice de subportadora (SIM) e precodificação de constelação linear agrupada (GLCP) como casos particulares. Para explorar a SSD, as n subportadoras dentro de um grupo são tratadas como $2n$ recursos reais. Entrelaçamento a nível de componente real é usado para quebrar a correlação entre subportadoras adjacentes. Então, uma análise de desempenho de erro revela que uma constelação de sinais real $2n$-dimensional deve ser projetada de acordo com o critério da SSD e da razão multiplicidade-por-distância produto. Sob certas restrições, o ganho máximo de diversidade de $2n$ pode ser alcançado com um projeto adequado. A segunda proposta considera uma abordagem completamente diferente para se projetar constelações multidimensionais com máxima SSD, cuja implementação é menos complexa e requer menor capacidade de armazenamento. O projeto consiste em encontrar boas permutações dos rótulos dos pontos em uma grade fixada. Foram consideradas grades com distribuição de pontos tanto uniforme quanto Gaussiana. O desempenho médio do *ensemble* de todas as constelações resultantes, baseado em uma análise enumerativa de eventos de erro, é obtido, esclarecendo alguns pontos do problema. Dois algoritmos de baixa complexidade são propostos para encontrar conjuntos de permutações que resultam em bom desempenho. Resultados de desempenho de erro, tanto analíticos quanto de simulações, são apresentados para as constelações construídas a partir das duas metodologias propostas. As constelações propostas apresentam um desempenho de erro superior aos esquemas de

referência. Portanto, elas podem ser consideradas como boas candidatas a serem adotadas em sistemas de comunicação futuros.

Palavras chave: Constelações com máxima diversidade modulação, distância produto, diversidade de espaço de sinais, entrelaçadores múltiplos, modulação por índice de portadora, precodificação de constelação linear agrupada, projeto de constelações multidimensionais, reticulados.

RESUMO EXPANDIDO

Introdução

Uma técnica eficiente para se alcançar ganho de diversidade em canais com desvanecimento é explorar o conceito de diversidade de espaço de sinais (SSD), introduzida por Boutros e Viterbo [1] vinte anos atrás. O ganho de diversidade é obtido pela rotação de uma constelação multidimensional de sinais, de tal forma que diferentes pontos da constellation tenham projeções diferentes em cada dimensão. Desta forma, se uma dimensão é afetada por um desvanecimento profundo, a informação ainda pode ser recuperada a partir das outras dimensões. Constelações multidimensionais podem ser construídas através do produto Cartesiano de modulações QAM, ou extraídas a partir de reticulados [2, 3]. Rotação pode então ser aplicada [4]. Além de ganho de diversidade, ganho de codificação em canais com desvanecimento também pode ser alcançado pela otimização da distância produto mínima [5]. Nos últimos anos, SSD tem sido explorada com sucesso em vários contextos, tais como em sistemas V-BLAST (do inglês *vertical-Bell laboratories layered space-time*) em múltiplos canais Rayleigh [6], comunicação cooperativa [7] e modulação codificada com entrelaçamento de bit e decodificação iterativa (BICM-ID) [8, 9]. Em [10], e em alguns trabalhos subsequentes, constelações multidimensionais rotacionadas se mostraram melhores não apenas em termos de desempenho de erro mas também em relação à informação mútua. A SSD também é explorada nos padrões da segunda geração de trasmissão de vídeo digital (DVB-T2) [11] e na próxima geração portátil DVB (DVB-NGH) [12]. Independentemente desses desenvolvimentos, várias técnicas têm sido recentemente propostas para melhorar a eficiência espectral e/ou o desempenho de erro de sistemas com múltiplas portadoras, tal como a multiplexação por divisão de frequência ortogonal (OFDM). Entre elas, a chamada modulação por índice de subportadora (SIM) [13] tem sido apontada como uma candidata promissora para as redes sem fio futuras. Nessa técnica, as portadoras são divididas em grupos, e dentro de cada grupo um índice portador de informação é associado a

um conjunto de subportadoras ativas. Existem variações e generalizações da SIM, tal como aquela reportada em [14], na qual diferentes constelações podem ser usadas em diferentes subportadoras ativas dentro de cada grupo. Em [15], os autores usaram entrelaçadores para melhorar o desempenho da SIM em regime de baixa razão sinal-ruído (SNR). Vários trabalhos subsequentes têm adotado a SIM entrelaçada (ISIM) para obter um bom desempenho. Entrelaçamento de coordenadas foi proposto em [16], em que cada componente, real e imaginária, de um símbolo complexo é transmitida em um instante de tempo diferente e através de diferentes antenas transmissoras. Modulação por índice em nível de componente foi introduzida em [17], e adaptada para o cenário de portadoras em [18, 19]. Além de todos esses desenvolvimentos, é sabido que OFDM convencional em canais de comunicação sem fio apresenta perda de diversidade de múltiplos percursos. A fim de recuperar essa perda, um técnica interessante chamada precodificação de constelação linear agrupada (GLCP) foi proposta em [20]. Na GLCP, o vetor contendo os símbolos de um grupo de n subportadoras é multiplicado por uma matriz de precodificação, a qual mistura os símbolos no domínio da frequência. Note que um grupo é formado por símbolos que são transmitidos por subportadoras separadas, ou seja, um entrelaçamento está implícito nesse agrupamento. Os autores mostraram que, sob certas condições, e para $n \geq L$, um ganho de diversidade L pode ser alcançado com essa técnica, em que L é o número de *taps* da resposta ao impulso do canal com desvanecimento seletivo em frequência. Recentemente, precodificação de constelação linear (LCP) foi combinada com SIM em [21], otimizando alguns critérios de projeto. No entanto, por ser uma técnica recente, inúmeras questões ainda não foram investigadas. Portanto, motivado pelo desejo de contribuir para a área de SIM e explorar o potencial das técnicas de SSD e GLCP, este trabalho foi desenvolvido.

Objetivos

O objetivo desta tese é propor soluções para o problema de projeto de constelações multidimensionais que explorem a máxima diversidade de espaço de sinais em canais com desvanecimento Rayleigh, em sistemas

com um único usuário e única antena. Além disso, espera-se de uma solução que ela seja generalizada e flexível, para que a sua utilização seja possível em diferentes cenários.

Metodologia

Para esta pesquisa, foram utilizados conceitos recentes que estão sendo investigados por pesquisadores do mundo todo, como a modulação por índice de subportadora, sistemas com múltiplas portadoras, projeto de constelações multidimensionais e diversidade de espaço de sinais. As etapas para o desenvolvimento desta tese foram: 1) Análise de desempenho para sistemas não codificados, em canais Rayleigh e com um único usuário e única antena, 2) Proposição de novas constelações multidimensionais, de acordo com os critérios obtidos na etapa anterior, baseadas em diferentes constelações originais (QAM, APSK, SIM, reticulados) combinadas com rotação e GLCP, 3) Comparação dos parâmetros teóricos das constelações construídas, 4) Proposição de uma nova metodologia para o projeto de constelações, sendo esta completamente diferente do que é encontrado na literatura, mais simples e generalizada do que a anterior, 5) Proposição de novas constelações seguindo a segunda metodologia de construção e também de acordo com os critérios obtidos na etapa 1, 6) Comparação dos parâmetros teóricos entre as duas metodologias de projeto de constelações, e 7) Desenvolvimento de simulações computacionais para confirmar os resultados analíticos obtidos.

Resultados e Discussão

As constelações (propostas) com os melhores parâmetros apresentaram o melhor desempenho, exceto para as constelações baseadas em APSK, mas para esses casos a inclinação das curvas simuladas em alta SNR tendem ao mesmo comportamento dos limitantes superiores. Explorar a máxima SSD proporciona um melhor desempenho em todos os cenários analisados. As constelações propostas baseadas em reticulados apresentaram o melhor desempenho em termos de erro de ponto para toda a faixa SNR, e em termos de erro de bit para média e alta SNR. Na comparação em termos de erro de bit para baixa e média SNR, as constelações propostas

baseadas em QAM e que exploram a máxima SSD apresentam o melhor desempenho. As constelações propostas baseadas na segunda metodologia têm desempenho melhor quando comparadas com as constelações baseadas em SIM.

Considerações Finais

O objetivo da tese foi alcançado, e duas metodologias para projetar constelações multidimensionais que exploram a máxima diversidade de espaço de sinais foram propostas. A primeira metodologia proposta segue a aborgadem clássica da literatura (constelações rotacionadas), combinando rotação e GLCP, e melhores resultados de desempenho são obtidos. A segunda metodologia proposta é totalmente diferente, abrindo caminho para uma nova perspectiva sobre o projeto de constelações, apresenta um bom resultado de desempenho (mas não o melhor de todos) e é uma alternativa mais simples, generalizada e flexível, permitindo o projeto de constelações com qualquer número de dimensões e de pontos. Os algoritmos propostos utilizados na segunda metodologia, além possuírem baixa complexidade, apresentam um grande potencial para serem utilizados em sistemas de acesso múltiplo por códigos esparsos (SCMA) após alguns ajustes. As constelações baseadas em SIM, embora consideradas por muitos autores como candidatas promissoras para sistemas de comunicação futuros, apresentaram um desempenho insatisfatório quando analisadas sob a perspectiva multidimensional.

Palavras chave: Constelações com máxima diversidade de modulação, distância produto, diversidade de espaço de sinais, entrelaçadores múltiplos, modulação por índice de portadora, precodificação de constelação linear agrupada, projeto de constelações multidimensionais, reticulados.

ABSTRACT

Previous transmission techniques for fading channels that exploit signal space diversity (SSD) are based on rotation or precoding of an original signal constellation. In this dissertation, two methodologies to design fully-diverse multidimensional constellations are proposed. The first proposal is a unified approach for orthogonal frequency-division multiplexing (OFDM) with grouped subcarriers which encompasses previous schemes such as subcarrier-index modulation (SIM) and grouped linear constellation-precoding (GLCP) as particular cases. To exploit SSD, the n subcarriers within a group are treated as $2n$ real resources. Interleaving at the real component level is used to break the correlation between adjacent subcarriers. Error performance analysis then reveals that a $2n$-dimensional real signal constellation (codebook) should be designed according to the SSD criterion and the multiplicity-to-product distance ratio criterion. Under certain constraints, the maximum diversity gain of $2n$ can be achieved by proper design. The second one is a completely different approach to design fully-diverse multidimensional codebooks whose implementation has low complexity and requires little storage. The design consists of finding good permutations of the labels of points in a fixed grid. Both the uniform and the Gaussian-shaped grids are considered. An ensemble average performance based on an enumerative analysis of the error events is presented, which brings some insight into the problem. Two low-complexity algorithms are proposed to find permutations sets yielding very good performance. Both analytical and simulation error performance results are presented for the codebooks constructed following the two methodologies. The proposed codebooks present a superior error performance. Therefore, they can be considered as good candidates for future communications systems.

Keywords: Codebook design, fully-diverse constellations, grouped linear constellation-precoding, lattices, multiple interleavers, product distance, signal space diversity, subcarrier-index modulation.

LIST OF FIGURES

LIST OF TABLES

CONTENTS

LIST OF ABBREVIATIONS AND ACRONYMS

BER	Bit Error Rate	47
DMT	Diversity-Multiplexing Tradeoff	49
SISO	Single-Input Single-Output	49
SIMO	Single-Input Multiple-Output	49
OFDMA	Orthogonal Frequency Division Multiple Access	49
SM	Spatial Modulation	49
ESIM	Enhanced Subcarrier-Index Modulation	51
SScM	Selecting Subcarriers Modulation	52
PAPR	Peak-to-Average Power Ratio	52
IM	Index Modulation	52
ICI	Inter-Carrier Interference	54
CFO	Carrier Frequency Offset	54
MED	Minimum Euclidean Distance	54
PAM	Pulse-Amplitude Modulation	54
GIM	Generalized Index Modulation	54
SMX	Spatial Multiplexing	55
GSFIM	Generalized Space-Frequency Index Modulation	55
MMSE	Minimum Mean Square Error	56
GAMP	Generalized Approximate Message Passing	56
AWGN	Additive White Gaussian Noise	59
PEP	Pairwise Codeword Error Probability	62
APSK	Amplitude Phase Shift Keying	74
BEP	Bit Error Probability	78
CEP	Constellation point error probability	79

LIST OF SYMBOLS

1 INTRODUCTION

In wireless communication systems, it is important that the adopted transmission techniques be robust against the channel adversities. A signal transmitted over a wireless channel is usually affected by severe fading, which makes it difficult to guarantee reliable communication. Incorporating diversity techniques into these systems is a good alternative to significantly improve the robustness of the signal and, consequently, the error performance. Diversity is a technique that provides the receiver with replicas of the signal affected by uncorrelated fading.

An efficient way to achieve diversity gain in fading channels is to exploit the concept of signal space diversity (SSD), introduced by Boutros and Viterbo [1] twenty years ago. The diversity gain is obtained by rotating a multidimensional signal constellation, in such a way that different signal points have different projections on every dimension. In this way, if a dimension is affected by a deep fading, the information can still be recovered from the other dimensions.

Multidimensional constellations can be constructed through the Cartesian product of conventional quadrature amplitude modulation (QAM), or they can be carved from lattices [2, 3]. Rotation can then be applied [4]. In addition to diversity gain, coding gain in fading channels can also be achieved by optimizing the minimum product distance [5].

In the last years, SSD has been successfully explored in various contexts such as in vertical Bell Laboratories layered space-time systems (V-BLAST) over multiple-input multiple-output (MIMO) Rayleigh channels [6], cooperative communication [7] and in bit-interleaved coded modulation with iterative decoding (BICM-ID) [8, 9]. In [10], and in some subsequent works, rotated multidimensional constellations are shown to improve not only the error performance but also the mutual information. SSD is also exploited in the second generation digital video broadcasting (DVB-T2) [11] and in the next-generation handheld DVB (DVB-NGH) [12] standards.

Independently of these developments, several techniques have re-

cently been proposed for improving the spectral efficiency and/or the error performance of multicarrier systems such as orthogonal frequency-division multiplexing (OFDM). Among them, the so-called subcarrier-index modulation (SIM) [13] has been pointed as a promising candidate for future wireless networks. In this technique, the subcarriers are divided into groups, and within each group an information-bearing index is associated with a subset of active subcarriers.

There have been variations and generalizations of SIM, such as the one in [14], where different constellations may be used in different active subcarriers within each group. In [15], the authors have independently used interleavers to improve the performance of SIM in the low signal-to-noise ratio (SNR) regime. Several subsequent papers have adopted the interleaved SIM (ISIM) to obtain a good performance. Coordinate interleaving was proposed in [16], where each component, real and imaginary, of a complex symbol is transmitted at a different time slot and through a different transmit antenna. In-phase/quadrature (I/Q) index modulation was introduced in [17], and adapted to the subcarriers scenario in [18, 19].

Apart from all these developments, it is well-known that conventional OFDM over wireless communications channels suffers from multipath diversity loss. In order to recover from this loss, an interesting technique called grouped linear constellation-precoding (GLCP) has been proposed in [20]. In GLCP, the vector containing the symbols within a group of n subcarriers is multiplied by a precoding matrix, which mixes the symbols in the frequency domain. Note that a group is formed by symbols that are transmitted through separated subcarriers, i.e., an interleaving is implicit in this grouping. The authors have shown that, under certain conditions and for $n \geq L$, a diversity gain of L can be achieved with this technique, where L is the number of taps of the frequency-selective fading channel impulse response.

Recently, linear constellation-precoding (LCP) was combined with SIM in [21], aiming to optimize the minimum squared Euclidean distance and the so-called minimum coding gain distance. However, for being a recent technique, numerous issues regarding SIM have not yet

been investigated. This work contributes to the area of SIM by exploiting the potential of SSD and GLCP techniques to improve the system's performance with manageable signal processing complexity.

1.1 MOTIVATION

Signal space diversity was introduced twenty years ago and it remains an important topic until today. In this technique, a rotation is commonly used for that the projection of a complex symbol is different from the projections of all other symbols in each dimension. This simple rotation operation improves the diversity gain in fading channels without sacrificing the spectral efficiency or increasing the transmission power. Subcarrier-index modulation is a recent technique that presents good performance in several scenarios. In a nutshell, while in conventional OFDM a symbol from a complex signal constellation is transmitted in every subcarrier, in subcarrier-index modulation some subcarriers are chosen to be inactive, as a way of carrying index information. Though extensively studied, this technique is still surrounded by open questions. In the present work, it has been observed that the signaling adopted both in OFDM and in the subcarrier-index modulation schemes can be seen as an instance of a more general approach based on multidimensional constellations. From this perspective, a natural question that arises is whether it is possible to design signal constellations with better parameters by further exploiting the channel characteristics to maximally extract signal space diversity. In this work, it will be shown that yes, it is possible.

1.2 DISSERTATION PROPOSAL

In this Ph.D dissertation, two methodologies are proposed to design fully-diverse multidimensional constellations for single-user, sigle-antenna systems over frequency-selective Rayleigh fading channels. In summary, this dissertation intends to present a concrete answer to the following question:

- *How to design in easy steps fully-diverse multidimensional constellations for obtaining good error performance over fading channels?*

1.2.1 General goal

The general goal of this proposal is to contribute to the success of the future wireless communications networks, based on multicarrier communications, by improving their error performance. The way to leverage these performance gains is to exploit the concept of signal space diversity in the frequency domain.

1.2.2 Specific objectives

In this document, we first present a theoretical background on signal space diversity, multidimensional constellations, grouped linear constellation-precoding and subcarrier-index modulation, as well as a review of related papers found in the literature. These previous ideas have inspired and motivated the present work.

The specific objectives are:

- To develop an error performance analysis for the considered scenario, which follows closely the analysis developed in [5, 3] for single-carrier systems.
- To propose an unified approach for designing fully-diverse multidimensional constellations for OFDM with grouped subcarriers.
- To propose a simple and generalized methodology for designing fully-diverse multidimensional codebooks without making use of rotation or precoding.
- To propose algorithms to finding a good set of permutations (or interleavers) with low complexity.
- To introduce an enumerative technique to obtain the average (squared) product distance spectrum of the ensemble of codebooks obtained with the uniform and Gaussian-shaped grids.

- To analyze the behavior of SIM-based codebooks from a multidimensional constellation perspective.

1.3 DOCUMENT STRUCTURE

The remainder of this document is organized as follows. Chapter 2 presents a theoretical background on the main schemes needed for the understanding of the proposed approaches. In Chapter 3, a performance analysis is first derived. Then, the first proposed approach for designing fully-diverse multidimensional constellations is presented. The proposed constellations are obtained, and a brief analysis of the known constellations under the multidimensional perspective is shown. The second proposal, a simple and generalized methodology for designing fully-diverse multidimensional codebooks without making uses of rotation or precoding, is presented in Chapter 4. The numerical results are presented in Chapter 5. Finally, Chapter 6 concludes this dissertation presenting a discussion of the results, the main contributions, and some suggestions for future work.

2 THEORETICAL FOUNDATION

2.1 INTRODUCTION

This chapter presents the theoretical background necessary to understand the proposal of this work. First, a brief introduction to OFDM is given. Then, the concept of signal space diversity, originally introduced for single-carrier systems, is presented. The simple idea of constellation rotation, a key ingredient to achieve SSD, is explained in simple terms and is then extended to multidimensional constellations. The main works related to these topics are also presented. In the next sections, grouped linear constellation-precoding and subcarrier-index modulation are detailed in a state-of-the-art level.

2.2 OFDM

One of the most popular multicarrier transmission techniques is orthogonal frequency division multiplexing. Due to its robustness to the frequency selectivity and to intersymbol interference (ISI), it has been included in many wireless communications standards, such as digital video broadcasting (DVB), IEEE 802.11 wireless local area network (WLAN), and long term evolution (LTE).

As OFDM is a well-known subject, in this document we will only present the main concept. For more details on OFDM the references [22, 23, 24, 25, 26] are suggested.

The main idea of the OFDM transmission scheme is to divide the wideband channel into N_s orthogonal narrowband subchannels, in such a way that the overlapping in the spectral domain does not affect the orthogonality and improves the bandwidth efficiency. OFDM is typically implemented in hardware. First, a sequence of complex data symbols is formed in the frequency domain. Then, by taking their inverse fast Fourier transform (IFFT) a sequence $x[t]$ of symbols in the time domain is formed. A cyclic prefix, consisting of the last μ symbols of the sequence $x[t]$, is appended to the beginning of $x[t]$ before transmission. The purpose of this operation if to avoid the ISI in an

easier way. The appropriate value of μ is related to the channel impulse response time duration. In the receiver, after removing the cyclic prefix, the fast Fourier transform (FFT) of $x[t]$ is taken in order to recover the data symbols, back in the frequency domain.

2.3 SSD AND MULTIDIMENSIONAL CONSTELLATIONS

It is well known that digital communications over fading channels require different transmission approaches for achieving a good performance when compared to additive white Gaussian noise (AWGN) channels. An important work evidencing this fact is the seminal paper by Viterbo and Boutros [1], which introduces the fundamental concept of signal space diversity, also known as modulation diversity. Consider a fast Rayleigh fading channel or, in case of a slowly-varying fading channel, assume that ideal interleaving is adopted which renders the channel i.i.d. To make it simple, assume also that a quaternary quadrature-amplitude modulation (4-QAM), like the one in Figure 1a, is used for transmission. Clearly, if (say) the quadrature component of the channel is in deep fading, then the two points on the left become indistinguishable; the same happens to the two points on the right. Of course, this event has a negative effect on the error performance.

Now if one allows for a simple rotation of the whole constellation, such as the one seen in Figure 1b, the four transmitted signals can still be recovered in spite of a deep fading in either component of the channel. Only under deep fading in the two dimensions is that the signal recovery becomes impossible. This translates into a two-fold diversity gain. While innocuous for the AWGN channel, constellation rotation is determinant in achieving full performance advantages in the Rayleigh fading channel.

Note that the signals need not be transmitted twice at different times or at different frequencies. So, this technique does not sacrifice the spectral efficiency nor increases the transmission power. The diversity gain comes from a tricky rotation operation imposed to the signal constellation. For that reason, Viterbo and Boutros have coined the

name modulation or signal space diversity for this behavior.

Figure 1 – Example of rotation of a 4-QAM constellation.

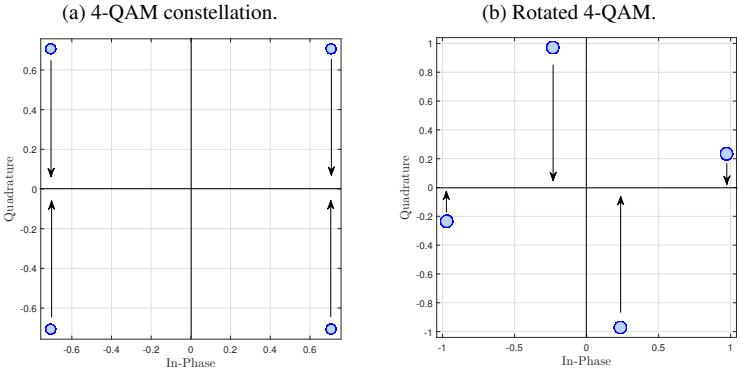

Rotations can also be applied to multidimensional constellations. A rotation in four-dimensions has been considered in [27]. A multidimensional constellation $\mathscr{C}$ is a finite set of points selected from an M-dimensional space. One can design an M-dimensional real constellation by performing the Cartesian product of $M/2$ two-dimensional QAM signal sets. In addition to diversity gain, a coding gain in fading channels can also be achieved by optimizing the minimum product distance [5].

Multidimensional constellations can also be carved from lattices [3, 28, 29]. An n-dimensional real lattice is an infinite discrete set of points in $\mathbb{R}^n$ consisting of all integer linear combinations of n fixed linearly independent vectors in $\mathbb{R}^n$. Lattices have several algebraic properties that make them an interesting object. They can be applied to the design and the analysis of signal constellations for communications. One such important property is that integer linear combinations of lattice points are also lattice points [30, 31, 4]. In [3] the authors have constructed some lattices that present a good performance over Rayleigh fading and Gaussian channels.

In the present work, two cases of study were considered, namely 8-dimensional and 4-dimensional signal constellations obtained from

the Gosset lattice, E_8, and the checkerboard lattice, D_4, respectively. Details and the application of these constellations will given in Section 3.5.2. The theory of lattices will not be covered here. For further details on this subject the references [3, 30, 2, 28, 29, 32, 33] are suggested.

Usually, maximum-likelihood (ML) detection is required to fully exploit all the benefits of the SSD. The ML detection complexity grows exponentially with the number of constellation points. This problem alleviated in [34] and [35], with sphere decoding and iterative methods based on Gaussian approximation, respectively.

In the last years, SSD has been successfully explored in various contexts. In [6, 36], through constellation rotation, the authors exploit the SSD in V-BLAST systems. In cooperative communication, an expanded constellation is obtained from a coordinate interleaving of a rotated quadrature phase shift keying (QPSK) constellation [7]. Performance analysis of this kind of system is presented in [37, 38]. Rotated constellations also are applied in BICM-ID systems [8, 9, 39], where the classical minimum product distance optimization criterion is replaced by the average mutual information. In terms of practical systems, modulation diversity is also exploited in the DVB-T2 standard [11]. What do all these works have in common? All of them exploit the SSD by rotating constellations with 2 real dimensions, where the maximum SSD is achieved and the error performance is improved.

Rotation of four-dimensional constellations is performed in DVB-NGH standard [12, 40], but full modulation diversity is not exploited. A few papers investigate the rotation of multidimensional constellations. Two interesting examples are [10] and [41], which propose multidimensional rotation matrices that exploit the SSD and optimize the mutual information in BICM-ID systems. In [10], the proposed rotation matrices are specifically for four-dimensional constellations, while in [41] the rotation matrices are restricted to constellations with dimensions which are power of 2.

2.4 GLCP IN OFDM SYSTEMS

Linear constellation precoding (LCP) was proposed in [20] as a way to improve the error performance of OFDM systems. Unlike previous techniques [42, 43], LCP does not add redundancy to the information. As a consequence, it does not sacrifice the transmission rate. In LCP, a precoding matrix operates on all, say, N_s digital modulation data symbols of the OFDM symbol. Therefore, in each subcarrier a linear combination of all data symbols is transmitted. Spreading the symbols across the frequency band like this creates a diversity effect which improves the error performance. However, in order to achieve this benefit, ML detection must be performed [20]. Unfortunately, the complexity of ML detection is $\mathscr{O}(N_s^S)$, where S is the signal constellation size. In practical scenarios, where N_s is large, LCP becomes too complex.

In order to reduce the decoding complexity, the authors in [20, 44] proposed to operate on groups of subcarriers, rather than on all subcarriers at once. The detection complexity is reduced to $\mathscr{O}(Gn^S)$, where n is the number of subcarriers in each group and G, the number of groups. It should be mentioned that the decoding complexity is reduced but the diversity and coding gains are preserved with this proposed approach, as long as n is sufficiently large and with respect to the channel diversity. This technique has been coined the name grouped linear constellation-precoding (GLCP). More details on GLCP follow next.

Let $\mathscr{I} = \{1, \ldots, N_s\}$ be the set of subcarrier indices. A subcarrier grouping is a partitioning of $\mathscr{I}$ into non-intersecting subsets $\mathscr{I}^{(g)}$, where $g = 1, \ldots, G$. In [20], the authors proposed an optimal subcarrier grouping, given by

$$\mathscr{I}^{(g)} = \{g, G+g, 2G+g, \ldots, (n-1)G+g\}. \tag{2.1}$$

Note that the symbols associated with a group are transmitted through separated subcarriers, i.e., an interleaving is implicit in this grouping, as can be seen in Figure 2.

Figure 2 – Optimal subcarrier grouping.

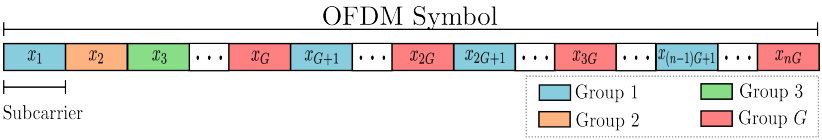

The $n = N_s/G$ symbols within a group are then submitted to a precoder, which is characterized by the following Vandermonde matrix [20]

$$\Theta = \frac{1}{\beta}\begin{bmatrix} 1 & \alpha_1 & \cdots & \alpha_1^{n-1} \\ 1 & \alpha_2 & \cdots & \alpha_2^{n-1} \\ \vdots & \vdots & \ddots & \vdots \\ 1 & \alpha_n & \cdots & \alpha_n^{n-1} \end{bmatrix}, \tag{2.2}$$

where β is a normalization factor which ensures the power constraint $\mathrm{tr}(\Theta\Theta^H) = n$. Alternatively, when n is a power of two, the precoding matrix is given as

$$\Theta = F_n \mathrm{diag}(1, \alpha_1, \ldots, \alpha_1^{n-1}), \tag{2.3}$$

where F_n is the Fourier matrix. As a result, after precoding each symbol in a given group becomes a combination of all the n symbols in the group.

The steps of the GLCP transmitter are illustrated in Figure 3. The matrix in (2.2) is designed to achieve the maximum multipath diversity and coding gains. However, as already mentioned, in order to achieve these gains, ML detection must be performed and the constraint $n \geq L$, where L is the number of taps of the frequency-selective fading channel impulse response, must be satisfied. In fact, there is a tradeoff between detection complexity and system performance in choosing n.

As the GLCP precoder is a non-redundant, unitary precoder[1], the energy and rate of the original constellation remain unchanged. In particular, the rate in bits per OFDM symbol is

$$R = N_s \log_2(S). \tag{2.4}$$

[1] When n is not power of two, the precoding can be non unitary in some cases [45].

Figure 3 – Block diagram of the GLCP transmitter.

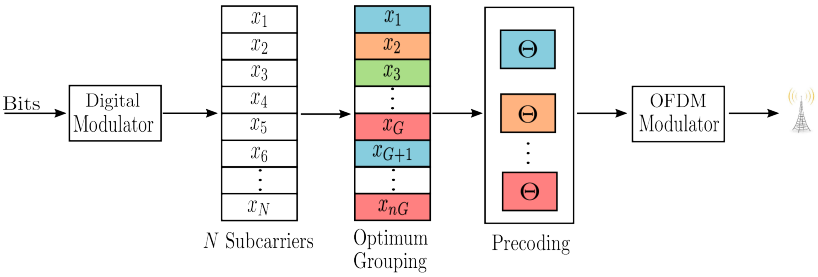

The constellation prior to precoding is a conventional digital modulation in each subcarrier. For illustration purpose, consider an OFDM system with 16-QAM modulation and 2 subcarriers per group. Figure 4a illustrates the projections of the 256 points in each real dimension of this resulting 4-dimensional constellation. Consider the application of the precoding matrix $\mathbf{\Theta}_{2\times 2}$ to all 256 possible sequences of 2 16-QAM symbols. The projections in each real dimension of the precoded constellation are presented in Figure 4b. Note that precoding, as well as rotation (see Figure 1b), increases the number of different projections in each dimension, which means that the modulation diversity is improved. The individual projections on the two complex dimensions of the resulting GLCP constellation, gathered together in a single complex plot is shown in Figure 5. The precoding matrix in equation (2.2) can be seen as a rotation matrix. After precoding, the constellation tends to a Gaussian-like set of points.

In [20, 20], the authors compared GLCP adopting the optimal grouping in eq. (2.1) with one using a suboptimal grouping, showing the superior performance of the former in terms of bit error rate (BER). Other issues were also investigated (see also [46, 47, 48]), such as the impact of using an alternative decoder with reduced complexity, and the effect of correlated and misestimated channels.

The good performance of GLCP motivated researchers around the world to do several others analyses and to propose new schemes based on this technique. In what follows, we point to some works that

Figure 4 – Projections of the 256 constellation points on each real dimension, for $n = 2$ and 16-QAM modulation.

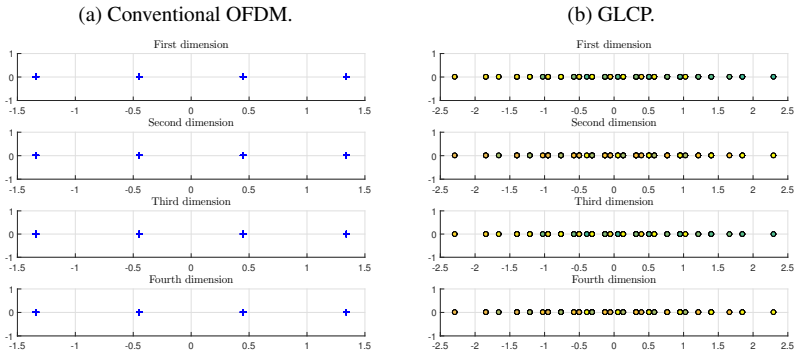

Figure 5 – GLCP constellation in a single complex plot.

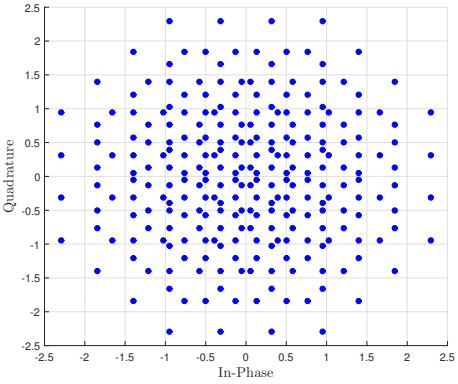

represent the state of the art of GLCP. In [49], the performance of the scheme was analyzed for different group sizes. In order to improve the error performance for low and medium SNR regions, the authors in [50] proposed to discard the subcarriers with poor SNR before detection. Elaborating on this proposal, the authors in [51] have weighted the signals received in the different subcarriers according to the subchannels' SNRs. This technique was shown to outperform both GLCP and the scheme in [50].

In the context of coded OFDM, the authors in [52, 53] explored

GLCP with convolutional codes, bit interleaving and iterative decoding, and designed rotation matrices to achieve full signal space diversity [1] for this scenario. In [54], the analysis was with respect to the diversity-multiplexing tradeoff (DMT) for SISO scenarios, while in [55] the same analysis occurs for the scenarios with multiple antennas (SIMO and MIMO). The authors in [56, 57, 58] analyzed the DMT of a combination of GLCP and OFDMA.

In [59, 60], a combination of GLCP and VBLAST was investigated, improving the performance over VBLAST alone. The authors in [61] proposed GLCP with transceivers having in-phase/quadrature (I/Q) imbalance and a suitable grouping. The results they obtained are at least as good as the ones without I/Q imbalance. Recently, the authors in [62] analyzed the performance of GLCP in a two-way relaying communication (TWRC) system. They proposed some modifications to the original scheme in order to achieve the maximum gains in this scenario. Recently, in [63], a scheme which combines spatial modulation for OFDM with GLCP has been proposed. The results indicate a significant improvement in performance when compared to the conventional SM-OFDM [64].

2.5 SUBCARRIER-INDEX MODULATION

Subcarrier-index modulation (SIM) was first proposed in [65]. The idea is analogous to that of spatial modulation (SM) [66, 67], where a new dimension is added to the system (in this latter case, the antennas indices) for sending additional information. In SM, where multiple antennas are used in the transmitter, the information is split into two parts. One part is mapped to a conventional digital modulation signal set. The other part of the information is used to select one antenna or a subset of antennas through which the signal or signals are transmitted. These are called the active antennas. By discovering the set of active transmit antennas selected in the transmitter, the receiver acquires both the information from the modulated symbol and that associated with the selection of the active antennas. Interestingly, the SM bits

travel for free as no extra energy is required for their transmission. Moreover, in SM the number of RF chains (which is equal to the number of active transmit antennas) is small, implying a hardware economy. With SIM [65], the antennas in SM are substituted with subcarriers.

The system in[65] does not use multiple antennas, i.e., it is a SISO system. Say the OFDM symbol has N_s subcarriers. The bitstream is divided into two parts. The first part consists of a sequence of N_s bits, each bit associated with a subcarrier. These bits are used to designate the active/inactive subcarriers. Since both the all-zero and the all-one sequences are valid information sequences, in order to avoid having all subcarriers inactive, the authors decided to associate the information bit value with higher occurrence in the sequence to an active subcarrier. If there are more zeros than ones in the sequence, then a zero would indicate an active subcarrier, and vice-versa. In this way, the number of active subcarriers is not less than $N_s/2$. The second part of the information consists of a sequence of bits whose length is random and depends on the instantaneous number of active subcarriers. These bits are mapped to a conventional digital modulation. The expected length of this bit sequence is $E[K]\log_2(S)$ bits, where $E[K]$ is the expected number of active subcarriers in an OFDM symbol, with $E[K] \geq N_s/2$.

From a constellation perspective, when a subcarrier is active a digital modulation symbol is transmitted through it and when a subcarrier is inactive the zero symbol (silent) is transmitted. Therefore, the SIM constellation can be seen as having a symbol at the origin, as shown in the example in Figure 6a. Another way of representing constellations is through the projections of their points on each real dimension, as illustrated in Figure 6b. Note that in this case, the projections are the same independently of the dimension.

One drawback of SIM is the need of an additional channel (*e.g.*, a dedicated subcarrier) to inform the receiver of which bit value represents an active subcarrier. This information may change from one OFDM symbol to another. Besides the spectral efficiency loss incurred by this, if this bit is in error, the whole OFDM symbol will also be in error.

Figure 6 – Example of the SIM constellation for 4-QAM.

(a) Conventional representation.

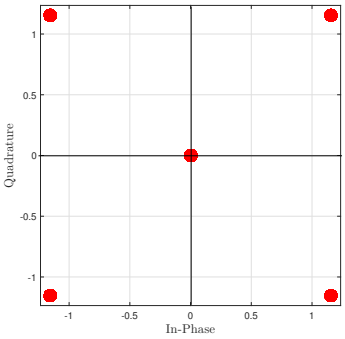

(b) Projection in each real dimension (in-phase or quadrature).

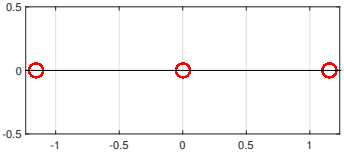

To remedy this problem, in [68] the authors proposed an improved version of SIM, called enhanced SIM (ESIM). In this scheme, a bit is associated with every two consecutive subcarriers, and indicates which of the two subcarriers is active. If the bit is 1, then say the first subcarrier is active, and if the bit is 0, then the second subcarrier is active. In this way, the new SIM does not require an additional channel as in the original SIM. The price paid for this solution is a reduction of spectral efficiency.

A further improvement of SIM was independently proposed in [69] and [13]. In this new approach the authors added the same basic idea of subcarrier grouping proposed in [20, 44] to SIM. For each group with n subcarriers, k subcarriers are chosen to be active according to part of the information. The remaining part of the information is mapped to k symbols from a conventional digital modulation, as illustrated in Figure 7. In this way, $k\log_2(S) + \lfloor \log_2 \binom{n}{k} \rfloor$ bits are transmitted per group of n subcarriers, where $\binom{n}{k}$ is the binomial coefficient and $\lfloor \cdot \rfloor$ is the floor function.

It should be mentioned that the energy savings from the inactive subcarriers can be used to amplify the signal constellation used in the active subcarriers. Also, on one hand, having many active subcarriers

(for $k > n/2$) increases the energy consumption and the amount of information associated with the digital modulatiom, but on the other hand it decreases the amount of information carried by the subcarrier indexing. In fact, there is a tradeoff between the number of active subcarriers, spectral efficiency, and the energy efficiency. In this regard, a related work, [70], analyzed the spectral and energy efficiencies for the scheme in [69] and [13], and obtained the optimal number of active subcarriers per group.

Figure 7 – Example of the subcarrier-index modulation idea proposed in [13] for $n = 4$, $k = 2$ and 4-QAM.

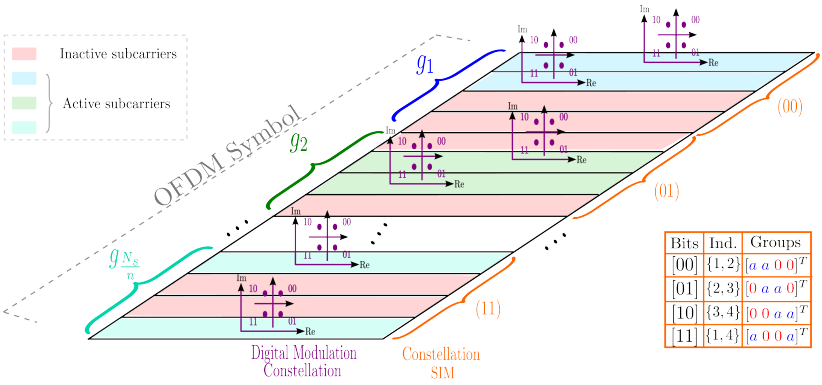

In [69], the authors called the new scheme "selecting subcarriers modulation" (SScM). They analyzed the proposed scheme in terms of power consumption and peak-to-average power ratio (PAPR) reduction. The authors in [13] called the scheme index modulation (IM). They analyzed the scheme in terms of error performance. Although the idea in [69, 13] is the same, there are some differences in implementations. The scheme IM in [13] is the more cited and the more adopted.

IM performs better than conventional OFDM for the range of medium to high SNR. Moreover, the scheme allows for different choices of groups and subcarrier activations and, consequently, it allows one to adjust the system spectral efficiency as desired.

Several works based on IM scheme have subsequently appeared.

The use of interleavers in IM was proposed in [15] and [71]. In these works, the scheme was called OFDM with interleaved subcarrier-index modulation (ISIM) and index modulated OFDM with interleaved grouping, respectively. These new schemes presented a better performance and a higher spectral efficiency when compared to IM. The interleaving process proposed in both papers is the same, the difference is in the channel models used and in the analyses. The block diagram of these schemes is illustrated in Figure 8.

Figure 8 – Block diagram for IM with interleavers proposed in [15].

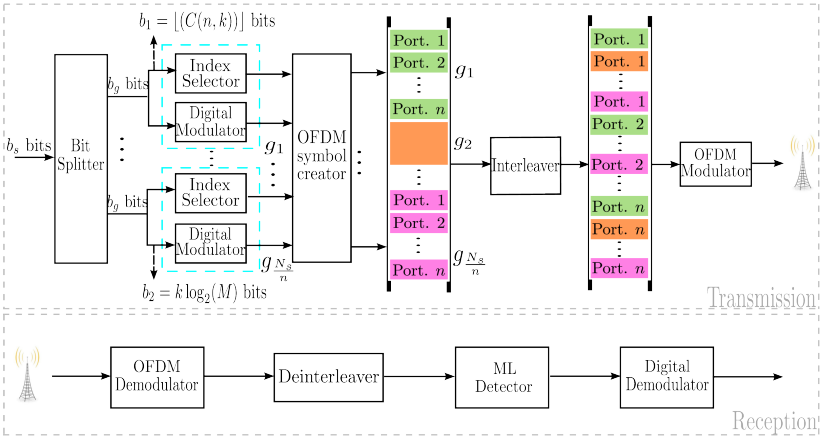

Interleaving was performed in the following way. After the division of the subcarriers into G groups, the symbols that would be transmitted through the first subcarrier of each group are reallocated to occupy the first G consecutives subcarriers in the interleaved OFDM symbol. In the sequel, the symbols that would be transmitted by the second subcarrier of each group are set to occupy the subcarriers $G+1$ to $2G$, sequentially, and so on. The procedure is illustrated in Figure 9.

We note that the interleaving proposed in [15, 71] is equivalent to the implicit interleaving in the optimal subcarrier grouping in [20]. The same can be said about the work [72], where the authors, aiming at optimizing the energy efficiency, analyzed the optimum number of active subcarriers in IM for some scenarios.

Figure 9 – Interleaving procedure proposed in [15].

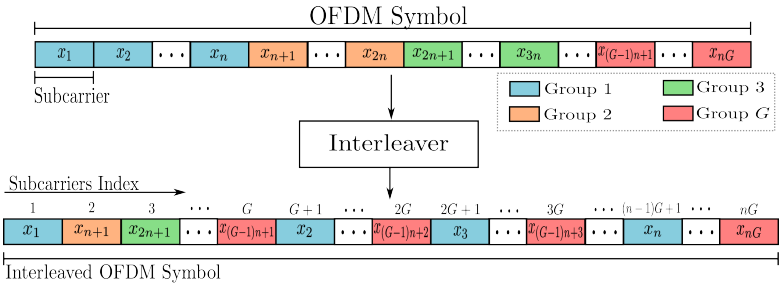

The authors in [73] have shown that ISIM presents a lower PAPR and a greater robustness to inter-carrier interference (ICI) in comparison to conventional OFDM. The robustness was also analyzed in [74], for scenarios with carrier frequency offset (CFO). The authors have found that ISIM outperforms both OFDM and IM. In [75], the achievable rate schemes and the effect of different constellation sizes of SIM were thoroughly studied. In [76], the authors showed that the SIM schemes are advantageous for scenarios with low transmission rate. In addition, they analyzed the PAPR, the minimum Euclidean distance (MED), the average mutual information and the performance with turbo codes. The MED was also analyzed in [15, 77] and the conclusions in these works are the same, namely, SIM constellation improves the MED.

With the aim of improving the spectral efficiency, the authors in [18] proposed some generalizations of the SIM schemes. One of them is to allow a variable number of active subcarriers k in each group. The second proposal is to attribute an independent index modulation for the in-phase and quadrature components, where each group with M real dimensions has k_d active dimensions. This means that each component can carry a S-ary pulse-amplitude modulation (S-PAM) symbol or a zero (inactive), and the resulting complex constellation will may have complex symbols with only real components, only imaginary components, or both. The scheme was called OFDM with generalized index modulation (GIM), and an interleaver at subcarrier level is used.

Besides improving the spectral efficiency, the scheme presented good performance.

In [78] the authors proposed a dependency between the indices of dimensions activation to further improve the spectral efficiency. Low-complexity detection for the GIM schemes is the proposal in [19], while in [21] the proposal is to apply linear constellation precoding, aiming to optimize the minimum squared Euclidean distance and the so-called minimum coding gain. In [79], an equiprobable subcarrier activation was proposed to reduce the need of a large storage of SAP. The method may as well be applied to the SIM and GIM schemes.

With several works showing that SIM with interleaving has very good performance, some works extending this idea to the MIMO scenario have recently appeared, such as [80, 81, 82]. Also, considering a MIMO scenario, in [16] an interleaving at the coordinate level was introduced, before the interleaving at the subcarrier level. To illustrate this idea, consider a group with $n = 4$ subcarriers of which $k = 2$ are active. Let $s_1^R + js_1^I$ and $s_2^R + js_2^I$ be the two complex symbols from a QAM constellation to be transmitted say in the first and third subcarriers of the group. After interleaving at the coordinate level, a possible configuration for the group could be: $[(s_1^R + js_2^I)\ 0\ (s_2^R + js_1^I)\ 0]$. The authors in [16] have also used others techniques to improve the performance, such as, for example, constellation rotation to increase the SSD [1] and convolutional codes. Constellation rotation also was used in [83], but therein the system combines rotated SIM with Alamouti-MIMO.

A generalization of spatial modulation [64], subcarrier-index modulation [13], and spatial multiplexing (SMX) [84] techniques, so-called generalized space-frequency index modulation (GSFIM), was proposed in [85]. The MIMO-OFDM scheme is also a particular case of the GSFIM, which presented better results in terms of achievable rates and error performance for the range of medium SNR. Other advantages of GSFIM is the energy savings due to transmission of large part of the information through the indices, and the flexibility of system settings in terms of spectral efficiency, due to the group structure and the several possibilities of index modulation. In [86], the authors further studied

GSFIM and proposed a form of coding based on combinatorial numerical systems to simplify the mapping of the index activation patterns when the number of patterns is large. Furthermore, a low-complexity detection algorithm was proposed based on a multi-stage message passing method which would facilitate the GSFIM implementation for more complex configurations in practical scenarios.

The recent works [80, 87] point to the MIMO-SIM as one of the possible candidates for the next generation of wireless communications systems, although many issues concerning this technique are still open. One of the important challenges cited in [87] is extending the SIM ideas to the multiuser scenario, recently approached with massive MIMO in [88, 89]. In this recent scheme, several single-antenna users transmit simultaneously to the base station, each one using SIM. At the receiver side, multiuser detection is made possible thanks to a large number of receiver antennas. Two detectors were considered therein: the minimum mean square error (MMSE) detector and the so-called generalized approximate message passing (GAMP), recently proposed in [90].

2.6 CHAPTER CONCLUSIONS

In Chapter 2, we have seen that the subcarrier grouping method is a very promising transmission method, for frequency-selective fading channels, that presents a good error performance with reasonable detection complexity. GLCP and SIM, two techniques that make use of grouped subcarriers, have been investigated independently. SSD is a key technique to improve the error performance without extra sacrifices and it is successfully exploited in different contexts. To the best of our knowledge, a scheme that fully exploits SSD along with these techniques has not yet been presented. This fact alone motivates us to pursue extended techniques aiming at further improving the error performance and the efficiency of these systems. The several concepts presented in this chapter are the basis for the proposal developed in the next chapters.

3 EXPLOITING SSD IN OFDM WITH GROUPED SUBCARRIERS

3.1 INTRODUCTION

This chapter presents the first proposal of this dissertation, namely, the design of multidimensional constellations for OFDM with grouped subcarriers, exploring signal space diversity in the frequency domain. First, the system model is presented, for a single user and SISO scenario. An interleaving at the real dimension level is also proposed. Then a performance analysis is given, which follows closely the analysis developed in [3, 5] for single-carrier systems. Based on design criteria, SSD and the proposed multiplicity-to-product distance ratio, obtained with the performance analysis, the design of new multidimensional constellations is sought, which may combine GLCP and/or constellation rotation. An analysis in terms of BER is made and a discussion is raised on the behavior of the constellations at low and medium SNR. Finally, the parameters of the constellations obtained so far are presented, which are compared to those of constellations found in the literature, all of them under a multidimensional perspective.

3.2 RELATED WORK

Motivated by the improvements obtained upon combining techniques, as described in the last chapter, in this chapter a unified approach for OFDM with grouped subcarriers is proposed, which encompasses some of the previous schemes as particular cases. As benchmark, conventional OFDM, GLCP [20] and ISIM [15] were adopted. The schemes proposed in [21] and [16] were left out because they focus on other objective functions (such as mutual information) or on a different scenario (such as MIMO). In this chapter, codebooks based on the SIM technique [13, 18] and GLCP [20] are proposed. As we will show, these codebooks perform quite well in fading channels. Therefore, they can be seen as an alternative for the ISIM [15].

The proposed approach goes beyond the combination of schemes,

making use of other ingredients not found in these previous techniques. More specifically, in order to exploit SSD [1], the transmitted signals in the subcarriers of a given group with, say, n subcarriers are seen as points in a space of $M = 2n$ real dimensions. Under this framework, we design new constellations in M real dimensions aiming at improving the SSD. The designed multidimensional constellations are carved from M-dimensional real lattices, such as the well-know 8-dimensional Gosset lattice, E_8, and 4-dimensional checkerboard lattice, D_4, both found in [2]. They may also be combined with GLCP [20] and rotations [1].

3.3 SYSTEM MODEL

As in the previous chapter, the OFDM symbol has N_s subcarriers, which are divided into G groups, where $n = N_s/G$ is the number of subcarriers per group. Through each subcarrier a complex symbol is transmitted with average energy E_s. Let $\check{\mathbf{x}}$ be the vector containing the N_s complex data symbols, given as

$$\check{\mathbf{x}} = [\check{\mathbf{x}}_1^T, \check{\mathbf{x}}_2^T, \ldots, \check{\mathbf{x}}_G^T]^T, \tag{3.1}$$

where

$$\check{\mathbf{x}}_g = [x_{ng-(n-1)}^{\mathrm{R}} + jx_{ng-(n-1)}^{\mathrm{I}}, \ldots, x_{ng}^{\mathrm{R}} + jx_{ng}^{\mathrm{I}}]^T \tag{3.2}$$

is a group vector of length n, for $g = 1, 2, \ldots, G$. Alternatively, we can see each component, in-phase (R) and in-quadrature (I), as a real dimension, and the vector $\check{\mathbf{x}}_g$ can be seen as a point in a M-dimensional real Euclidean space, where $M = 2n$, given as

$$\mathbf{x}_g = [x_{ng-(n-1)}^{\mathrm{R}}, x_{ng-(n-1)}^{\mathrm{I}}, \ldots, x_{ng}^{\mathrm{R}}, x_{ng}^{\mathrm{I}}]^T \in \mathscr{C}. \tag{3.3}$$

Analogously, we define

$$\mathbf{x} = [\mathbf{x}_1^T, \mathbf{x}_2^T, \ldots, \mathbf{x}_G^T]^T, \tag{3.4}$$

which will prove useful in our development. $\mathscr{C}$ is a M-dimensional real constellation (codebook). We design $\mathscr{C}$ following rules obtained from the performance analysis presented in Section 3.4.

We propose an interleaving at the real component level in such a way that the interleaved version of $\check{\mathbf{x}}$ in (3.1) is given by

$$\tilde{\mathbf{x}} = [(\tilde{\mathbf{x}}_1^{\mathrm{R}})^T, (\tilde{\mathbf{x}}_1^{\mathrm{I}})^T, \ldots, (\tilde{\mathbf{x}}_f^{\mathrm{R}})^T, (\tilde{\mathbf{x}}_f^{\mathrm{I}})^T, \ldots, (\tilde{\mathbf{x}}_n^{\mathrm{R}})^T, (\tilde{\mathbf{x}}_n^{\mathrm{I}})^T]^T, \tag{3.5}$$

which has been restructured to consist of n pairs of blocks with $G/2$ complex-valued elements each. For $f = 1, 2, \ldots, n$, the first complex block of the f-th pair, $\tilde{\mathbf{x}}_f^{\mathrm{R}}$, is given by

$$\tilde{\mathbf{x}}_f^{\mathrm{R}} = [x_f^{\mathrm{R}} + jx_{f+n}^{\mathrm{R}}, x_{f+2n}^{\mathrm{R}} + jx_{f+3n}^{\mathrm{R}}, \ldots, x_{f+(G-2)n}^{\mathrm{R}} + jx_{f+(G-1)n}^{\mathrm{R}}]^T. \tag{3.6}$$

The second complex block of the same pair, $\tilde{\mathbf{x}}_f^{\mathrm{I}}$, is similarly described (same subscripts, superscript changed to I). Note that the proposed interleaving in equations (3.5) and (3.6) is similar to the one implicit in the optimal subcarrier grouping in equation (2.1) and to the procedure proposed in [15, 71]. Herein, the interleaving is at the real component level, whereas in these previous papers it is at the subcarrier level.

The IFFT and the FFT steps as well as the cyclic prefix insertion and removal, inherent to the OFDM modulation, will be suppressed in this development since they are standard.

After transmission of the OFDM symbol in (3.5), the received vector is given by

$$\tilde{\mathbf{y}} = \mathrm{diag}(\tilde{\mathbf{h}})\tilde{\mathbf{x}} + \tilde{\mathbf{w}}, \tag{3.7}$$

where

$$\tilde{\mathbf{h}} = [\tilde{h}_1, \tilde{h}_2, \ldots, \tilde{h}_{N_s}]^T \tag{3.8}$$

is the zero-mean complex Rayleigh fading coefficients vector with unit variance per dimension ($E[|\tilde{h}_i|^2] = 1$), and

$$\tilde{\mathbf{w}} = [\tilde{w}_1, \tilde{w}_2, \ldots, \tilde{w}_{N_s}]^T \tag{3.9}$$

is the zero-mean complex additive white Gaussian noise (AWGN) vector with variance $N_0/2$ per dimension. The signal-to-noise ratio per complex symbol is given by $\mathrm{SNR} = E_s/N_0$.

To recover the original data vector $\check{\mathbf{x}}$ in (3.1), first the following processing of the received symbol $\tilde{\mathbf{y}}$ is performed:

$$\bar{\mathbf{y}} = \left[\frac{\tilde{h}_1^*}{|\tilde{h}_1|}\tilde{y}_1, \frac{\tilde{h}_2^*}{|\tilde{h}_2|}\tilde{y}_2, \ldots, \frac{\tilde{h}_{N_s-1}^*}{|\tilde{h}_{N_s-1}|}\tilde{y}_{N_s-1}, \frac{\tilde{h}_{N_s}^*}{|\tilde{h}_{N_s}|}\tilde{y}_{N_s} \right]. \tag{3.10}$$

For the purpose of illustration, as a result of this processing, the first element of $\bar{\mathbf{y}}$ in (3.10) develops as

$$\begin{aligned}
\frac{\tilde{h}_1^*}{|\tilde{h}_1|}[(x_1^{\mathrm{R}}+jx_{1+n}^{\mathrm{R}})(\tilde{h}_1^{\mathrm{R}}+j\tilde{h}_1^{\mathrm{I}})+\tilde{w}_1] &= \frac{\tilde{h}_1^*}{|\tilde{h}_1|}[(x_1^{\mathrm{R}}\tilde{h}_1^{\mathrm{R}}-x_{1+n}^{\mathrm{R}}\tilde{h}_1^{\mathrm{I}})+ \\
&\quad j(x_{1+n}^{\mathrm{R}}\tilde{h}_1^{\mathrm{R}}+x_1^{\mathrm{R}}\tilde{h}_1^{\mathrm{I}})+\tilde{w}_1] \\
&= \frac{\tilde{h}_1^{\mathrm{R}}-j\tilde{h}_1^{\mathrm{I}}}{|\tilde{h}_1|}[(x_1^{\mathrm{R}}\tilde{h}_1^{\mathrm{R}}-x_{1+n}^{\mathrm{R}}\tilde{h}_1^{\mathrm{I}})+ \\
&\quad j(x_{1+n}^{\mathrm{R}}\tilde{h}_1^{\mathrm{R}}+x_1^{\mathrm{R}}\tilde{h}_1^{\mathrm{I}})+\tilde{w}_1] \\
&= \frac{1}{|\tilde{h}_1|}\{x_1^{\mathrm{R}}(\tilde{h}_1^{\mathrm{R}})^2+x_1^{\mathrm{R}}(\tilde{h}_1^{\mathrm{I}})^2+ \\
&\quad j[x_{1+n}^{\mathrm{R}}(\tilde{h}_1^{\mathrm{R}})^2+x_{1+n}^{\mathrm{R}}(\tilde{h}_1^{\mathrm{I}})^2]\}+\bar{w}_1 \\
&= \frac{1}{|\tilde{h}_1|}\{x_1^{\mathrm{R}}[(\tilde{h}_1^{\mathrm{R}})^2+(\tilde{h}_1^{\mathrm{I}})^2]+ \\
&\quad jx_{1+n}^{\mathrm{R}}[(\tilde{h}_1^{\mathrm{R}})^2+(\tilde{h}_1^{\mathrm{I}})^2]\}+\bar{w}_1 \\
&= \frac{|\tilde{h}_1|^2(x_1^{\mathrm{R}}+jx_{1+n}^{\mathrm{R}})}{|\tilde{h}_1|}+\bar{w}_1 \\
&= |\tilde{h}_1|(x_1^{\mathrm{R}}+jx_{1+n}^{\mathrm{R}})+\bar{w}_1. \qquad (3.11)
\end{aligned}$$

Applying the same processing to the other elements, we can rewrite $\bar{\mathbf{y}}$ as

$$\bar{\mathbf{y}} = [|\tilde{h}_1|(x_1^{\mathrm{R}}+jx_{1+n}^{\mathrm{R}}),\ldots,|\tilde{h}_{Gn}|(x_{Gn-n}^{\mathrm{I}}+jx_{Gn}^{\mathrm{I}})]^T+\bar{\mathbf{w}}, \qquad (3.12)$$

where

$$\bar{\mathbf{w}} = \left[\frac{\tilde{h}_1^*}{|\tilde{h}_1|}\tilde{w}_1,\frac{\tilde{h}_2^*}{|\tilde{h}_2|}\tilde{w}_2,\ldots,\frac{\tilde{h}_{N_s-1}^*}{|\tilde{h}_{N_s-1}|}\tilde{w}_{N_s-1},\frac{\tilde{h}_{N_s}^*}{|\tilde{h}_{N_s}|}\tilde{w}_{N_s}\right]. \qquad (3.13)$$

As we will see next, this processing along with deinterleaving will give rise to a simple system model in which the M real components of the transmitted point $\mathbf{x}_g$ in (3.3) are affected by quasi-uncorrelated Rayleigh fading coefficients. After deinterleaving, we obtain an *equivalent real system model*:

$$\mathbf{y} = \mathrm{diag}(\mathbf{h})\mathbf{x}+\mathbf{w}, \qquad (3.14)$$

where $\mathbf{x}$ and $\mathbf{w}$ are the *real* expanded versions of the vectors $\check{\mathbf{x}}$ and $\bar{\mathbf{w}}$, respectively, and

$$\mathbf{h} = [\mathbf{h}_1^T, \mathbf{h}_1^T, \mathbf{h}_2^T, \mathbf{h}_2^T, \ldots, \mathbf{h}_{G/2}^T, \mathbf{h}_{G/2}^T]^T, \tag{3.15}$$

where, for $\gamma = 1, \ldots, G/2$, the group channel vector $\mathbf{h}_\gamma$ in (3.15) is given by

$$\mathbf{h}_\gamma = [|\tilde{h}_\gamma|, |\tilde{h}_{\gamma+\frac{G}{2}}|, |\tilde{h}_{\gamma+2\frac{G}{2}}|, \ldots, |\tilde{h}_{\gamma+(M-1)\frac{G}{2}}|]^T. \tag{3.16}$$

It should be noted that in this channel model, the transmission of an OFDM symbol corresponds to the transmission of a sequence of G points in a M-dimensional real Euclidean space. Each real component of a point is multiplied by a real (Rayleigh distributed) channel gain and is affected by AWGN. These channel gains are as uncorrelated as they can be with interleaving/deinterleaving[1], although consecutive points are, two by two, affected by the same channel gains vector.

For the real system model in (3.14), the ML detection (at the group level), for $g = 1, \ldots, G$ and $\gamma \stackrel{\Delta}{=} \lceil g/2 \rceil$, is given as

$$\hat{\mathbf{x}}_g = \arg\min_{\mathbf{x}'_g \in \mathscr{C}} \|\mathbf{y}_g - \mathrm{diag}(\mathbf{h}_\gamma)\mathbf{x}'_g\|^2, \tag{3.17}$$

whose complexity is essentially the same as that for all grouped-OFDM schemes.

A summary of the system model adopted in this chapter is presented in Figure 10, where the block Π represents the interleaver. The input bits are mapped into G independent $2n$-dimensional codewords of a codebook $\mathscr{C}$. Each codeword $\mathbf{x}_g$ is associated with a group of subcarriers. The G codewords are arranged to produce the vector $\mathbf{x}$.

3.4 PERFORMANCE ANALYSIS

The constellation point (codeword) error probability, i.e, the probability that the detected point $\hat{\mathbf{x}}_g$ in (3.17) is different from the

[1] The correlation level will still depend on the number of taps of the frequency-selective fading channel (L), the total number of subcarriers (N_s), and the frequency bandwidth.

Figure 10 – The block diagram of the system model.

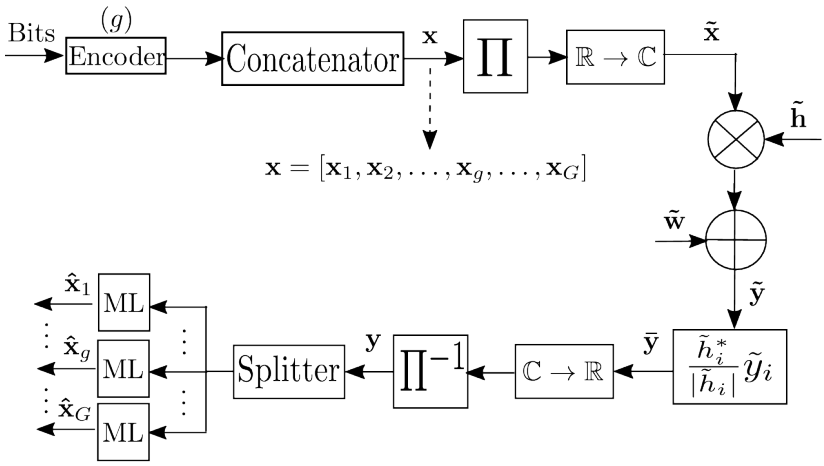

transmitted point can be upper bounded by [5]

$$P_e(\mathscr{C}) \leq \frac{1}{|\mathscr{C}|} \sum_{\mathbf{x}_g} \sum_{\mathbf{x}'_g \neq \mathbf{x}_g} P(\mathbf{x}_g \to \mathbf{x}'_g), \tag{3.18}$$

where $P(\mathbf{x}_g \to \mathbf{x}'_g)$ is the pairwise codeword error probability (PEP).

The conditional PEP is given by

$$\begin{aligned} P(\mathbf{x}_g \to \mathbf{x}'_g \mid \mathbf{h}_\gamma) &= P\left(\|\mathbf{y}_g - \text{diag}(\mathbf{h}_\gamma)\mathbf{x}'_g\|^2 \leq \|\mathbf{y}_g - \text{diag}(\mathbf{h}_\gamma)\mathbf{x}_g\|^2 \mid \mathbf{x}_g\right) \\ &= P\left(\|\text{diag}(\mathbf{h}_\gamma)\mathbf{x}_g + \mathbf{w}_g - \text{diag}(\mathbf{h}_\gamma)\mathbf{x}'_g\|^2 \leq \|\text{diag}(\mathbf{h}_\gamma)\mathbf{x}_g \right. \\ &\quad \left. + \mathbf{w}_g - \text{diag}(\mathbf{h}_\gamma)\mathbf{x}_g\|^2\right) \\ &= P\left(\|\text{diag}(\mathbf{h}_\gamma)(\mathbf{x}_g - \mathbf{x}'_g) + \mathbf{w}_g\|^2 \leq \|\mathbf{w}_g\|^2\right). \end{aligned} \tag{3.19}$$

Expanding the term $\|\text{diag}(\mathbf{h}_\gamma)(\mathbf{x}_g - \mathbf{x}'_g) + \mathbf{w}_g\|^2$ in (3.19), we have

$$\begin{aligned} \|\text{diag}(\mathbf{h}_\gamma)(\mathbf{x}_g - \mathbf{x}'_g) + \mathbf{w}_g\|^2 &= \|\text{diag}(\mathbf{h}_\gamma)(\mathbf{x}_g - \mathbf{x}'_g)\|^2 + \|\mathbf{w}_g\|^2 + \\ &\quad \text{tr}\left(\text{diag}(\mathbf{h}_\gamma)(\mathbf{x}_g - \mathbf{x}'_g)\mathbf{w}_g^H + \right. \\ &\quad \left. \mathbf{w}_g(\mathbf{x}_g - \mathbf{x}'_g)^H \text{diag}(\mathbf{h}_\gamma)^H\right), \end{aligned} \tag{3.20}$$

where $\text{tr}(C) \triangleq \sum_{i=1}^{n} c_{i,i}$ is the trace of the $n \times n$ matrix C, with the properties $\text{tr}(AB) = \text{tr}(BA)$ for any $n \times m$ and $m \times n$ matrices A and

B, respectively, $\mathrm{tr}(AB) = AB$ if $n = 1$. The term $\|\mathrm{diag}(\mathbf{h}_\gamma)(\mathbf{x}_g - \mathbf{x}'_g)\|^2$ in (3.20) expands as

$$\|\mathrm{diag}(\mathbf{h}_\gamma)(\mathbf{x}_g - \mathbf{x}'_g)\|^2 = \mathrm{tr}\left((\mathbf{x}_g - \mathbf{x}'_g)^H \mathrm{diag}(\mathbf{h}_\gamma)^H \cdot \mathrm{diag}(\mathbf{h}_\gamma)(\mathbf{x}_g - \mathbf{x}'_g)\right). \tag{3.21}$$

Since $\mathrm{diag}(\mathbf{h}_\gamma)$ is a diagonal matrix, whose diagonal elements are real and positive, then $\mathrm{diag}(\mathbf{h}_\gamma)^H \mathrm{diag}(\mathbf{h}_\gamma) = \mathrm{diag}(\mathbf{h}_\gamma)^2$. Also, as $\mathbf{x}_g$ and $\mathbf{w}_g$ are real, $(\cdot)^H$ can be replaced by $(\cdot)^T$. Thus, we have

$$\begin{aligned} \mathrm{tr}\left((\mathbf{x}_g - \mathbf{x}'_g)^T \mathrm{diag}(\mathbf{h}_\gamma)^2 (\mathbf{x}_g - \mathbf{x}'_g)\right) &= (\mathbf{x}_g - \mathbf{x}'_g)^T \mathrm{diag}(\mathbf{h}_\gamma)^2 (\mathbf{x}_g - \mathbf{x}'_g) \\ &= \sum_{i=1}^{M} h_\gamma^2(i)(x_g(i) - x'_g(i))^2. \end{aligned} \tag{3.22}$$

Working on the term $\mathrm{tr}\left(\mathrm{diag}(\mathbf{h}_\gamma)(\mathbf{x}_g - \mathbf{x}'_g)\mathbf{w}_g^T + \mathbf{w}_g(\mathbf{x}_g - \mathbf{x}'_g)^T \mathrm{diag}(\mathbf{h}_\gamma)^T\right)$ in (3.20), we have

$$\begin{aligned} &\mathrm{tr}\left(\mathrm{diag}(\mathbf{h}_\gamma)(\mathbf{x}_g - \mathbf{x}'_g)\mathbf{w}_g^T + \mathbf{w}_g(\mathbf{x}_g - \mathbf{x}'_g)^T \mathrm{diag}(\mathbf{h}_\gamma)^T\right) = \\ &\quad \mathrm{tr}\left(\mathbf{w}_g^T \mathrm{diag}(\mathbf{h}_\gamma)(\mathbf{x}_g - \mathbf{x}'_g)\right) + \mathrm{tr}\left((\mathbf{x}_g - \mathbf{x}'_g)^T \mathrm{diag}(\mathbf{h}_\gamma)^T \mathbf{w}_g\right) \\ &\quad = 2\sum_{i=1}^{M} h_\gamma(i)(x_g(i) - x'_g(i))w_g(i). \end{aligned} \tag{3.23}$$

Substituting equations (3.22) and (3.23) in (3.19), we have that

$$P(\mathbf{x}_g \to \mathbf{x}'_g \mid \mathbf{h}_\gamma) = P\{\Omega \le 0\}, \tag{3.24}$$

where

$$\Omega = \sum_{i=1}^{M} h_\gamma^2(i)(x_g(i) - x'_g(i))^2 + 2\sum_{i=1}^{M} h_\gamma(i)(x_g(i) - x'_g(i))w_g(i). \tag{3.25}$$

Note that, for fixed $\mathbf{x}_g$, $\mathbf{x}'_g$ and $\mathbf{h}_\gamma$, Ω is Gaussian, i.e., $\Omega \sim \mathscr{G}(\mu_\Omega, \sigma_\Omega^2)$, where

$$\mu_\Omega = \mathrm{E}_{\mathbf{w}}[\Omega] = \sum_{i=1}^{M} h_\gamma^2(i)(x_g(i) - x'_g(i))^2, \tag{3.26}$$

and

$$\sigma_\Omega^2 = \mathrm{E}_{\mathbf{w}}[(\Omega - \mu_\Omega)^2] = 4\mathrm{E}\left[\left(\sum_{i=1}^{M} h_\gamma(i)(x_g(i) - x'_g(i))w_g(i)\right)^2\right]. \tag{3.27}$$

Note that the cross-terms in (3.27) have the factor $\mathrm{E}_{\mathbf{w}}[w_g(i)w_g(k)] = 0$. Thus, we have

$$\begin{aligned}\sigma_\Omega^2 &= 4\sum_{i=1}^{M} h_\gamma(i)^2 (x_g(i) - x'_g(i))^2 \mathrm{E}_{\mathbf{w}}[w_g(i)^2] \\ &= 2N_0 \sum_{i=1}^{M} h_\gamma(i)^2 (x_g(i) - x'_g(i))^2 = 2N_0\mu_\Omega. \end{aligned} \tag{3.28}$$

The conditional PEP in (3.19) then becomes

$$P(\mathbf{x}_g \to \mathbf{x}'_g \mid \mathbf{h}_\gamma) = P(\Omega \le 0) = Q(\mu_\Omega/\sigma_\Omega) \tag{3.29}$$

$$= Q(\mu_\Omega/\sqrt{2N_0\mu_\Omega}) = Q\left(\sqrt{\frac{\mu_\Omega}{2N_0}}\right), \tag{3.30}$$

where

$$Q(z) = \frac{1}{2\pi}\int_z^\infty \exp(-t^2/2)dt. \tag{3.31}$$

Using the Chernoff bound

$$Q(z) \le \frac{1}{2}\exp(-z^2/2), \tag{3.32}$$

the conditional PEP can be upper bounded as

$$P(\mathbf{x}_g \to \mathbf{x}'_g \mid \mathbf{h}_\gamma) \le \frac{1}{2}\exp\left(-\frac{1}{4N_0}\sum_{i=1}^{M} h_\gamma(i)^2 \left(x_g(i) - x'_g(i)\right)^2\right). \tag{3.33}$$

The PEP can be evaluated as

$$P(\mathbf{x}_g \to \mathbf{x}'_g) = \int P(\mathbf{x}_g \to \mathbf{x}'_g \mid \mathbf{h}_\gamma) f_{\mathbf{h}_\gamma}(\mathbf{h}) d\mathbf{h}, \tag{3.34}$$

where the multidimensional integral is over the sample space of $\mathbf{h}_\gamma$, which has joint probability density function (PDF)

$$f_{\mathbf{h}_\gamma}(\mathbf{h}) = f_{\mathbf{h}_\gamma(1)}(\mathbf{h}(1)) \ \ldots \ f_{\mathbf{h}_\gamma(M)}(\mathbf{h}(M)). \tag{3.35}$$

All marginal PDFs have the same (normalized) Rayleigh distribution:

$$f_{\mathbf{h}(i)}(h) = 2he^{-h^2}. \tag{3.36}$$

Hence, equation (3.34) becomes

$$\begin{aligned} P(\mathbf{x}_g \to \mathbf{x}'_g) &\leq \frac{1}{2}\prod_{i=1}^{M}\int_0^{\infty} \exp\left(-\frac{1}{4N_0}h_\gamma(i)^2\left(x_g(i)- x'_g(i)\right)^2\right) f_{\mathbf{h}(i)}(h)dh_\gamma(i) \\ &= \frac{1}{2}\prod_{i=1}^{M}\int_0^{\infty} \exp\left(-\frac{1}{4N_0}h_\gamma(i)^2\left(x_g(i)- x'_g(i)\right)^2\right) 2h_\gamma(i)e^{-h_\gamma(i)^2}dh_\gamma(i) \\ &= \frac{1}{2}\prod_{i=1}^{M}\int_0^{\infty} 2h_\gamma(i)\exp\left(-\frac{1}{4N_0}h_\gamma(i)^2\left(x_g(i)- x'_g(i)\right)^2 - h_\gamma(i)^2\right) dh_\gamma(i) \\ &= \frac{1}{2}\prod_{i=1}^{M}\int_0^{\infty} 2h_\gamma(i)\exp\left(-C(i)h_\gamma(i)^2\right) dh_\gamma(i), \end{aligned} \tag{3.37}$$

where

$$C(i) = 1 + \frac{(x_g(i) - x'_g(i))^2}{4N_0}. \tag{3.38}$$

Solving the integral in (3.37), we have

$$P(\mathbf{x}_g \to \mathbf{x}'_g) \leq \frac{1}{2}\prod_{i=1}^{M}\frac{1}{C(i)}. \tag{3.39}$$

Substituting (3.39) in (3.18), yields

$$\begin{aligned} P_e(\mathscr{C}) &\leq \frac{1}{|\mathscr{C}|}\sum_{\mathbf{x}_g}\sum_{\mathbf{x}'_g\neq\mathbf{x}_g}\frac{1}{2}\prod_{i=1}^{M}\frac{1}{C(i)} \\ &= \frac{1}{|\mathscr{C}|}\sum_{\mathbf{x}_g}\sum_{\mathbf{x}'_g\neq\mathbf{x}_g}\frac{1}{2}\prod_{i=1}^{M}\frac{1}{1+\frac{(x_g(i)-x'_g(i))^2}{4N_0}} \qquad (3.40) \\ &= \frac{1}{|\mathscr{C}|}\sum_{\mathbf{x}_g}\sum_{\mathbf{x}'_g\neq\mathbf{x}_g}\frac{1}{2}\prod_{i\in\mathscr{I}(\mathbf{x}_g,\mathbf{x}'_g)}\frac{1}{\frac{|\mathbf{x}_g-\mathbf{x}'_g|^2}{4N_0}} \qquad \text{(for high SNR)} \\ &= \frac{1}{|\mathscr{C}|}\sum_{\mathbf{x}_g}\sum_{\mathbf{x}'_g\neq\mathbf{x}_g}\frac{1}{2}\frac{1}{\left(\frac{E_s}{4\eta N_0}\right)^{|\mathscr{I}(\mathbf{x}_g,\mathbf{x}'_g)|}\delta_p(\mathbf{x}_g,\mathbf{x}'_g)^2}, \qquad (3.41) \end{aligned}$$

where $\mathscr{I}(\mathbf{x}_g, \mathbf{x}'_g)$ is the set of indices $i \in \{1, \ldots, M\}$ for which $x_g(i) \neq x'_g(i)$, i.e., $|\mathscr{I}(\mathbf{x}_g, \mathbf{x}'_g)| = d_H(\mathbf{x}_g, \mathbf{x}'_g)$ is the *Hamming distance* between $\mathbf{x}_g$ and $\mathbf{x}'_g$, and $D \leq |\mathscr{I}(\mathbf{x}_g, \mathbf{x}'_g)| \leq M$. The parameter η is the spectral efficiency measured in bits per two dimensions and D is the *minimum Hamming distance* of the codebook $\mathscr{C}$, which has been termed SSD (or *modulation diversity*) in [1]. The (normalized) *product distance*, $\delta_p(\mathbf{x}_g, \mathbf{x}'_g)$, is defined as

$$\delta_p(\mathbf{x}_g, \mathbf{x}'_g)^2 = \frac{\prod\limits_{i \in \mathscr{I}(\mathbf{x}_g, \mathbf{x}'_g)} |\mathbf{x}_g(i) - \mathbf{x}'_g(i)|^2}{(E_c/M)^{|\mathscr{I}(\mathbf{x}_g, \mathbf{x}'_g)|}}, \tag{3.42}$$

where E_c is the average energy of the constellation point. Asymptotically, (3.41) is dominated by the term $1/(E_s/4\eta N_0)^D$, and can be approximated as

$$P_e(\mathscr{C}) \approx \frac{\Delta_D}{2|\mathscr{C}|\,(E_s/4\eta N_0)^D}, \tag{3.43}$$

where

$$\Delta_D = \sum_{\delta_p : |\mathscr{I}(\mathbf{x}_g, \mathbf{x}'_g)| = D} \tau_p^{\delta_p} / \delta_p^2 \tag{3.44}$$

should be minimized. The parameter $\tau_p^{\delta_p}$ is the multiplicity. Note that the overall system diversity is limited by $D_{\text{sys}} = \min(L, D)$ [84].

3.5 CODEBOOK DESIGN

From the design criteria derived in the previous section, we will now propose some good M-dimensional codebooks. We consider two cases of study. The first case has $M = 8$ real dimensions and the second one has $M = 4$ real dimensions, both with $N = 256$ constellation points. The first proposed schemes are simply a combination of SIM [13] or GIM [18] and GLCP [20]. The APSK constellation, rather than QAM constellation, in GLCP schemes has also been tested. Next, two codebooks are obtained from the 8-dimensional Gosset lattice, E_8, and the 4-dimensional checkerboard lattice, D_4 [2, 3]. An extra rotation is also

proposed for all codebooks with GLCP, both from literature and proposed, to better explore the design criteria.

The benchmarks schemes adopted in this work are the conventional OFDM, SIM [13] and GLCP [20]. In the conventional OFDM and GLCP schemes, each group of n subcarriers can be seen as an M-dimensional point, corresponding to the Cartesian product of n conventional complex QAM signal sets. For the first case of study, we choose 4-QAM as the digital modulation and $n = 4$ for the benchmarks, where for the SIM technique the same rate is obtained by setting $k = 3$ (out of $n = 4$) active subcarriers. The inactive subcarriers are always assumed to transmit the symbol zero. For the second case of study, 16-QAM was chosen as the digital modulation for the benchmarks, and each group has $n = 2$ subcarriers.

3.5.1 SIM-based constellations

In general, we can consider an OFDM symbol with N_s subcarriers, divided into G groups, each group having n subcarriers, of which k are active. In each active subcarrier, an S-QAM symbol is transmitted. The group vector $\check{\mathbf{x}}_g$ of the OFDM symbol was defined in equation (3.2). For the SIM schemes, $n-k$ elements of this vector are zero. As seen in Section 2.4, the GLCP operation does not modify the rate, which is the same as the ones of the schemes in [13] and [15], namely,

$$R_{\text{SIM}} = G\{\lfloor \log_2 \tbinom{n}{k} \rfloor + k \log_2(S)\} \quad \text{(bits per OFDM symbol)}. \tag{3.45}$$

After applying GLCP to the SIM scheme, new (precoded) group vector is obtained as

$$\dot{\mathbf{x}}_g = \Theta \check{\mathbf{x}}_g, \tag{3.46}$$

where Θ was given in equation (2.2). For the SIM scheme with $n = 4$ and $k = 3$ described above, we have, in Figure 11a, the projections on each real dimension of the proposed constellation GLCP-SIM (for $E_s = 2$). The proposed GLCP-SIM has 256 points, some of them with overlapping projections. In Figure 11b, we show the projections of the four complex dimensions gathered together in a single complex plot.

Note the Gaussian-like shape of the points distribution, with a denser concentration of points with lower energie. This characteristic of the codebook yields a shapping gain, as defined in [91]. The parameters of this codebook are given in Section 3.6, Table 4.

Figure 11 – Projections of the proposed GLCP-SIM constellation, for $n = 4$ and 4-QAM.

(a) Projections on each real dimension.

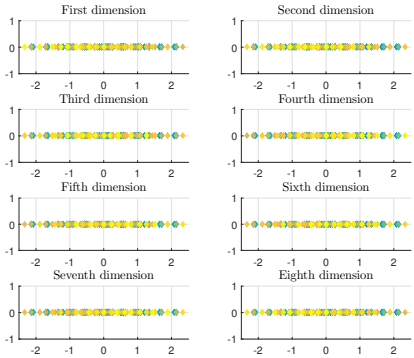

(b) Projections of the four complex dimensions in a single complex plot.

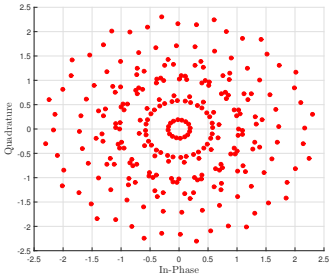

From (3.46), the expanded (precoded) real group vector is given as

$$\dot{\mathbf{x}}_g = [\dot{x}^{\mathrm{R}}_{ng-(n-1)}, \dot{x}^{\mathrm{I}}_{ng-(n-1)}, \ldots, \dot{x}^{\mathrm{R}}_{ng}\ ,\ \dot{x}^{\mathrm{I}}_{ng}]^T. \tag{3.47}$$

All the development in Section 3.3 applies, except for the ML detection which, for the proposed GLCP-SIM, is

$$\hat{\mathbf{x}}_g = \underset{\mathbf{x}'_g \in \mathscr{C}}{\arg\min} \parallel \mathbf{y}_g - \mathrm{diag}(\mathbf{h}_\gamma)\dot{\mathbf{x}}'_g \parallel^2. \tag{3.48}$$

For the second case of study, all previous procedure is similar, except that we adopt GIM technique [18] instead of SIM [13]. In this case, each group with $n = 2$ subcarriers is seen as a group of $M = 4$ real dimensions, of which $k_d = 3$ are independent real dimensions are active. In each active real dimension, a 4-PAM symbol is transmitted, and the complex symbols of the resulting constellation may have only the in-phase component, the quadrature component, or both.

The precoded group vector of the proposed GLCP-GIM is as defined in equation (3.47), with each symbol a linear combination of the real symbols in the active real dimensions. The rate, in terms of bits per OFDM symbol, is given as [18]

$$R_{\text{GIM}} = G\{\lfloor \log_2 \binom{M}{k_d} \rfloor + k_d \log_2(S)\}. \tag{3.49}$$

The projections on each real dimension of our proposed GLCP-GIM constellation are shown in Figure 12a, while the projections of the two complex dimensions gathered together are in Figure 12b, both for $E_s = 2$. Again, a Gaussian-like shape is observed. The parameters of interest of this codebook is presented in Table 5.

Figure 12 – Projections of the proposed GLCP-GIM constellation, for $n = 2$ and 4-PAM.

(a) Projections on each real dimension.

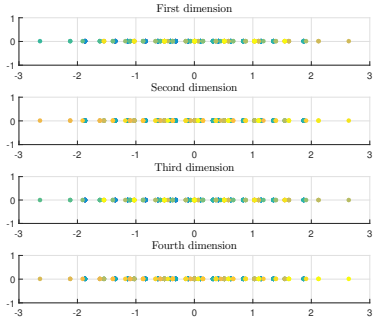

(b) Projections of the two complex dimensions in a single complex plot.

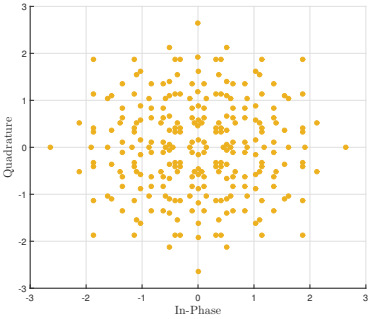

3.5.2 Lattice-based constellations

The Gosset lattice, referred to as E_8, is a well-known 8-dimensional real lattice described as [2]

$$\{(x_1, \ldots, x_8) \in \mathbb{Z}^8 \cup (\mathbb{Z} + 1/2)^8 : \sum_{q=1}^{8} x_q \equiv 0 \pmod 2\}. \tag{3.50}$$

To form our codebook, 256 codewords were chosen from the points of lowest norm in E_8, presented in Table 1. For the nonzero components of

the points shown, the two possible polarities ($\pm$) are available. In the case of the points shown as $(\pm1,\pm1,0,0,0,0,0,0)$, we considered all $\binom{8}{2}$ combinations, associated with the different positions the two nonzero components can take, and for each one of them the 4 possible polarities. This results in a total of 112 points/codewords. The same idea applies to the points in the fourth row of the table. The 15 codewords were chosen among the $16\binom{8}{4}$ points of norm 4, in such a way that the parameters of interest shown is Section 3.4 are optimized.

Table 1 – Selected points from the lattice E_8 for the proposed codebook.

	No. of points	Points	Norm
$\mathscr{C}_{E_8}^{O}$	1	(0,0,0,0,0,0,0,0)	0
	128	$(\pm1/2,\pm1/2,\pm1/2,\pm1/2,\pm1/2,\pm1/2,\pm1/2,\pm1/2)$	2
	112	$(\pm1,\pm1,0,0,0,0,0,0)$	2
	15[a]	$(\pm1,\pm1,\pm1,\pm1,0,0,0,0)$	4

[a] Codewords chosen (all with positive polarity): $[(1,1,1,1,0,0,0,0),(1,1,1,0,1,0,0,0),(1,1,1,0,0,1,0,0),(1,1,1,0,0,0,1,0),(1,1,1,0,0,0,0,1),(1,1,0,1,1,0,0,0),(1,1,0,1,0,1,0,0),(1,1,0,1,0,0,1,0),(1,1,0,1,0,0,0,1),(1,1,0,0,1,1,0,0),(1,1,0,0,1,0,1,0),(1,1,0,0,1,0,0,1),(1,1,0,0,0,1,1,0),(1,1,0,0,0,1,0,1),(1,1,0,0,0,0,1,1)]$.

In Table 1, the codebook $\mathscr{C}_{E_8}^{O}$ is not centralized (as is usually the case when a subset is carved from a lattice). When this happens, a centralized version of the codebook must be obtained through translation, in order to make the codebook more energy-efficient. This can be accomplished by adding a vector, called *dither*, to all points of the codebook, as described next.

The dither is given by

$$\mathbf{v}_d = \frac{1}{|\mathscr{C}_{E_8}^{O}|}\sum_{\mathbf{c}\in\mathscr{C}_{E_8}^{O}}\mathbf{c}, \tag{3.51}$$

which corresponds to the average vector and $\mathbf{c}$ represents a codeword from the subset carved from the lattice. The centralized codebook, denoted by $\mathscr{C}_{E_8}^{C}$, is given by

$$\mathscr{C}_{E_8}^{C} = \mathscr{C}_{E_8}^{O} - \mathbf{v}_d \triangleq \left\{\mathbf{c}-\mathbf{v}_d \;:\; \mathbf{c}\in\mathscr{C}_{E_8}^{O}\right\}. \tag{3.52}$$

Let $E(\mathscr{C}_{E_8}^C)$ be the average energy of the centralized codebook, given by

$$E(\mathscr{C}_{E_8}^C) = \frac{1}{|\mathscr{C}_{E_8}^C|} \sum_{\mathbf{c} \in \mathscr{C}_{E_8}^C} \|\mathbf{c}\|^2. \tag{3.53}$$

The proposed centralized M-dimensional codebook, denoted by $\mathscr{C}_{E_8}$, with a given point average energy E_c, is obtained as

$$\mathscr{C}_{E_8} = \sqrt{\frac{E_c}{E(\mathscr{C}_{E_8}^C)}} \mathscr{C}_{E_8}^C. \tag{3.54}$$

Since we cannot draw in 8-dimensions, the proposed constellation is presented, as done before, in terms of the projections on each real dimension and on the four complex dimensions gathered together in a single complex plot. The result is shown in Figure 13. The average energy per complex symbol is $E_s = 2$ (or $E_c = 8$).

Figure 13 – Projections of the proposed $\mathscr{C}_{E_8}$ constellation, for $n = 4$ and $N = 256$.

(a) Projections on each real dimension.

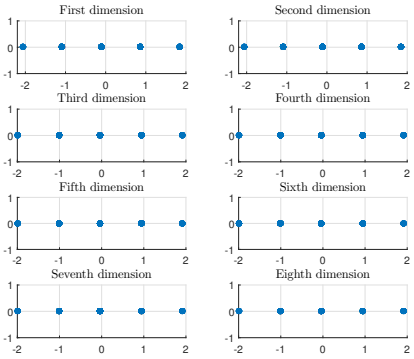

(b) Projections of the four complex dimensions in a single complex plot.

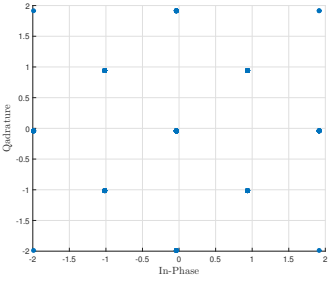

It should be beared in mind that the four complex dimensions in the group are correlated (as in a coded scheme) due to the multidimensional design. In other words, although each complex dimensions has 13 points (due to the overlapping, in Figure 13b), not all of the

$13^4 = 28561$ sequences belong to the multidimensional constellation. Instead, there are only 256 8-dimensional points in the constellation. In fact, this correlation is what causes the performance improvement of the multidimensional design.

This proposed constellation was also combined with GLCP. Figure 14 shows the projections, as in the previous cases, of the proposed constellation $\mathscr{C}_{E_8}$ with GLCP, herein called GLCP-$\mathscr{C}_{E_8}$.

Figure 14 – Projections of the proposed GLCP-$\mathscr{C}_{E_8}$ constellation, for $n = 4$ and $N = 256$.

(a) Projections on each real dimension.

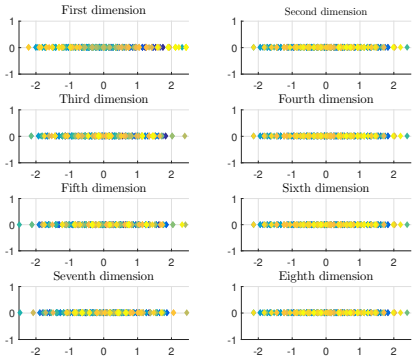

(b) Projections of the four complex dimensions in a single complex plot.

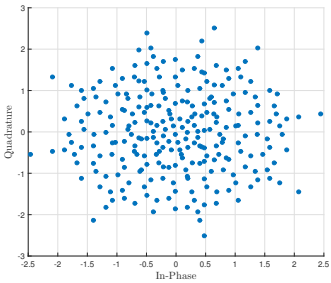

The checkerboard lattice, D_4, is described as [2]:

$$\{(x_1, x_2, x_3, x_4) \in \mathbb{Z}^4 : \sum x_i = \text{even}\}. \tag{3.55}$$

To form our 4-dimensional codebook, 256 points of lowest norms were chosen from D_4, according to Table 2.

Table 2 – Selected points from the lattice D_4 for the proposed codebook.

	# of Points	Points	Norm	# of Points	Points	Norm
$\mathscr{C}^O_{D_4}$	1	(0,0,0,0)	0	96	$(\pm1, \pm1, \pm2, 0)$	6
	24	$(\pm1, \pm1, 0, 0)$	2	24	$(\pm2, \pm2, 0, 0)$	8
	16	$(\pm1, \pm1, \pm1, \pm1)$	4	48	$(\pm1, \pm3, 0, 0)$	10
	8	$(\pm2, 0, 0, 0)$	4	39	$(\pm1, \pm1, \pm2, \pm2)$	10

The point $(\pm1, \pm1, \pm2, \pm2)$ with norm 10 has 96 possible permutations, but only 39 points among them have been chosen. As $\binom{96}{39}$ is a very large value, 10000 random combinations were tested. The 39 points were chosen according to the criteria for optimization the parameters of interest in Section 3.4 and are listed in Table 3.

Table 3 – The 39 points chosen among $\binom{96}{39}$ possible combinations.

Selected points			
$(-2,-2,-1,-1)$	$(-2,-1,2,-1)$	$(-2,2,-1,-1)$	$(-1,-2,2,-1)$
$(-2,-2,-1,1)$	$(-2,-1,2,1)$	$(-2,2,-1,1)$	$(-1,-2,2,-1)$
$(-2,-2,1,-1)$	$(-2,1,-2,-1)$	$(-2,2,1,-1)$	$(-1,-1,-2,-2)$
$(-2,-2,1,1)$	$(-2,1,-2,1)$	$(-2,2,1,1)$	$(-1,-1,-2,2)$
$(-2,-1,-2,-1)$	$(-2,1,-1,-2)$	$(-1,-2,-2,-1)$	$(-1,-1,2,-2)$
$(-2,-1,-2,1)$	$(-2,1,-1,2)$	$(-1,-2,-2,1)$	$(-1,-1,2,2)$
$(-2,-1,-1,-2)$	$(-2,1,1,-2)$	$(-1,-2,-1,-2)$	$(-1,1,-2,-2)$
$(-2,-1,-1,2)$	$(-2,1,1,2)$	$(-1,-2,-1,2)$	$(-1,1,-2,2)$
$(-2,-1,1,-2)$	$(-2,1,2,-1)$	$(-1,-2,1,-2)$	$(-1,1,2,-2)$
$(-2,-1,1,2)$	$(-2,1,2,1)$	$(-1,-2,1,2)$	–

As in the first case, the proposed M-dimensional codebook, denoted by $\mathscr{C}_{D_4}$, had to be centralized according to equation (3.53), yielding

$$\mathscr{C}_{D_4} = \sqrt{\frac{E_c}{E(\mathscr{C}^C_{D_4})}}\mathscr{C}^C_{D_4}. \tag{3.56}$$

For the second case of study, we focus on the precoded only schemes and on the rotated and precoded schemes, which will be presented in Section 3.5.4. For this reason, we present only the proposed constellation GLCP-$\mathscr{C}_{D_4}$, which is illustrated in Figure 15, in terms of the individual projections and of the two overllaped complex projections. A more uniform point distribution is obtained. The symbol average energy is $E_s = 2$, then $E_c = 4$. The parameters of interest of this codebook is presented in Table 5.

Figure 15 – Projections of the proposed GLCP-$\mathscr{C}_{D_4}$ constellation, for $n = 2$ and $N = 256$.

(a) Projections on each real dimension.

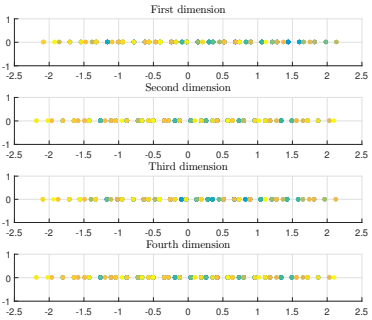

(b) Projections of the four complex dimensions in a single complex plot.

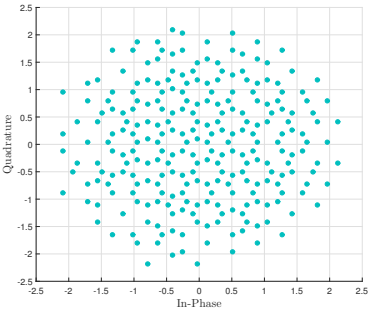

3.5.3 APSK-based constellations

The authors in [9] proposed to exploit the SSD with BICM-ID with amplitude phase shift keying modulation (APSK). They used rotation [1] to improve the modulation diversity order of the proposed constellations, and they obtained good results for coded systems.

For this reason, we decided to investigate the performance of APSK constellations associated to GLCP and rotation for uncoded systems in order to complement our second case of study. The principle of the proposed scheme is the same as for the conventional GLCP [20], the only difference is that instead of using S-QAM we use S-APSK in each subcarrier. The proposed constellation (GLCP with 16-APSK) is presented in Figure 16 for $n = 2$, resulting in a constellation with 256 points. The symbol average energy is the same as the one for the other schemes in this case of study ($E_s = 2$).

3.5.4 Rotations and a search algorithm

According to [1], constellation rotations may improve the modulation diversity. With that in mind, a search has been performed to find the best rotation angles for each scheme.

Figure 16 – Projections of the proposed GLCP constellation with 16-APSK, for $n = 2$ and $N = 256$.

(a) Projections on each real dimension.

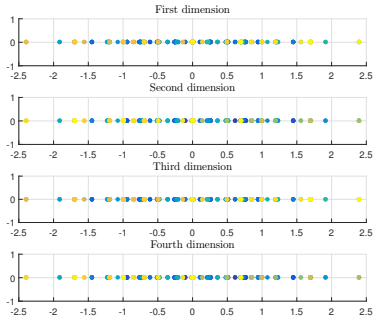

(b) Projections of the four complex dimensions in a single complex plot.

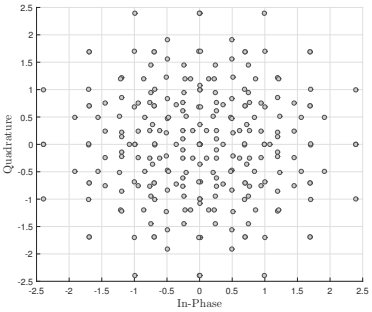

Let $\mathscr{C}$ be an M-dimensional real codebook (or equivalently, an n-dimensional complex codebook, where $M = 2n$) and let $\check{\mathbf{x}}_g$ be a generic point in $\mathscr{C}$ (see (3.2)). Denote the angle vector by $\boldsymbol{\phi} = [\phi_1, \ldots, \phi_n]$. Denote the multidimensional constellation rotated by the angle vector $\boldsymbol{\phi}$ by $\mathscr{C}(\boldsymbol{\phi})$, which is given by

$$\mathscr{C}(\boldsymbol{\phi}) = \left\{ \boldsymbol{\Phi} \check{\mathbf{x}}_g : \check{\mathbf{x}}_g \in \mathscr{C} \right\}, \tag{3.57}$$

where the matrix $\boldsymbol{\Phi}$, of size $n \times n$, is given as

$$\boldsymbol{\Phi} = \mathrm{diag}([e^{j\phi_1}, \ldots, e^{j\phi_n}]). \tag{3.58}$$

Denote by $D(\boldsymbol{\phi})$ and $\Delta_D(\boldsymbol{\phi})$ the two corresponding parameters of codebook $\mathscr{C}(\boldsymbol{\phi})$, listed in order of importance. The optimum rotation angle is the one that produces the rotated codebook with the optimal parameters D^{opt} and Δ_D^{opt}, according to the criteria presented in Section 3.4.

To avoid a complex search, a good and feasible solution can be obtained by constraining the search space to a finite set. Let such set be denoted by $\mathscr{Q} = \{\phi_1, \ldots, \phi_A\}$, of size $|\mathscr{Q}| = A$. Define also the sets $\mathscr{P}(\boldsymbol{\phi})$ as the set of all pairs of distinct codewords (points) in codebook $\mathscr{C}(\boldsymbol{\phi})$. With some abuse of notation, denote by D^{opt} the best parameter

D obtained under the restricted search space:

$$D^{\text{opt}} = \max_{\phi'_a \in \mathscr{Q}} D(\phi'_a) = \max_{\phi'_a \in \mathscr{Q}} \left\{ \min_{(\ddot{\mathbf{x}}_g, \ddot{\mathbf{x}}'_g) \in \mathscr{P}(\phi'_a)} d_H(\ddot{\mathbf{x}}_g, \ddot{\mathbf{x}}'_g) \right\}, \tag{3.59}$$

where

$$\ddot{\mathbf{x}}_{\mathbf{g}} = \mathbf{\Phi} \check{\mathbf{x}}_g, \tag{3.60}$$

and $\ddot{\mathbf{x}}_g \in \mathscr{C}(\phi)$. Consider now the set of all angles in $\mathscr{Q}$ which maximize the SSD, given as

$$\mathscr{Q}_D = \left\{ \phi_a \in \mathscr{Q} : D(\phi_a) = D^{\text{opt}} \right\}. \tag{3.61}$$

The next step is to find the best parameter Δ_D^{opt} (multiplicity-to-product distance ratio) under the restricted search space $\mathscr{Q}_D$. Again, with some abuse of notation, we have

$$\Delta_D^{\text{opt}} = \min_{\phi'_a \in \mathscr{Q}_D} \Delta_D(\phi'_a) = \min_{\phi'_a \in \mathscr{Q}_D} \left\{ \sum_{\delta_p : d_H(\ddot{\mathbf{x}}_g, \ddot{\mathbf{x}}'_g) = D^{\text{opt}}} \frac{\tau_p^{\delta_p}}{\delta_p(\ddot{\mathbf{x}}_g, \ddot{\mathbf{x}}'_g)^2} \right\}. \tag{3.62}$$

The best rotation angle vector is given by

$$\phi^{\text{opt}} = \arg\min_{\phi'_a \in \mathscr{Q}_D} \Delta_D(\phi'_a) \tag{3.63}$$

For conventional OFDM, some works have investigated the problem of angle optimization aiming at maximizing the SSD, as for example [1, 92]. In contrast, for SIM constellations the only work exploiting the benefits of constellations rotation is [16], which has different optimization criteria not applicable to the present work. For GLCP constellations, no previous work dealing with rotations has been found in the literature. Therefore, the rotated GLCP constellations found in this work are novel. Then, we have a new group vector (point) given as

$$\mathring{\mathbf{x}}_g = \mathbf{\Theta}\mathbf{\Phi}\check{\mathbf{x}}_g. \tag{3.64}$$

Note that, when one of these precoded codebooks (with GLCP, rotation or both) is used, appropriate changes should be made in the analysis, such as considering the matrices $\mathbf{\Phi}$, $\mathbf{\Theta}$ or $\mathbf{\Theta\Phi}$ in equation (3.17).

Other possibility is to replace the group vector in (3.2) by one of the group vectors in (3.46), (3.60) or (3.64) and, consequently, in all other equations in the development.

Some comments regarding GLCP can be drawn. First, note from (2.2) that GLCP already has an implicit rotation. However, this rotation was obtained in [20] considering other optimization parameters and adopting an interleaving at the (complex) subcarrier level, which yields a maximum diversity order of n. It is possible to find a single rotation as a result of the product $\mathrm{diag}(\alpha_1,\ldots,\alpha_1^{n-1})\mathrm{diag}(e^{j\phi})$, but the implicit rotation in the GLCP has a different angle for each complex dimension. Considering a search of 360 angles for each complex dimension, we would have 360^n combinations to be tested, which is too complex. For this reason, we have to re-optimize the rotation matrix Φ using, for simplicity, the same angle for all complex dimensions. We also adopt interleaving at the real dimension level, which can offer a diversity order of up to $2n$.

3.6 NUMERICAL RESULTS

In our search for the best rotation, the angle ϕ varied between $0°$ and $360°$ with step $0.5°$ and we consider $\phi_i = \phi$ in (3.58) for all $i = 1,\ldots,n$ and for any codebook. The codebooks with the best rotations and their parameters found in this work are listed in Table 4.

As can be seen, rotation alone changes the minimum modulation diversity from $D = 1$ to $D = 2$, as in [1]. The use of GLCP in the constellations further improves the diversity order, reaching $D = n = 4$. However, our proposal, which performs interleaving at the real dimension level and combines GLCP and rotation, is able to achieve full diversity $D = M = 8$. Moreover, if we compare the schemes with the same D, lattice-based constellations presented the lowest Δ_D.

For the 4-dimensional codebooks, the same behavior as in the previous case is observed. The schemes with the best rotation and their parameters found in this chapter are listed in Table 5. For this case of study, we present results only for the precoded schemes, to show

Table 4 – Codebooks parameters before and after rotation for 8-dimensional schemes, where the highlighted cells correspond to the proposed schemes.

Schemes	Without Rotation		With Rotation		
	D	Δ_D	D	Δ_D	$\phi(^\circ)$
OFDM	1	512	2	938.12	29.5
ISIM [15]	1	288	2	395.77	29.5
$\mathscr{C}_{E_8}$	1	14.71	2	104.46	13
GLCP [20]	4	1782.5	8	1.39×10^{10}	14.5
GLCP-SIM	4	1133.6	8	2.78×10^{10}	75
GLCP-$\mathscr{C}_{E_8}$	4	254.54	8	4.41×10^{9}	52

Table 5 – Codebooks parameters before and after rotation for 4-dimensional precoded schemes, where the highlighted cells correspond to the proposed schemes.

Schemes	Without rotation		With rotation		
	D	Δ_D	D	Δ_D	$\phi(^\circ)$
GLCP (16-QAM) [20]	2	1.32×10^{4}	4	7.55×10^{7}	31
GLCP (16-APSK)	1	9.54	2	57.53	164.5
GLCP-GIM	2	9.831,98	4	6.71×10^{8}	124,5
GLCP-$\mathscr{C}_{D_4}$	2	5 048.21	4	7.21×10^{7}	55,5

the strength of our proposal.

3.7 ON THE BIT ERROR RATE

As shown in (3.41), for high SNR the main constellation parameters are, in order of importance, the SSD, the minimum product distance, and the multiplicity, where the last is frequently ignored to reduce the design complexity. The bit error probability (BEP) in this case can be upper bounded by a modified version of the constellation

point error probability (CEP) in (3.41) as

$$P_b(\mathscr{C}) \leq \frac{1}{|\mathscr{C}|\log_2(|\mathscr{C}|)} \sum_{\mathbf{x}_g} \sum_{\mathbf{x}'_g \neq \mathbf{x}_g} \frac{1}{2} \frac{d_H(\ell(\mathbf{x}_g), \ell(\mathbf{x}'_g))}{\left(\frac{E_s}{4\eta N_0}\right)^{|\mathscr{I}(\mathbf{x}_g, \mathbf{x}'_g)|} \delta_p(\mathbf{x}_g, \mathbf{x}'_g)^2}, \quad (3.65)$$

where $\ell(\mathbf{x}_g)$ represents the bit label of the M-dimensional point $\mathbf{x}_g$, and $d_H(\ell(\mathbf{x}_g), \ell(\mathbf{x}'_g))$ is the Hamming distance between two distinct labels.

In contrast, it can be shown by expanding the product in (3.40) that for low SNR the squared Euclidean distance becomes more relevant to the error probability than the squared product distance. On the other hand, it is well-known that the effect of bit labeling on the BEP is more prominent at low SNR. Therefore, in order to design good labelings that can reduce the BEP, one should focus on the low SNR region and adopt the squared Euclidean metric.

In general terms, a good labeling is one for which $d_H(\ell(\mathbf{x}_g), \ell(\mathbf{x}'_g))$ is small if the codebook points $\mathbf{x}_g$ and $\mathbf{x}'_g$ are close to each other in the signal space. For the codebooks designed as the cartesian product of the constellations QAM or PAM, Gray labeling can be used in each complex constellation, and the label of the multidimensional codebook point is taken as the concatenation of the constituent complex symbols labels. Interestingly, since rotation and GLCP are unitary transformations, the squared Euclidean distances between codebook points are preserved after the operation in (3.64). Therefore, a good labeling for an original codebook will do as good for its rotated and/or precoded version.

The problem becomes far more complicated for codebooks based on multidimensional lattices. It is well known from the literature that labeling in this case is a complex problem. The Gray labeling can not be used and, therefore, another solution have to be sought.

3.7.1 Binary switching algorithm

An interesting solution to this problem is obtained with the so-called binary switching algorithm (BSA) [93], which is widely used in the literature in different contexts to find a suboptimal labeling. The main idea of this algorithm is to do a switching between labels in order

to minimize the total cost of the codebook. As a result, a quasi-Gray labeling is obtained. From the literature [94, 95], the total cost function (CF) of a codebook for fading channels is a function of the squared Euclidean distance, and is given as [94]

$$\mathrm{CF} = \frac{1}{m2^m} \sum_{i=1}^{m} \sum_{b=0}^{1} \sum_{\mathbf{x}_g \in \mathscr{X}_i^b} \sum_{\mathbf{x}'_g \in \mathscr{X}_i^{\bar{b}}} \frac{1}{\delta_E(\mathbf{x}_g, \mathbf{x}'_g)^2}, \tag{3.66}$$

where $m = \log_2(|\mathscr{C}|)$ and $\mathscr{X}_i^b$ is the set of codewords whose i-th bit-label is b. $\bar{b}$ is the complement of b and $\delta_E(\mathbf{x}_g, \mathbf{x}'_g)^2$ is the squared Euclidean distance, given by

$$\delta_E(\mathbf{x}_g, \mathbf{x}'_g)^2 = \|\mathbf{x}_g - \mathbf{x}'_g\|^2. \tag{3.67}$$

The individual cost function, i.e., the cost associated with a codeword $\mathbf{x}_g$ of the codebook, is given as

$$\mathrm{ICF}(\mathbf{x}_g) = \frac{1}{m} \sum_{i=1}^{m} \sum_{\mathbf{x}'_g \neq \mathbf{x}_g, \mathbf{x}'_g \in \mathscr{X}_i^{\bar{b}}} \frac{1}{\delta_E(\mathbf{x}_g, \mathbf{x}'_g)^2}, \tag{3.68}$$

where now b is determined by the label of the codeword $\mathbf{x}_g$.

The steps of the BSA are described below:

1. Set the current labeling to (possibly random) initial labeling for the codebook.

2. Calculate the CF in (3.66) based on the current labeling of the codebook.

3. Calculate the ICF in (3.68) based on the current labeling for each codeword of the codebook.

4. Switch the bit-label of the codeword having the highest cost (the reference codeword) with the bit-label of each codeword of the codebook, and calculate the CF for each switch. If this action does not reduce CF, we take the next most costly codeword as the reference codeword to make the switch, until CF is reduced or until no switch, among all possible switches, is able to reduce the CF.

5. If CF has been reduced, updated the current labeling and go to step 3.

6. Return the current labeling as the best labeling.

3.7.2 Results obtained

In Table 6, the 8-dimensional codebooks are compared in terms of the total cost in (3.66) and the minimum squared Euclidean distance, denoted as d_E^2. Herein, only the codebooks with maximum SSD are listed.

As can be seen in Table 6, rot. GLCP presents the smallest CF. Although rot. GLCP-$\mathscr{C}_{E_8}$ has the largest minimum squared Euclidean distance, a larger multiplicity factor (number of neighboring codewords) in (3.66) and (3.68) renders its CF value the highest. The best CF found for rot. GLCP-$\mathscr{C}_{E_8}$, after testing some different initial labelings on the BSA, is shown in the last column of the table.

Table 6 – Comparison of the total cost function (CF) of the 8-dimensional schemes with $D = 8$.

Scheme	d_E^2	Total cost function (CF)		
		Initial labeling	Optimized labeling	
			Gray	BSA
rot. GLCP	4	7.97[a]	7.97	–
rot. GLCP-SIM	5.33	8.54[b]	8.54	–
rot. GLCP-$\mathscr{C}_{E_8}$	7.62	9.35[c]	–	8.60

[a] Natural labeling at QAM level.
[b] Natural labeling at QAM level and random labeling for the subcarrier activation pattern.
[c] Random labeling.

For the second case of study, results are presented in Table 7. Again, as expected, the codebooks based on constellations with Gray labeling have the smallest CF. The BSA has produced a very good result for rot. GLCP-$\mathscr{C}_{D_4}$: the second best CF. For the codebook based

Table 7 – Comparison of the total cost function (CF) of the 4-dimensional schemes with $D = 4$.

Scheme	d_E^2	Total cost function (CF)		
		Initial labeling	Optimized labeling	
			Gray	BSA
rot. GLCP (16-QAM)	0.8	23.70[a]	20.85	–
rot. GLCP (16-APSK)	0.5	24.22[b]	–	–
rot. GLCP-GIM	0.53	24.10[c]	23.32	–
rot. GLCP-$\mathscr{C}_{D_4}$	1.16	25.13[d]	–	21.72

[a] Natural labeling at QAM level.
[b] Natural labeling at APSK level.
[c] Natural labeling at PAM level and random labeling for the dimension action pattern.
[d] Random labeling.

on APSK, natural and Gray labeling presented the same CF and the BSA was not able to find anything better.

In the remainder of this chapter, we present some numerical results in order to better illustrate the problem of low squared Euclidean distance associated with large average number of neighbors, which causes a low CF for lattice-based codebooks.

The average number of neighbors at distance δ_E^2 is given as

$$\overline{v}(\delta_E^2) = \frac{\text{no. of pairs at distance } \delta_E^2}{N/2}. \tag{3.69}$$

The collection $\{\overline{v}(\delta_E^2)\}$ for all distances δ_E^2 is called the distance spectrum, which is shown for the 8- and 4-dimensional schemes in Figures 17 and 18, respectively. We observe from these figures that the lattice-based codebooks have larger distances but they associated to larger multiplicities.

We have also obtain the average number of bit errors as a function of the squared Euclidean distance between pairs of codewords,

Figure 17 – Distance spectra of the 8-dimensional schemes with $D = 8$.

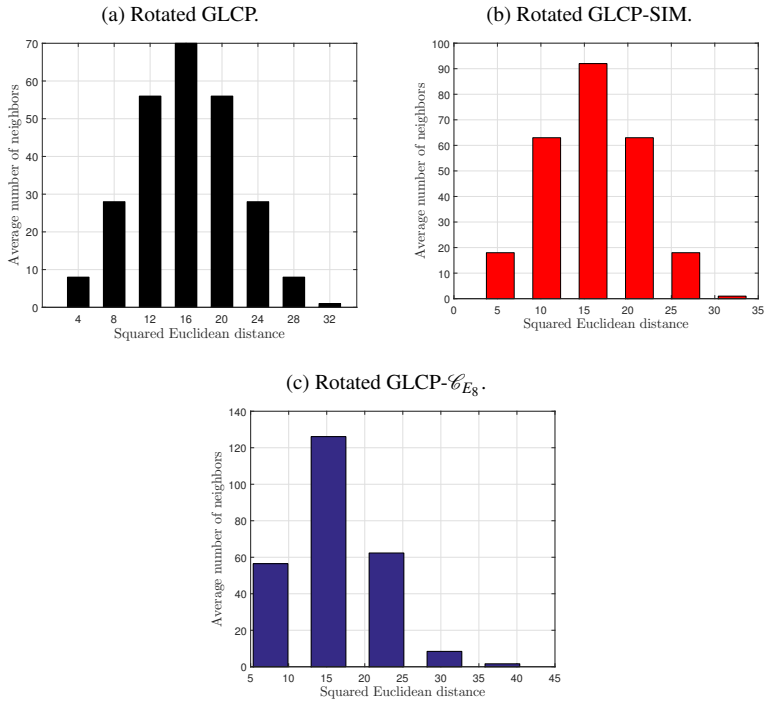

given as

$$\overline{b}_e(\delta_E^2) = \frac{\sum \delta_H \text{ of all pairs at distance } \delta_E^2}{\text{no. of pairs at distance } \delta_E^2}. \tag{3.70}$$

Results are presented in Figures 19 and 20. For the 8-dimensional codebooks, as can be seen in 19a, the QAM-based codebook has the best bit errors distribution, where all codeword pairs tat d_E^2 have labels that differ by only 1 bit. As the squared Euclidean distance increases, the average number of bit error increases linearly.

The SIM-based codebook has a worse distribution but follows the same trend: it has an increasing distribution. The worse result comes from the fact that part of the bits comes from the index modulation, which is not related to the Euclidean distance. In 19c, we can see that the BSA was capable of reducing the average number of bit errors from

Figure 18 – Distance spectra of the 4-dimensional schemes with $D = 4$.

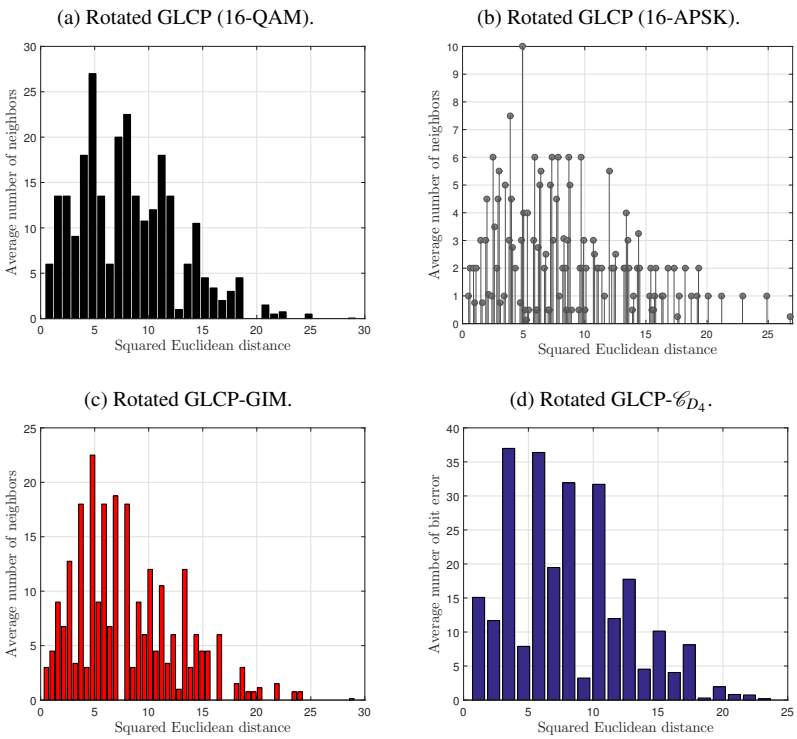

3.92 to 2.77, for d_E^2. An increasing spectrum is also observed for the lattice-based codebook.

The average bit error distributions for the 4-dimensional codebooks are shown in Figure 20. The QAM-based codebook continues to have the best distribution, where the three smaller distances have the three smaller average number of bit errors with Gray labeling. For the constellation based on APSK, which presents the worst CF for this scenario, we tried some different strategies to improve the CF. For example, we tried the labeling proposed in [9], the Gray labeling at 16-APSK level and we run the BSA search, but no improvement has been obtained. As in the previous case, the BSA provided a good improvement of the CF for the lattice-based codebook, but not enough

Figure 19 – Average number of bit errors versus squared Euclidean distance for the 8-dimensional schemes with $D = 8$.

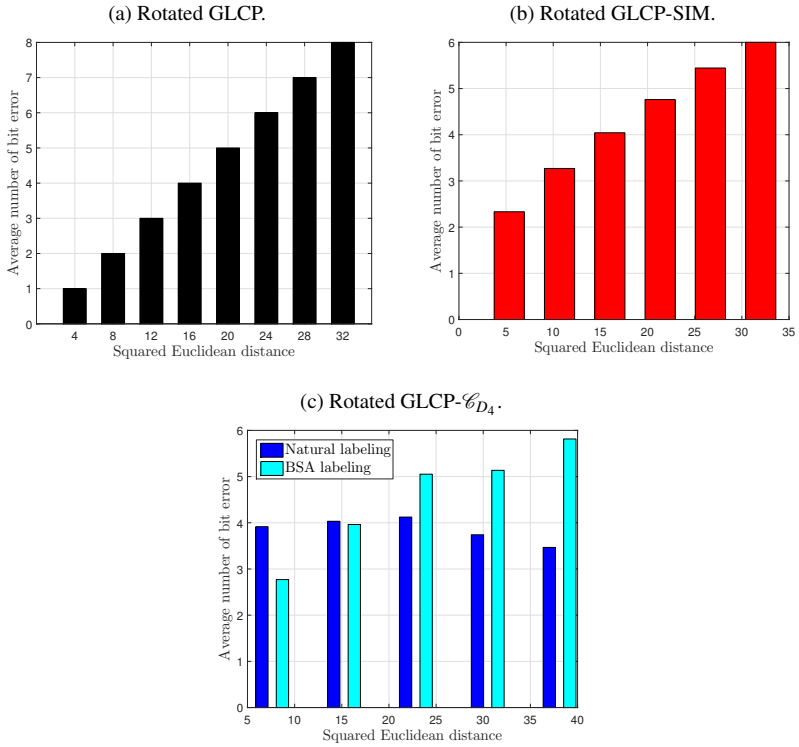

to outperform the QAM-based codebook.

3.8 CHAPTER CONCLUSIONS

This chapter presented the system model adopted in this dissertation. Some 8-dimensional and 4-dimensional constellations were proposed. The first were the SIM-based codebooks, which presented better parameters when compared with the schemes in the literature: GLCP [20] and ISIM [15]. Then, leaving aside the index modulation concept and looking for all constellations under the multidimensional perspective, multidimensional constellations carved from the Gosset

Figure 20 – Average number of bit errors versus squared Euclidean distance for the 4-dimensional schemes with $D = 4$.

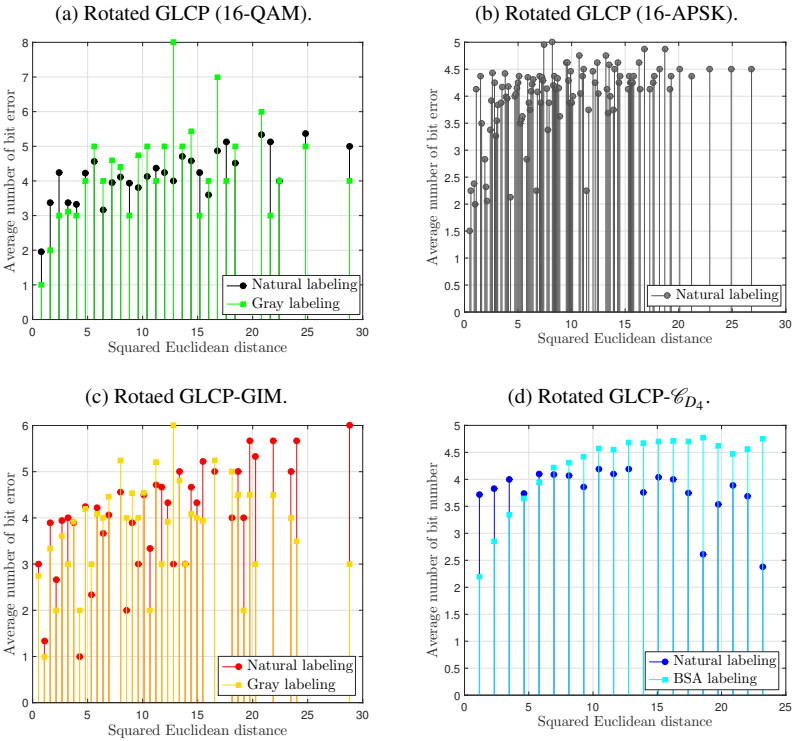

and D_4 lattices presented better parameters for some scenarios. Different digital modulations, which serve as a basis for constructing multidimensional constellations, were investigated under this perspective. Constellations with maximum modulation diversity, yielding a performance better than that of their predecessors, were obtained with an extra rotation of the GLCP constellations. Finally, the codeword labeling problem and its impact on the bit error rate performance, at low and medium SNR regime, were investigated. The binary switching algorithm was used to obtain an improved bit labeling, yielding a lower bit error probability. Both simulation and analytical results showing these improvements are presented and discussed in Chapter 5.

4 FULLY-DIVERSE MULTIDIMENSIONAL CODEBOOK DESIGN: A COMBINATORIAL APPROACH

4.1 INTRODUCTION

This chapter presents the second proposal of this dissertation, namely, the design of fully-diverse multidimensional codebooks by a combinatorial approach. Although this proposal is not restricted to OFDM systems with grouped subcarriers, the same system model of the previous chapter is assumed to better compare the different proposals. First, the problem statement is presented. Then, we explain the operation of the proposed methodology. An enumerative technique is developed by which an average (squared) product distance spectrum of an ensemble of codebooks is obtained. Two algorithms for systematically constructing good codebooks are presented. Finally, the codebook parameters are tabulated and compared to those of the codebooks of the previous chapter.

4.2 PROPOSED APPROACH FOR DESIGNING FULLY-DIVERSE MULTIDIMENSIONAL CODEBOOKS

Traditionally, the approach to improve the diversity gain over fading channels is to consider a rotation of the signal constellation [1, 3, 92], as considered in the previous chapter and illustrated in Fig. 21b for a QPSK constellation. It should be noted that, after rotation, all the four points of the constellation are distinguishable when projected on either one of the two dimensions. It means that, if one dimension is affected by a deep fading, the information can still be recovered from the other dimension [1]. This is the reason why the diversity gain is equal to two with the constellation in Fig. 21b. In contrast, with the standard QPSK in Fig. 21a, the two dimensions are required in order to recover the information. Thus, the so-called SSD is not properly exploited in this case.

From Section 3.3, if $|\mathscr{I}(\mathbf{x}_g, \mathbf{x}'_g)| = M$ for all pairs of distinct codebook points, i.e., if $D = M$, the codebook is said to be *fully-*

Figure 21 – Illustration of the proposed approach for codebook design.

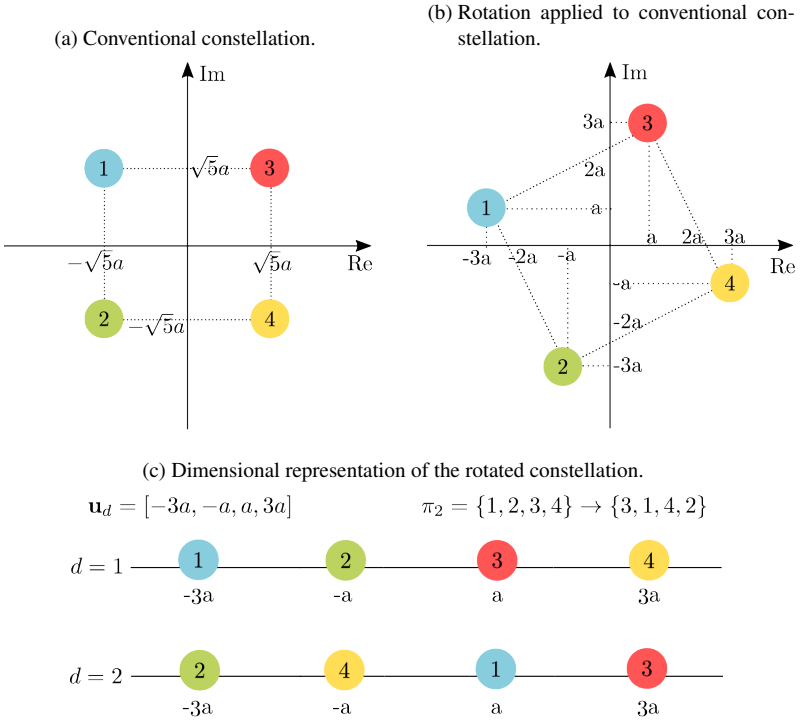

diverse [1, 5], in which case the best performance (maximum diversity gain) is achieved for moderate-to-high SNR.

The rotation illustrated in Fig. 21b or, more generally, the principle of constellation precoding [20] is usually applied to a complex (2-dimensional real) constellation. Symbols from this precoded constellation are then transmitted sequentially in different channel resources. In the previous chapter, a unified approach to design multidimensional codebooks for fading channels has been proposed. In particular, a multidimensional real constellation was carved from a real lattice, and then rotation and precoding were applied to finally produce a fully-diverse multidimensional codebook.

In this chapter, we introduce a different approach to produce a

fully-diverse codebook. Instead of departing from a standard constellation, herein we start with a fixed set of grids of points which represent the projection of an ensemble of fully-diverse codebooks on all dimensions. In other words, all codebooks in the ensemble are projected onto the same set of grids, and each grid is associated with a dimension and contains exactly the same N projected marks. Different codebooks in the ensemble are obtained by different sets of label permutations, as explained next.

Without loss of generality, we can label the N points of any codebook $\mathscr{C}$ in the ensemble as $1,2,\ldots,N$, according to the order in which their projections are positioned along the first dimension, as shown in the upper part of Fig. 21c, for $N=4$ and $M=2$. In this way, the first dimension of all codebooks in the ensemble look exactly the same in terms of projected marks and labels ordering. What differentiate one codebook from another are the labels orderings in the other dimensions.

Now, for a given codebook $\mathscr{C}$, by piling all other dimensions along with the projections (again, see Fig. 21c), one readily obtain a set of $M-1$ permutations of the elements $1,2,\ldots,N$ as the labels of the points. We may refer to a point in $\mathscr{C}$ as its label (an integer) or as the column vector whose entries are the point coordinates in all dimensions, depending on the context. In the latter case, the point i is conveniently referred to as the vector $\mathbf{x}^{(i)}$.

Under the traditional constellation rotation, the projections of the codebook on different dimensions usually result in different sets of points (although, typically, they all have a similar Gaussian shape). Herein, we have exactly the same set of points in all dimensions, for simplicity of design and analysis.

In a recent work, Bao et al. [96] has used a similar idea in a different context, namely, sparce code multiple access (SCMA). In contrast to our approach, in their specific problem several codewords were intentionally projected onto the same point in a given dimension. The aim was to reduce the complexity of the associated message-passing decoder. Therein, the authors recognize the high complexity of the problem, and restrict their codebooks to only two dimensions, and per-

mutations of no more than eight points. Also, in [96], no analyses or systematic procedures to produce good permutations are provided. Instead, the authors present exhaustive search results for their small case of study. Unlike the work of Bao et al., herein we provide an ensemble average analysis and propose two low-complexity algorithms tp obtain good permutations. The development is presented next.

Let us first focus on the labels ordering. For $d = 1,\ldots,M$, let $\pi_d : \{1,\ldots,N\} \to \{1,\ldots,N\}$ denote the permutation mapping of the labels $1,\ldots,N$ in dimension d. The point $i \in \{1,\ldots,N\}$ in the codebook, whose projection on the first dimension occupies the position i, is mapped by this mapping to the element $\pi_d[i] \in \{1,\ldots,N\}$, which represents the position occupied by the projection of the point i on dimension d. In the example of Fig. 21c, we have $\pi_2[1] = 3$. By convention, π_1 is the trivial permutation, i.e., $\pi_1[i] = i$ for all i.

Having defined the labels ordering in the grids, let us now describe the grids themselves. Let $\mathbf{u}_d$ denote the $1 \times N$ vector whose elements are the (ordered) real coordinates of the projections of the points in $\mathscr{C}$ on dimension d where, by convention, $\mathbf{u}_d[i] < \mathbf{u}_d[j]$ for $i < j$. In the example of Fig. 21c, we have $\mathbf{u}_d = [-3a, -a, a, 3a]$ for $d = 1$ and 2.

In the developments ahead, we also need to define the permuted version of the grids. Let $\mathbf{c}_d$ denote the $1 \times N$ vector whose i-th element corresponds to the coordinate of the projection of the point i in $\mathscr{C}$ on dimension d. In mathematical terms, we have $\mathbf{c}_d[i] = \mathbf{u}_d[\pi_d[i]]$. In our example of Fig. 21c, we have $\mathbf{c}_2[1] = a$. Based on this definition, the coordinates (projections) of the point i in all dimensions are the column vector $\mathbf{x}^{(i)} = [\mathbf{c}_1[i],\ldots,\mathbf{c}_M[i]]^T$.

In matrix notation, we have

$$\mathbf{c}_d = \mathbf{u}_d \mathbf{P}_d, \tag{4.1}$$

where $\mathbf{P}_d$ is the permutation matrix which arises from the permutation mapping π_d. Clearly, if we arrange all the points in $\mathscr{C}$ (as column

vectors) in a matrix, from point 1 to point N, we have the relation

$$\left[\mathbf{x}^{(1)},\ldots,\mathbf{x}^{(N)}\right] = \begin{bmatrix} \mathbf{c}_1[1] & \ldots & \mathbf{c}_1[N] \\ \vdots & & \vdots \\ \mathbf{c}_M[1] & \ldots & \mathbf{c}_M[N] \end{bmatrix} = \begin{bmatrix} \mathbf{c}_1 \\ \vdots \\ \mathbf{c}_M \end{bmatrix}, \tag{4.2}$$

which we call the *codebook matrix*.

In our proposed approach for fully-diverse codebook design, knowing the number of points, N, and the number of dimensions, M, we first set the grids $\mathbf{u}_d$ for $d = 1,\ldots,M$. The fact that each grid $\mathbf{u}_d$ is a set of N distinct coordinates suffices to guarantee full diversity. Therefore, the fully-diverse codebook design problem reduces to the one of finding the best permutation set $\Pi = \{\pi_2,\ldots,\pi_d,\ldots,\pi_M\}$, i.e., the one that minimizes the parameter Δ_M. In the example of Fig. 21c, among the $4! = 24$ distinct permutations π_2, only two yield the best performance (minimal Δ_2). One of them is shown in the figure.

In summary, the proposed fully-diverse codebook design can be described by the following steps:

1. Knowing N and M, pile the M dimensions, each of them containing a grid of N points (projections);

2. Without loss of generality, label the projections on the first dimensions as $1,2,\ldots,N$;

3. Search over all $(N!)^{M-1}$ possible permutation sets Π to find the one that minimizes Δ_M in (3.43);

4. Adopt the resulting codebook in the real communication system in (3.14).

It is important to mention that having the same grid on all dimensions (as opposed to having slightly different ones) is not a significant constraint. This allows us to find good codebooks. Furthermore, the structure enables some analyses of the ensemble which are useful. The grid can be chosen, for instance, as a set of uniformly spaced points or as having a Gaussian shape. We study both types of grid next.

4.3 DISTANCE SPECTRA AND ENSEMBLE AVERAGE PERFORMANCE

In this section, we derive closed-form expressions for the product distance spectrum, averaged out over all possible sets of permutations Π. These expressions follow from an enumeration of all possible distance events for all possible codebooks in the ensemble. With this, an ensemble average performance is obtained through the corresponding average value of Δ_M.

We begin with the analysis of the uniform grid, and then present the results for the Gaussian grid. As a first step, the Euclidean distance spectrum is derived. Then, a slight modification in this polynomial is introduced, yielding the desired (squared) product distance spectrum. Moreover, by evaluating this new polynomial at a particular value of X directly yields the parameter Δ_M, averaged out over all possible codebooks in the ensemble as we wish.

The distance spectrum of a codebook or an ensemble of codebooks with N points has the general form:

$$\overline{P}(X) = \sum_{\delta} \tau_{\delta} X^{\delta}, \tag{4.3}$$

where τ_{δ} is the average number of neighbors (multiplicity) at distance δ from a reference signal. Clearly, from the double sum in (3.41), we must have

$$\lim_{X \to 1} \overline{P}(X) = \sum_{\delta} \tau_{\delta} = N(N-1). \tag{4.4}$$

4.3.1 Uniform grid

In order to facilitate the enumerations, we consider initially the uniform grid illustrated in Fig. 22, which is presented without centralization and normalization. A proper adjustment is done at the end of

the analysis. The δ_d for all values of i is given as

$$\delta_d = \begin{cases} [1,1,2,2,\ldots,(i-1),(i-1),i, \\ (i+1),\ldots,(N-i)] & 1 \le i \le N/2 \\ [1,1,2,2,\ldots,(N-i),(N-i), \\ (N-i+1),(N-i+2),\ldots,(i-1)] & N/2+1 \le i \le N \end{cases} . \quad (4.5)$$

Figure 22 – The (unnormalized and uncentralized) uniform grid in the d-th dimension and the associated distances to neighbouring signal components when the reference signal component is at position i, $1 \le i \le N/2$.

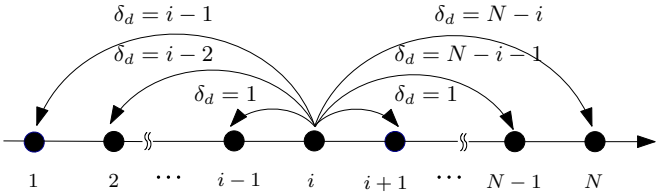

In our analysis, let ℓ denote the label of signal $\mathbf{x}^{(\ell)}$ and let i denote the position of its projection on each dimension d, where $\ell, i = 1,2,\ldots,N$ and $d = 1,\ldots,M$. From the previous section, in the first dimension the labels of the signals follow the trivial ordering, i.e., $i = \ell$. In the other dimensions, the labels can follow any ordering according to all possible permutations. Therefore, these two cases must be analyzed separately.

For $\ell = 1,\ldots,N$, let $\mathbf{x}^{(\ell)}$ be the reference signal, whose projection on the first dimension, as we know, occupies position ℓ. Then, we can obtain the distance enumerator polynomial for the first dimension based on the distances presented in Fig. 22 and according to (4.6), where we set $d = 1$ and $i = \ell$. This has to be counted only once for each reference signal, since by convention the labels ordering in the first dimension is fixed for all codebooks.

The distance enumeration polynomial associated with the first

dimension is then given as[1]

$$\begin{aligned} P_{\mathrm{l,u}} &= \sum_{i=1}^{N/2}\left[\sum_{j=1}^{i-1}2X^j+\sum_{j=i}^{N-i}X^j\right]+\sum_{i=N/2+1}^{N}\left[\sum_{j=1}^{N-i}2X^j+\sum_{v=N-i+1}^{i-1}X^j\right] \\ &= \frac{2X(X^N-NX+N-1)}{(X-1)^2}. \end{aligned} \tag{4.6}$$

For the other dimensions, the signals taken as the reference signal, $\mathbf{x}$, and the concurrent signal, $\mathbf{x}'$, are themselves irrelevant for the distance enumeration. The only thing that counts in this regard are the positions of their projections on dimension d, for $d=2,\ldots,M$. Therefore, in order to account for the enumeration over all possible codebooks, it suffices to have the projection of the reference signal occupy any of the N positions i in the grid and, for each one of them, the projection of the concurrent signal occupy any of the other $N-1$ positions in the grid.

Interestingly, this symmetrizes the enumeration problem in such a way that the distance enumeration polynomial associated with the d-th dimension, for $d=2,\ldots,M$, is also given by (4.6). That is to say

$$P_{d,\mathrm{u}}(X)=P_{\mathrm{l,u}}(X),\ \text{ for } d=1,\ldots,M. \tag{4.7}$$

It should be observed that the factor $N(N-1)$ coming from the double sum in (3.41) has be included in the enumerations of all the M dimensions. To have the proper average, yielding the condition in (4.4), a normalization factor is required. From equations (4.6) and (4.7), the Euclidean distance spectrum is given by

$$\overline{P}_{\mathrm{E,u}}(X) = \frac{1}{[N(N-1)]^{M-1}}P_{\mathrm{l,u}}(X)P_{d,\mathrm{u}}(X)^{M-1} \tag{4.8}$$

$$= \frac{1}{[N(N-1)]^{M-1}}\left(\frac{2X(X^N-NX+N-1)}{(X-1)^2}\right)^M \tag{4.9}$$

$$= \frac{1}{[N(N-1)]^{M-1}}\left(\sum_{i=1}^{N-1}2(N-i)X^i\right)^M. \tag{4.10}$$

[1] In (4.6), we have replaced the exponent j^2 of X for the squared Euclidean distance by j in order to have the closed-form expression in (4.6). We consider the squared distance later on when we present the desired (squared) product distance spectrum.

Indeed, we have

$$\lim_{X\to 1} \overline{P}_{\mathrm{E,u}}(X) = N(N-1). \tag{4.11}$$

However, in this subsection we are interested in the (squared) product distance spectrum and, more specifically, in the parameter Δ_M, for the centralized and normalized N-PAM grid.

We observe that, in the enumeration for obtaining the Euclidean distance spectrum, we have used the basic exponent rule:

$$\tau X^{\delta_1} X^{\delta_2} = \tau X^{\delta_1+\delta_2}. \tag{4.12}$$

To substitute the addition (without squaring) with a squared product, we only need the following modification:

$$\tau X^{2\log(\delta_1)} X^{2\log(\delta_2)} = \tau X^{\log(\delta_1^2\delta_2^2)}. \tag{4.13}$$

With this modification applied to $\overline{P}_{\mathrm{E,u}}(X)$ in (4.10), the (squared) product distance spectrum for the uniform grid is presented as

$$\overline{P}_{\mathrm{P,u}}(X) = \frac{1}{[N(N-1)]^{M-1}} \left(\sum_{i=1}^{N-1} 2(N-i) X^{2\log(qi)} \right)^M, \tag{4.14}$$

where the scaling factor q has been introduced to account for centralization and normalization of the uniform grid, and is given by $q = \sqrt{\frac{12}{N^2-1}}$.

Finally, note that evaluating (4.13) at $X = e^{-1}$ yields

$$\tau X^{\log(\delta_1^2\delta_2^2)}\Big|_{X=e^{-1}} = \frac{\tau}{\delta_1^2\delta_2^2}. \tag{4.15}$$

Correspondingly, the parameter Δ_M required in the expression for the error probability bound in (3.43), averaged out over all codebooks in the ensemble, can be obtained as

$$\overline{\Delta}_{M,\mathrm{u}} = \overline{P}_{\mathrm{P,u}}(X)\big|_{X=e^{-1}}. \tag{4.16}$$

As a technical issue, it is important to say that, although (4.14) does not simplify nicely as in (4.9) and, in fact, its expanded version for large N and M is hard to obtain even with powerful mathematical softwares, the evaluation of Δ_M, as given in (4.16), can be obtained in no time.

***Example* 1** *Consider the ensemble of codebooks obtained from the situation presented in Fig. 21, where we have $N = 4$ points in $M = 2$ real dimensions. The distance spectrum in (4.14) for this case can be written as:*

$$\overline{P}_{P,u}(X) = \frac{1}{12} X^{2\log(4/5)} \left(6 + 4X^{2\log(2)} + 2X^{2\log(3)}\right)^2, \tag{4.17}$$

from which the parameter $\overline{\Delta}_{M,u}$ obtained from (4.16) is 6.7917. For comparison, the best codebook in this ensemble (i.e., the one presented in Fig. 21c) has $\Delta_M = 3.8194$.

4.3.2 Gaussian grid

The Gaussian grid considered in this work is a set of N centralized points whose distribution follow a Gaussian shape specified by two parameters, namely, the standard deviation of the Gaussian pulse, σ, and the tail truncation point, κ. These parameters can be optimized to reduce Δ_M. In order to obtain this grid, consider the area under the Gaussian-like pulse as

$$A = ((N-1))^{-1} \int_{-\kappa}^{+\kappa} \exp\left(\frac{-x^2}{2\sigma^2}\right) dx. \tag{4.18}$$

The first (left most) point in the grid is $\mathbf{u}_1[1] = -\kappa$. Then, for $\ell = 2,\ldots,N$, the ℓ-th point in the grid is obtained by solving for $\mathbf{u}_1[\ell]$ the following recursive equation:

$$A = \int_{\mathbf{u}_1[\ell-1]}^{\mathbf{u}_1[\ell]} \exp\left(\frac{-x^2}{2\sigma^2}\right) dx. \tag{4.19}$$

Clearly, we have $\mathbf{u}_1[N] = +\kappa$ and

$$\sum_{\ell=2}^{N} \int_{\mathbf{u}_1[\ell-1]}^{\mathbf{u}_1[\ell]} \exp\left(\frac{-x^2}{2\sigma^2}\right) dx = (N-1)A. \tag{4.20}$$

After obtaining the grid points, $\mathbf{u}_1[\ell]$, for $\ell = 1,\ldots,N$, a proper normalization of these points can be realized (e.g., to yield unitary average point energy).

The Gaussian shape grants a denser cloud of points close to the center of the grid, yielding a shaping gain [91].

Since the points in the Gaussian grid are not integers, its (squared) product distance spectrum can only be obtained as

$$\overline{P}_{\mathrm{P,G}}(X) = \frac{1}{[N(N-1)]^{M-1}} \left(\sum_{i=1}^{N} \sum_{\substack{j=1, \\ i \neq j}}^{N} X^{2\log(|\mathbf{u}_1[i]-\mathbf{u}_1[j]|)} \right)^{M}, \qquad (4.21)$$

which has no closed form. Nevertheless, the parameter Δ_M for the Gaussian grid, averaged out over all codebooks in the ensemble, can still be easily obtained as

$$\overline{\Delta}_{M,\mathrm{G}} = \overline{P}_{\mathrm{P,G}}(X)\big|_{X=e^{-1}}. \qquad (4.22)$$

Example 2 *Consider the normalized Gaussian grid with $N = 4$ points and the somewhat optimized parameters $\sigma = 3.5$ and $\kappa = 1.1$ (as explained above):*

$$\mathbf{u}_1 = [-1.3482, -0.4271, 0.4271, 1.3482].$$

The ensemble of codebooks of $M = 2$ real dimensions obtained with this grid has $\overline{\Delta}_{M,G} = 6.74981$, as obtained in (4.22). For comparison, the codebook obtained from the best permutation (the same one as for the uniform grid case), given by $\pi_2[1] = 3$, $\pi_2[2] = 1$, $\pi_2[3] = 4$, and $\pi_2[4] = 2$, has $\Delta_M = 3.746$. Note that, as expected, there is an improvement in these parameters as compared to the respective ones in Example 1, due to the shaping gain.

Remark 1: It should be noted that the best codebooks have much better performance than the average performance. We elaborate on that in the next section.

Remark 2: Small values of N and M have been considered in this section for easy of presentation and for reproducibility purposes. From now on, we focus on two scenarios which are more likely to be used in practical systems: 1) $N = 256$ and $M = 8$ and 2) $N = 256$, $M = 4$.Both the uniform and the Gaussian grids are considered. The paramenters σ and κ of the Gaussian grid were not optimized.

4.4 SEARCH APPROACHES FOR FINDING GOOD PERMUTATIONS SETS

From Section 4.2, the number of distinct codebooks in the ensemble is $(N!)^{M-1}$, which corresponds to the number of permutations sets $\boldsymbol{\Pi}$. It means that the exhaustive search for the best codebook in the ensemble (i.e., the one that minimizes Δ_M) is not practical, except for very small values of N and M (see the examples above). To circumvent this combinatorial problem, in this section we discuss the random search and then propose two approaches for finding a good permutations set $\boldsymbol{\Pi}$ with reduced or essentially no complexity, for any number of points N.

4.4.1 Random permutations search

Selecting permutations sets randomly renders the parameter Δ_M a random variable. In Fig. 23, we present the empirical cumulative distribution function (CDF) of Δ_M based on 10^5 random permutations sets or codebooks from the ensemble formed by the Gaussian grid with $N = 256$ and $M = 8$.

As can be seen, typically the random codebooks have a Δ_M varying from 10^{14} to 10^{17}, while the ensemble average, $\Delta_{M,\mathrm{G}}$, shown in the figure, is of the order of 10^{19}. The fact that the average performance is quite far from the typical performance is because a fraction of the codebooks performs extremely poor, as for instance the codebook obtained from the trivial permutations set (i.e., the same labels ordering in all dimensions), whose Δ_M is 7.66×10^{32}.

Although we have used a negligible number of samples to obtain the empirical CDF of Fig. 23, namely, 10^5 from a total of $(256!)^7 \approx 10^{3548}$ samples, we can see that not much effort is needed in order to find a codebook whose performance is significantly better than the average performance. Note in Fig. 23 that just a few random samples suffice to obtain Δ_M of the order of 10^{14}. On the other hand, not even 10^5 attempts are enough to reduce Δ_M below 10^{13} (see the best sample in Fig. 23), when we know that Δ_M of the order of 10^9 is reachable (see

the black square in the figure).

Figure 23 – Cumulative distribution function of Δ_M based on 10^5 randomly chosen codebooks from the Gaussian grid based ensemble with $N = 256$ and $M = 8$.

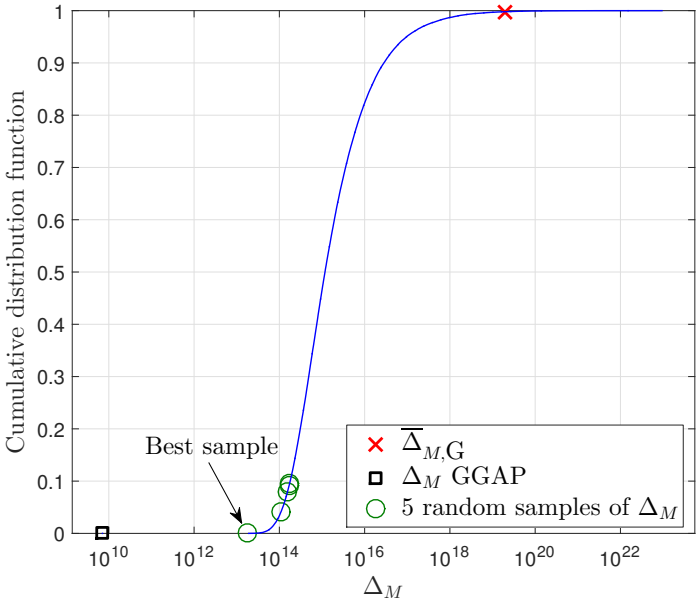

Some additional figures corroborate these findings. The number of good permutations within the set of $(N!)^{M-1}$ possible permutations is very small. For instance, for $N = 4$ and $M = 2$, there are $N! = 24$ possible permutations only two among which are good. For $N = 8$ and $M = 3$, among 40320 possible permutations, only 1695 are considered good for the second dimension, while after choosing one of them, the number of good permutations for the third dimension is further reduced. The fraction of good codes tend to become more and more negligible as N and M grow.

In summary, finding a very good codebook is a needle-in-a-haystack problem, and therefore any clever, low complexity method to accomplish this goal is of greatest interest. In the next subsections, we believe we take a step in this direction.

4.4.2 Permutations based on P-interleavers

In this section, we propose a codebook design based on the construction of a set of permutation mappings allowing a large overall product distance. In the context of turbo-codes, different interleaver constructions have been proposed to avoid short cycles in the associated Tanner graph. Among those constructions, we can cite the so-called S-random interleaver [97] and the L-random interleaver [98], [99] that maximize the minimum primary cycle, $\min_{i,j,i\neq j} |i-j| + |\pi[i] - \pi[j]|$.

Following the same strategy, we propose the P-random interleaver maximizing the minimum product distance of a 2-dimensional codebook defined as

$$\min_{i,j,i\neq j} \left|\mathbf{u}_1[i] - \mathbf{u}_1[j]\right| \cdot \left|\mathbf{u}_2[\pi_2[i]] - \mathbf{u}_2[\pi_2[j]]\right|. \tag{4.23}$$

The algorithm for the construction of a P-random interleaver is given in Algorithm 1, where the *test 1* in step 6 is defined as

$$\left|\mathbf{u}_1[i] - \mathbf{u}_1[j]\right| \cdot \left|\mathbf{u}_2[\pi_2[i]] - \mathbf{u}_2[\pi_2[j]]\right| \geq p_2, \qquad \forall j < i. \tag{4.24}$$

The proposed interleaver construction can be extended to construct successively the set of $M-1$ permutation mappings for a M-dimensional codebook. In that case, the d-th permutation ($2 \leq d \leq M$) will be obtained using the same algorithm by simply replacing the test 1 by the test d defined as

$$\left|\mathbf{u}_1[i] - \mathbf{u}_1[j]\right| \prod_{l=2}^{d} \left|\mathbf{u}_l[\pi_l[i]] - \mathbf{u}_l[\pi_l[j]]\right| \geq p_d, \qquad \forall j < i. \tag{4.25}$$

The values $p_2, p_3, \ldots, p_d$ must be adjusted in order to achieve a solution.

The proposed codebook, which follows this solution, is referred as Gaussian Grid with P-Interleavers (GGPI). Considering the second case of study, where $M = 4$ and $N = 256$, the individual projections of the GGPI are presented in Figure 24a. Note that in the first dimension, where the projections follows the trivial order, the colors range from dark blue to yellow. As we adopt the same grid for all dimensions,

Algorithm 1 P-random interleaver algorithm

1: **procedure** P-INTERLEAVER($N, \{\pi_2, \ldots, \pi_{d-1}\}$)
2: $i = 1$
3: $\mathscr{E} = \{1, 2, \ldots, N\}$
4: $\mathscr{A} = \mathscr{E}$
5: pick randomly $\pi_d[i]$ in $\mathscr{A}$
6: **if** test 1 is satisfied **then**
7: $\mathscr{E} = \mathscr{E} \setminus \pi_d[i]$
8: $i = i + 1$
9: **if** $\mathscr{E} = \varnothing$ **then**
10: construction succeeded
11: **else**
12: **goto** step 4
13: **end if**
14: **else**
15: $\mathscr{A} = \mathscr{A} \setminus \pi_d[i]$
16: **if** $\mathscr{A} = \varnothing$ **then**
17: construction failed
18: **else**
19: **goto** step 5
20: **end if**
21: **end if**
22: **return** π_d ▷ The d-th interleaver is π_d
23: **end procedure**

we can see different mixtures of the colored dots in the other three dimensions as result of the P-interleavers. Figure 24b presents the projections of the two complex dimensions gathered together in a single complex plot.

Figure 24 – Projections of the proposed GGPI constellation, for $M = 4$ and $N = 256$.

(a) Projections on each real dimension.

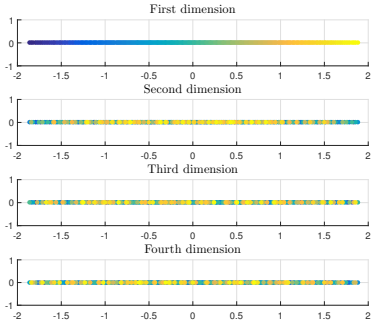

(b) Projections of the two complex dimensions in a single complex plot.

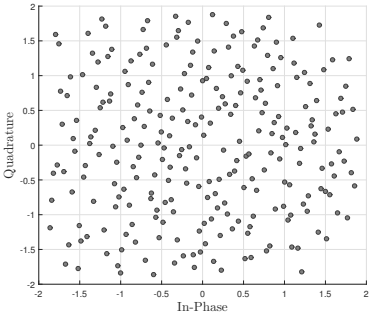

4.4.3 Algebraic permutations constructions

In this section, we propose an algebraic construction to design good permutations sets $\mathbf{\Pi}$. The main idea is to select the next permutation $\boldsymbol{\pi}_{d+1}$ in such a way that whenever the projections of two codebook points on the current dimension are neighbors, the projections of the same points on the next dimension are chosen to be further apart. The algebraic permutations can be associated to the uniform grid or the Gaussian grid, and a good permutation set tends to yield good performance in both cases. The algorithm for the algebraic construction is presented in Algorithm 2.

In step 4, in order to obtain the minimum Δ_M, the shift parameter s must be taken from a set $\mathscr{S}$ of "magic" numbers[2], which can be

[2] Certainly, the good performance obtained with these shift parameters could be explained by a number-theoretic analysis. However, this is beyond the realm of the present work.

Algorithm 2 Algebraic permutations algorithm

procedure ALGEBRAIC PERMUTATIONS($N, s \in \mathscr{S}, M$)
  for $i = 1, \ldots, N$ **do**
    $\pi_1[i] = i$
    $\pi_2[i] = [s\,i \pmod N] + 1$
    if $\pi_2[i] = \pi_2[i']$ for some $i' < i$ **then**
      $\pi_2[i] = \pi_2[i] + \left\lceil \frac{i}{s} \right\rceil$
    end if
  end for
  for $d = 3, ..., M$ **do**
    for $i = 1, \ldots, N$ **do**
      $\pi_d[i] = \pi_{d-1}[\pi_2[i]]$
    end for
  end for
  return Π ▷ The set of permutations is Π
end procedure

obtained experimentally using a uniform grid. Since the search space for determining the good shift sets $\mathscr{S}$ is the range $2 \leq s \leq N-1$, the complexity of this search, as well the complexity of the algorithm as a whole is linear in N. This can be considered a negligible complexity compared with the exponential-of-a-factorial growth of the ensemble. More important, the performance achieved with this permutations set is considerably better than the typical (random) performance, as we show next.

We have constructed algebraic permutation sets and provided the "magic" numbers for several values of N and M. The permutations themselves are not listed as they can be easily obtained by running Algorithm 2. The best shifts based on the uniform grid are listed in Table 8. The codebooks obtained in this chapter based on the algebraic permutations applied to the uniform (resp., Gaussian) grid are referred to as UGAP (resp. GGAP), which stands for Uniform (resp., Gaussian) Grid with Algebraic Permutations.

Table 8 – Set $\mathscr{S}$ with the best shifts for the uniform grid and different values of M and N.

M	$N = 2^M$	$\mathscr{S}$	$N \neq 2^M$	$\mathscr{S}$
2	4	$\{2\}$	3	$\{2\}$
3	8	$\{4,6\}$	6	$\{3,4\}$
4	16	$\{3,11\}$	256	$\{74\}$
5	32	$\{26\}$	45	$\{21\}$
6	64	$\{25,41\}$	83	$\{54\}$
7	128	$\{75,99\}$	35	$\{30\}$
8	256	$\{117,221\}$	80	$\{66\}$
9	512	$\{35,395\}$	250	$\{13\}$
10	1024	$\{43,643\}$	415	$\{121\}$

For $N = 256$ and $M = 8$, and considering the Gaussian grid, we have found a GGAP with $\Delta_M = 7.11 \times 10^9$, which will be detailed in Section 4.6. This result is shown in Fig. 23. From the CDF, we can see that the probability of obtaining this same Δ_M from a random permutations set is nearly zero.

Figure 25 – Projections of the proposed GGAP constellation, for $M = 8$ and $N = 256$.

(a) Projections on each real dimension.

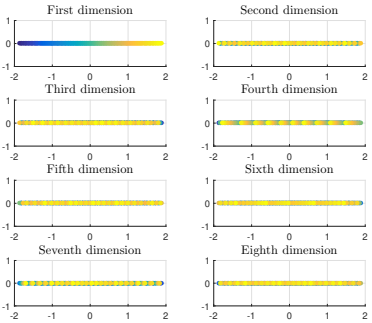

(b) Projections of the two complex dimensions in a single complex plot.

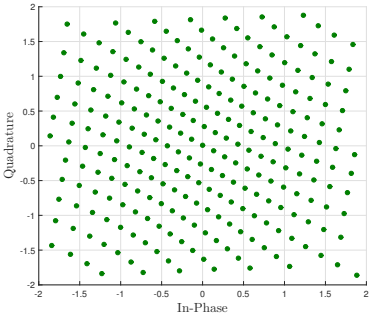

For the two cases of study of the previous chapter, four constellations based on algebraic permutations were designed, two for each grid (uniform and Gaussian). The 8-dimensional GGAP and UGAP are

shown in Figures 25 and 26, respectively, for $E_s = 2$. The individual projections of each constellation, Figures 25a and 26a, follows the same behavior of the GGPI. In the first dimension we can see the ordered projections in a color scale and in the other dimensions they appear in different patterns of colored dots.

Figure 26 – Projections of the proposed UGAP constellation, for $M = 8$ and $N = 256$.

(a) Projections on each real dimension.

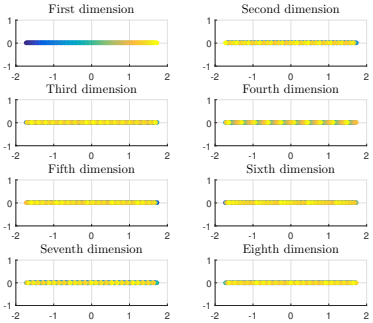

(b) Projections of the two complex dimensions in a single complex plot.

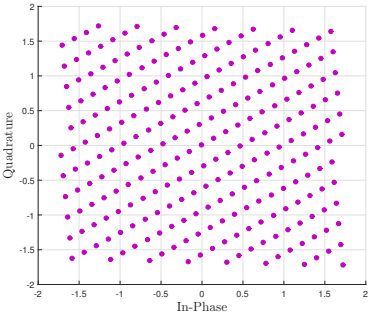

The 4-dimensional GGAP and UGAP are presented, respectively, in Figures 27 and 28. Note that for this case of study, GGAP and GGPI (Figure 24) have the same grid, with only different permutations, which is sufficient to change significantly the shape of the constellation in a single plot (compare Figures 27b and 24b) and its parameters, as will be seen in Section 4.6. Another curious fact is that, unlike the constellations based on rotation and GLCP, whose projections in a single plot have a more circular shape, the GGAP and UGAP constellations have a square shape with diagonal lines, as can be seen in Figures 25b, 26b, 27b and 28b.

4.5 COMPLEXITY AND STORAGE ISSUES

In the first proposed approach for designing fully-diverse codebooks, the $M/2$-fold Cartesian product of a conventional QAM constel-

Figure 27 – Projections of the proposed GGAP constellation, for $M = 4$ and $N = 256$.

(a) Projections on each real dimension.

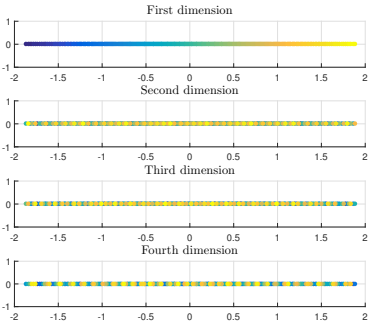

(b) Projections of the two complex dimensions in a single complex plot.

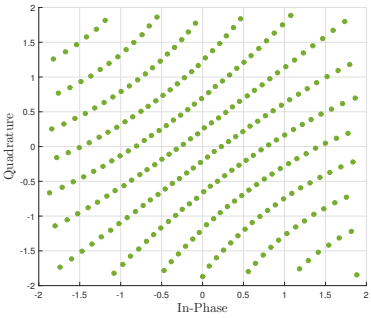

Figure 28 – Projection of the proposed UGAP constellation, for $M = 4$ and $N = 256$.

(a) Projections on each real dimension.

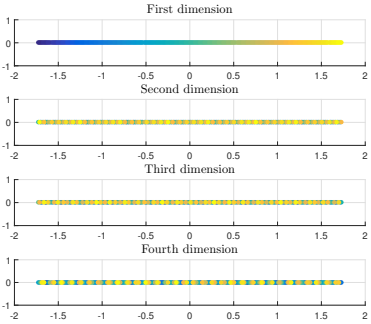

(b) Projections of the two complex dimensions in a single complex plot.

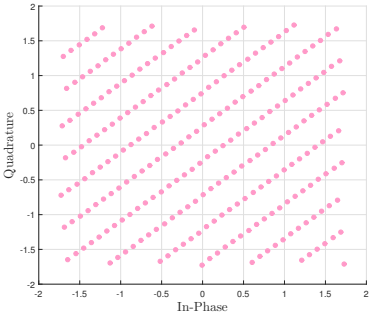

lation (possibly with some zero symbols in the case of SIM) or a set of points carved from a M-dimensional real lattice (according to the Chapter 3) is first prepared, and then a proper rotation and GLCP are applied. Usually, the same 2-dimensional rotation applied to each complex dimension suffices for a good result, and the complexity of finding the optimal or close to optimal rotation is not high (a few hundred trials are enough).

On the other hand, the good results of the lattice-based codebooks in the previous sections rely on the existence of a good M-dimensional real lattice, which may not be the case for general M. Thus, obtaining a good set of points following the proposed approach in Chapter 3 may not always be easy.

Designing the GLCP matrix is not a simple task either. These precoding matrices have been tabulated in [20, Table I]) for $M \leq 16$. For larger values of M, some matrix optimization following some restrictions is required, and in some cases the resulting precoding matrix may be non-unitary [45].

In any case, if say $\check{\mathbf{x}}$ in (3.1) is the original $M \times N$ codebook matrix, whose corresponding codebook is not fully-diverse, the fully-diverse codebook $\mathring{\mathbf{x}} = [\mathring{\mathbf{x}}_1^T, \mathring{\mathbf{x}}_2^T, \ldots \mathring{\mathbf{x}}_G^T]$ is obtained according to (3.64), where $\mathbf{\Phi}$ and $\mathbf{\Theta}$ are the rotation and the GLCP matrices, respectively, and $\check{\mathbf{x}}_g$ is the codeword. In this way, the matrices $\check{\mathbf{x}}$, $\mathbf{\Phi}$, and $\mathbf{\Theta}$ must be stored and the aforementioned matrix multiplications need to be done both at the transmitter and the receiver, which yields a large complexity.

Alternatively, the matrix $\mathring{\mathbf{x}}$ can be precomputed offline, and then stored at the transmitter and the receiver. This reduces both the complexity and the storage requirements. Note that $\mathring{\mathbf{x}}$ consists of NM real numbers.

In the approach proposed of this chapter, designing the fully-diverse codebook amounts first to preparing a grid of N real points, which is a trivial task, and then designing offline the good permutations set $\mathbf{\Pi}$, a procedure whose complexity is negligible if the algebraic construction is adopted. Moreover, we only need to store a grid consisting of N real numbers and $M-1$ permutations of the elements $1, 2, \ldots, N$. Each such permutation can be stored in the form of a vector with N integer elements. In summary, N real numbers and $N(M-1)$ integers must be stored at the transmitter and the receiver.

Therefore, for large N or M, the proposed approach in this chapter for designing a good fully-diverse codebook is clearly less complex and requires less storage than its predecessors.

4.6 NUMERICAL RESULTS

To compare the codebooks obtained with the methodology presented in this chapter with the codebooks proposed in Chapter 3, we adopt the same scenarios of Section 3.6.

The proposed 8-dimensional fully-diverse codebooks are listed in Table 9. As can be seen the GGAP presents a smaller Δ_M than the UGAP. The Gaussian grid was obtained with the parameters $\sigma = 5$, $\kappa = 2.5$ and $s = 139$. In some cases, the shift found for the uniform grid (see Table 8) is not the best one for the Gaussian grid. In these cases, the search of the best shift must be specific to the Gaussian grid. Comparing GGAP and UGAP with the fully-diverse codebooks in Table 4, the rotated GLCP-$\mathscr{C}_{E_8}$ presents the best Δ_M.

Table 9 – Codebooks parameters of the schemes based on the combinatorial approach with $M = D = 8$ and $N = 256$.

Schemes	Δ_M
GGAP	7.11×10^9
UGAP	8.06×10^9

For the second scenario, the proposed 4-dimensional fully-diverse codebooks are presented in Table 10. Once again, the GGAP has the smallest Δ_M compared with UGAP and GGPI. However, compared with the fully-diverse codebooks in Table 5, the rotated GLCP-$\mathscr{C}_{D_4}$ and rotated GLCP are better. The Gaussian grid for this case was obtained with the paramenters $\sigma = 1.07$ and $\kappa = 1.65$. The shift s used for both grids is given in Table 8.

4.7 ON THE BIT ERROR RATE

As mentioned in Section 3.7, the most important optimization criteria can change at low SNR and in terms of BEP. Therefore, in the next section the schemes based on the combinatorial approach will be analyzed for this scenario. The BEP upper bound and the BSA

Table 10 – Codebooks parameters of the schemes based on the combinatorial approach with $M = D = 4$ and $N = 256$.

Schemes	Δ_M
GGAP	1.42×10^8
UGAP	1.56×10^8
GGPI	1.97×10^8

solution, presented in Sections 3.7 and 3.7.1, respectively, are adopted here.

In Table 11, the proposed 8-dimensional codebooks are compared in terms of the total cost in (3.68) and the minimum squared Euclidean distance. As can be seen, UGAP presents a smaller CF than the GGAP after the BSA optimization. However, the obtained values are worse than the values of the rotated and precoded schemes in Table 6.

Table 11 – Comparison of the total cost function (CF) of the 8-dimensional schemes based on the combinatorial approach, for $N = 256$.

Scheme	d_E^2	Total cost function (CF)		
		Initial labeling[a]	Optimized labeling	
			Gray	BSA
UGAP	2.88	9.73	–	8.96
GGAP	2.88	9.80	–	9.02

[a] Random labeling.

The distance spectrum and the average number of bit errors, both versus δ_E^2, of the proposed schemes are presented in Figure 29 and 30, respectively. Similar to the schemes in Figure 18, the δ_E^2 were discretized. Although the distance spectrum of the proposed schemes present a small number of neighbors for the first distances δ_E^2, the average number of bit errors for these distances are greater than they should be, which results in a larger CF.

The distance spectrum and the average number of bit errors, both versus δ_E^2, of the proposed schemes are presented in Figure 29 and 30, respectively. Similar to the schemes in Figure 18, the δ_E^2 were discretized. Although the distance spectrum of the proposed schemes present a small number of neighbors for the first distances δ_E^2, the average number of bit errors for these distances are greater than they should be, which results in a larger CF.

Figure 29 – Distance spectra of the 8-dimensional schemes based on the combinatorial approach, for $N = 256$.

(a) UGAP. (b) GGAP.

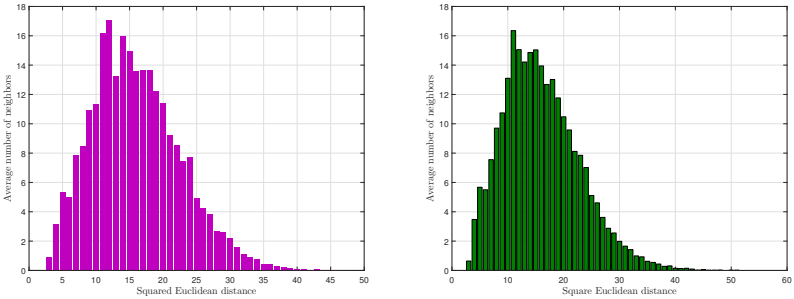

Figure 30 – Average number of bit errors versus δ_E^2 for 8-dimensional schemes based on the combinatorial approach, for $N = 256$.

(a) UGAP. (b) GGAP.

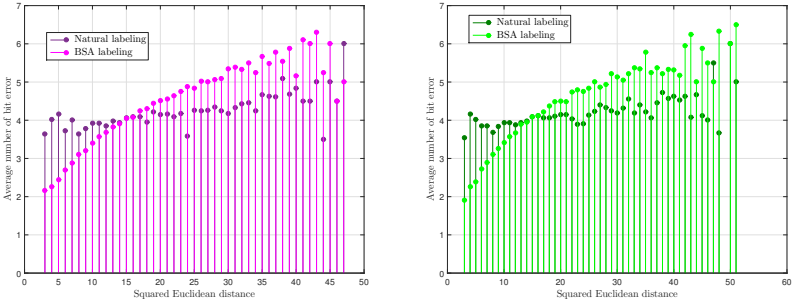

For the second case of study, the proposed 4-dimensional code-

books are listed in Table 12. As can be seen, the GGPI presents the smallest CF compared to the UGAP and GGAP. However, compared with the schemes in Table 7, they are only better than the rotated GLCP-GIM. The minimum squared Euclidean distances of the schemes in Table 11 and 12 are also the worst compared with the schemes in the previous chapter, but as this criterion is not important for the channel adopted, it was not optimized.

Table 12 – Comparison of the total cost function (CF) of the 4-dimensional schemes based on the combinatorial approach, for $N = 256$.

Scheme	d_E^2	Total cost function (CF)		
		Initial labeling[a]	Optimized labeling	
			Gray	BSA
GGPI	0.2	26.07	–	22.67
UGAP	0.3	27.24	–	23.05
GGAP	0.5	27.25	–	23.15

[a] Random labeling.

The distance spectrum of the proposed 4-dimensional schemes are illustrated in Figures 31. As can be seen, they present a similar behavior as the previous case. An interesting fact is that, the schemes GGPI and GGAP have exactly the same grid, they only differ in terms of permutations, but the distance spectrum are different. This means that the permutations plays an important role for the schemes' performance. As the labeling problem and, consequently, the distance spectrum were investigated after all optimization process, these criteria were not optimized. It means that the performance of these proposed schemes can be further improved by some optimization.

Some attempts with different initial labeling were made to found the BSA labeling, and the best labelings found are shown in Figure 32. One of the attempts was to pass as initialization to the BSA a labeling that ensured that the label of each constellation point differed from

Figure 31 – Distance spectra of the 4-dimensional schemes based on the combinatorial approach, for $N = 256$.

(a) UGAP.

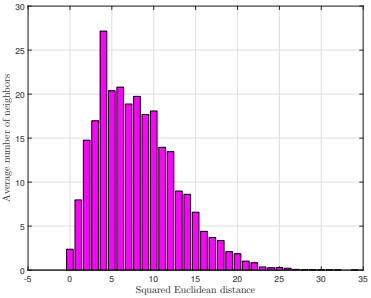

(b) GGAP.

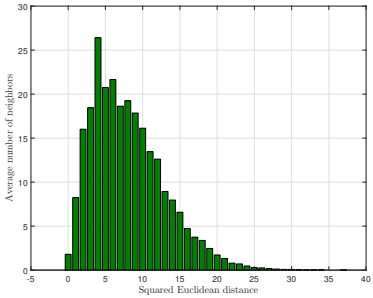

(c) GGPI.

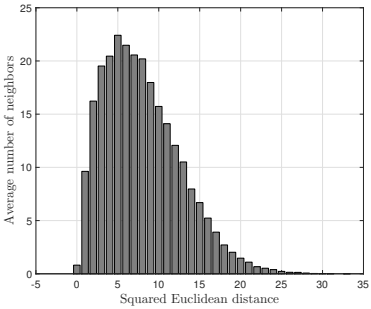

the ones of the nearest neighbors (the two smallest δ_E^2) by only one bit. However, the labeling found by the algorithm was not so good, which led us to believe that this optimization process is more complex than previously thought, and left as future work.

4.8 CHAPTER CONCLUSIONS

In this chapter, a totally different methodology to design fully-diverse multidimensional constellations has been presented. Two algorithms for finding good permutations were proposed. A comparison between the proposed solution and the approach that chooses a random permutations set is made and it becomes evident how difficult it

Figure 32 – Average number of bit errors versus δ_E^2 for 4-dimensional schemes based on the combinatorial approach, for $N = 256$.

(a) UGAP.

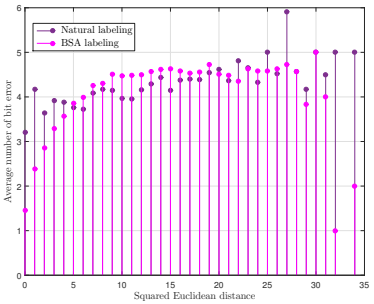

(b) GGAP.

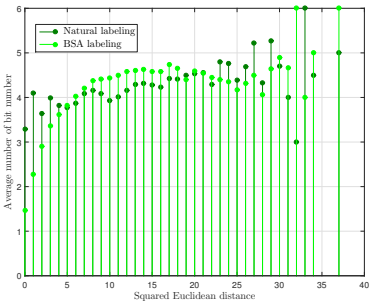

(c) GGPI.

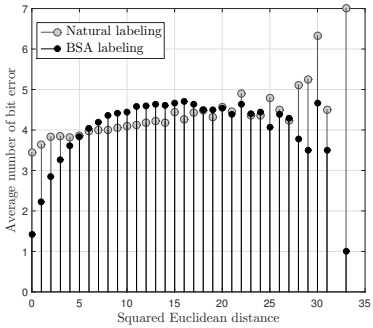

is to design a good fully-diverse codebook. As in the previous chapter, some 8-dimensional and 4-dimensional codebooks were proposed. Although the paramenters obtained are not the best of this work, this methodology presents interesting features: simplicity, generality and fully flexible design, in addition to complexity and storage benefits.

5 NUMERICAL RESULTS

5.1 INTRODUCTION

In this chapter, the performance of the benchmarks and of the constellations proposed in Chapters 3 and 4 are evaluated. More specifically, the constellation point error rate and the bit error rate, respectively, versus SNR are presented. As a way to measure the quality of labeling, we use the ratio between CER and BER. The performance results are compared to the analytical upper bounds obtained in this dissertation.

5.2 SIMULATION PARAMETERS

In the Monte Carlo simulations, we consider an OFDM system with bandwidth $B = 20$ MHz. Each OFDM symbol has $N_s = 256$ subcarriers and the adopted Rayleigh channel is the extended vehicular A (EVA) channel model [100] with Doppler spread of 5 Hz. In [100], 9 taps are considered in the channel impulse response. Herein, we adopt $L = M$ taps, so that maximum diversity can always be achieved. Proper interleaving at the real component level is performed to break channel correlation, as described in Section 3.3. Maximum likelihood detection is considered in the receptor.

Simulations results are presented, for different codebooks and settings, under the condition of same average energy per real M-dimensional point, $E_c = ME_s/2$, where E_s is the standard average energy per complex symbol.

5.3 FIRST CASE OF STUDY

In this case, it is considered for all schemes that the N_s subcarriers are divided into $G = 64$ groups with $n = 4$ subcarriers each. Each group carries $m = 8$ bits, which leads us to compare codebooks with $N = 2^8 = 256$ constellation points with $M = 2n = 8$ real dimensions. All schemes have the same rate $R = 512$ bits per OFDM the symbol.

The codebooks with $M = 8$ and $N = 256$ were designed in Sections 3.5 and 4.4.3. As the benchmark schemes, we adopte conventional OFDM, ISIM [15], and GLCP [20].

5.3.1 Performance comparison in terms of CER

Besides the Monte Carlo simulations results for the constellation point error rate (CER), the analytical performance in terms of the CER upper bound (UB) in (3.43), with the corresponding values of Δ_M, is also presented. Although the analytical upper bounds are not tight for low and medium SNRs, they give a good error performance indication in the high-SNR regime as the analytical performance curves of the different schemes preserve the same ordering as the one of the corresponding simulated curves.

Figure 33 – Constellation point error rates (simulated and theoretical UBs) of the benchmark codebooks, OFDM and ISIM [15], the proposed $\mathscr{C}_{E_8}$ and their rotated versions, for $D = 1$ and $D = 2$, $M = 8$ and $N = 256$.

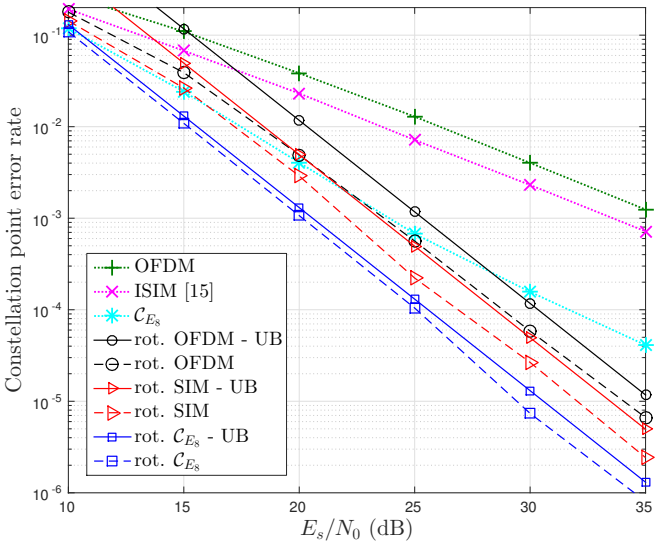

In Figure 33, the proposed codebooks and the ones in the literature are compared (see Table 4), all with modulation diversities $D = 1$ (without rotation) and $D = 2$ (with rotation). For the two cases, the proposed codebook $\mathscr{C}_{E_8}$ presents a significant SNR gain over the other schemes. It can also be seen that simulated points and upper bounds are coherent.

Figure 34 – Constellation point error rates (simulated and theoretical UBs) of the benchmark codebook GLCP [20] and the proposed GLCP-SIM and GLCP-$\mathscr{C}_{E_8}$, for $D = 4$, $M = 8$ and $N = 256$.

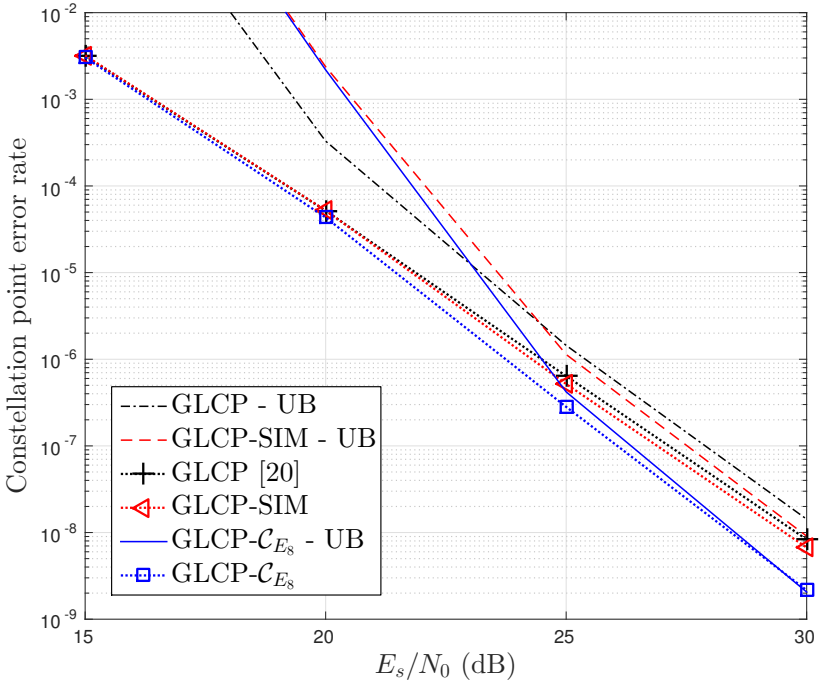

The precoded schemes are presented in Figure 34. It can be seen that GLCP reduces the performance advantage of SIM-based codebooks over QAM-based codebooks. The proposed GLCP-SIM outperforms the bechmark scheme GLCP [20] by only 0.2 dB for an error

probability of 10^{-6}. Comparing with the other SIM-based codebooks in Figure 33, GLCP-SIM presents a significant gain. For a SNR of 20 dB, for example, the error probability for GLCP-SIM is of the order of 10^{-5} while for the codebooks rot. SIM and ISIM [15] the error probabilities are of the order of 10^{-3} and 10^{-2}, respectively. However, the best performance is still achieved by the lattice-based codebook, where the GLCP-$\mathscr{C}_{E_8}$ presents a gain of 0.55 dB over GLCP-SIM.

Figure 35 – Constellation point error rates (simulated and theoretical upper bounds) of the proposed fully-diverse codebooks for $M = 8$ and $N = 256$.

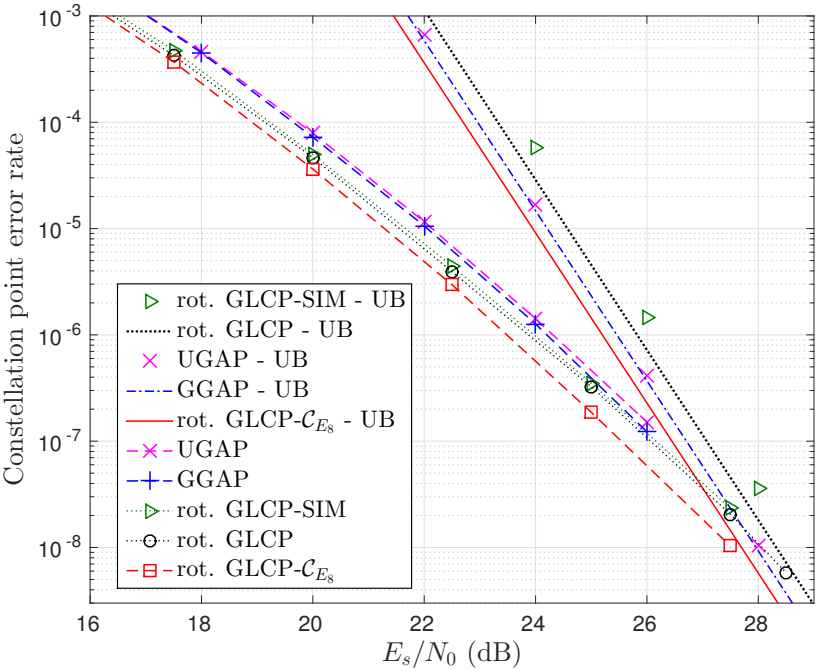

In Figure 35, all fully-diverse proposed codebooks are compared (see Tables 4 and 9). The proposed scheme rot. GLCP-$\mathscr{C}_{E_8}$ outperforms all the other codebooks in this scenario, including the proposed codebooks GGAP and UGAP, by 0.63 dB and 0.75 dB, respectively,

for an error probability of 10^{-4}. The codebooks GGAP and UGAP outperform rot. GLCP and rot. GLCP-SIM as the SNR increases, according to the UBs behavior.

5.3.2 Performance comparison in terms of BER

In this section, we presente simulations results in terms of BER. The analytical performance, i.e., the UB, in (3.65) is also presented. Similar to Section 5.3.1, the analytical upper bounds may be not tight for low and medium SNRs. They are useful to give a good error performance indication in the high-SNR regime as the analytical performance curves of the different schemes preserve the same ordering as the one of the corresponding simulated curves.

As dicussed in Section 3.7, comparing the different schemes in terms of BER, especially at low and medium SNRs, is in order due to the different behavior of the BER observed in this SNR range when compared to CER. This behavior makes us believe that a different set of criteria should be used to improve the BER performance of these schemes.

Figure 36 presents a comparison between the schemes with SSD $D = 1$ and $D = 2$, in terms of BER, for the first case of study. The QAM-based codebooks employ Gray labeling at the digital modulation level, labeled as "Gray lab." in the legends. The parameters of the presented schemes are listed Table 6. For the lattice-based codebooks the optimized labeling obtained through BSA is used, corresponding to "BSA lab." in the legends. As can be seen, for both modulation diversities, the proposed codebooks $\mathscr{C}_{E_8}$ and rot. $\mathscr{C}_{E_8}$ outperform the concurrent schemes from 13 dB and 12 dB on, respectively. A similar behavior is not observed when comparison is made in terms of CER. At low SNR (0 up to 11 dB), rot. OFDM presents the best performance. This behavior is in accordance with the criterion CF in Table 6 and the distance spectrum discussed in Section 3.7.2. Note that the SSD plays an important role to the performance of rot. OFDM compared to conventional OFDM.

Figure 36 – Bit error rates (simulated) of the schemes with $D = 1$ and $D = 2$ and for $M = 8$ and $N = 256$.

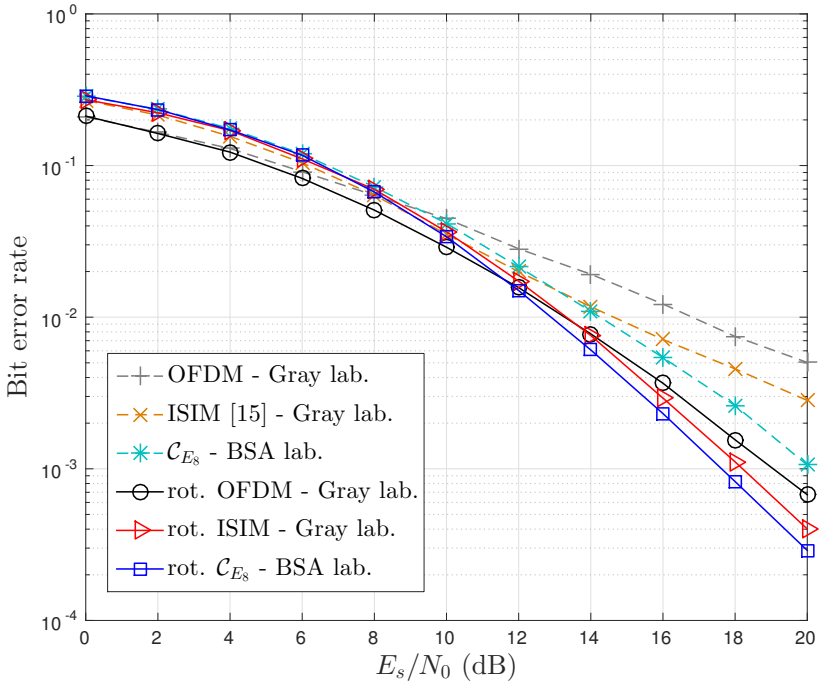

The same comparison is presented for the precoded schemes ($D = 4$) in Figure 37. It can be observed that GLCP [20] presents the best performance for a larger SNR range, from 0 up to 20 dB, which evidences the importance of a good labeling and a good neighbors distribution. For an error probability of 10^{-3}, the gain of the GLCP is of 0.6 dB and 0.8 dB, compared with, respectively, the proposed GLCP-$\mathscr{C}_{E_8}$ and GLCP-SIM. For larger SNRs (> 20 dB), the proposed schemes present the best performance, which is consistent with the behavior of their bounds.

In Figure 38, the proposed fully-diverse codebooks are shown. The best performance at low to medium SNR is achieved by the proposed rot. GLCP, which is based on conventional digital modulation. Rot. GLCP presents a gain of ≈ 0.8 dB, ≈ 0.9 dB, ≈ 1.2 dB, and

Figure 37 – Bit error rates (simulated and theoretical UBs) of the precoded schemes with $D = 4$, for $M = 8$ and $N = 256$.

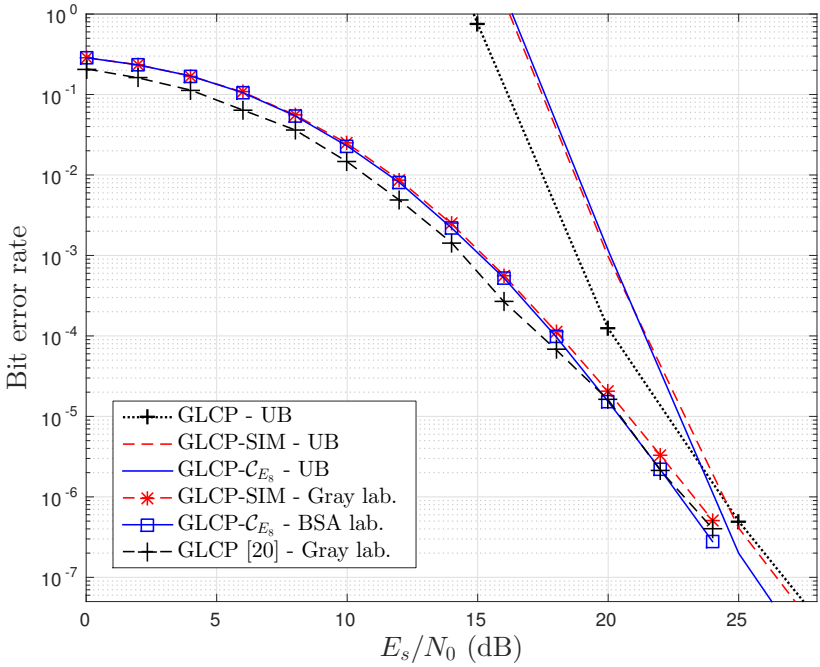

≈ 1.3 dB over rot. GLCP-$\mathscr{C}_{E_8}$, rot. GLCP-SIM, GGAP, and UGAP, respectively, for an error probability of 10^{-2}. At 22 dB, the proposed rot. GLCP-$\mathscr{C}_{E_8}$ has practically the same performance as rot. GLCP, while, according to the upper bounds, rot. GLCP-$\mathscr{C}_{E_8}$, GGAP, and UGAP outperform rot. GLCP at higher SNRs.

Figure 39 presents the best schemes, in terms of BER, at low and medium SNR regime. Only the best scheme of each modulation diversity is presented. Although the performance gain of rot. GLCP is tiny compared to the GLCP [20] for SNRs up to 18 dB, the SSD appears to be the most important criterion in the optimization process, independently of the SNR regime.

In Figure 40, the CER/BER ratio of the simulated curves is presented. This metric indicates how good a labeling is, where the closer

Figure 38 – Bit error rates (simulated and theoretical UBs) of the proposed fully-diverse schemes ($D = M$), for $M = 8$ and $N = 256$.

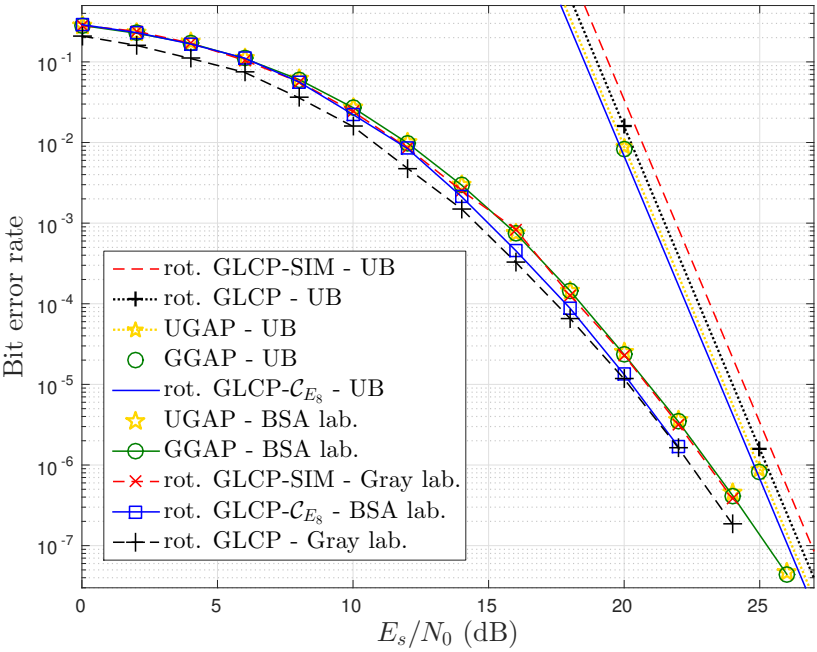

to $\log_2|\mathscr{C}|$ the better. As can be seen, for all SSD, the QAM-based codebooks present the best labeling, which is in accordance with the criteria analyzed in Section 3.7.2. However, for QAM- and SIM-based codebooks, which present a similar behavior, as the SSD increases, the CER/BER ratio decreases. For the lattice-based codebooks, the CER/BER ratio exhibits little or no variation as SSD increases. Another fact is, the improvements obtained with the BSA labeling compared to the natural labeling are more significant for the codebooks based on the combinatorial approach: UGAP and GGAP, although their performances are worse than that of rot. GLCP-$\mathscr{C}_{E_8}$.

Figure 39 – Bit error rates (simulated) of the best schemes with $M = 8$ for several SSD and at low SNR regime.

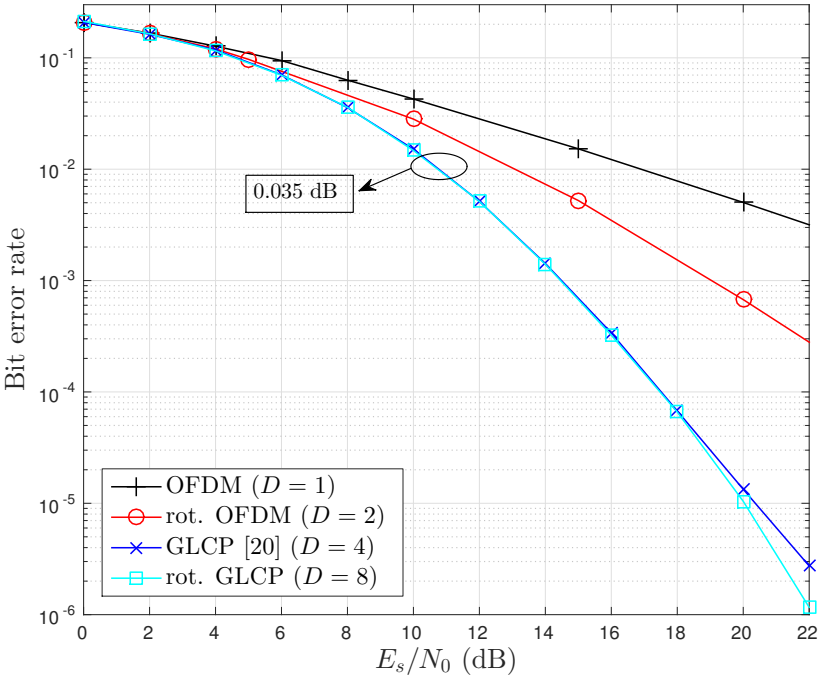

5.4 SECOND CASE OF STUDY

For this case, it is considered for all schemes that the 256 subcarriers are divided into $G = 128$ groups with $n = 2$ subcarriers each. As in the previous case, each group carries $m = 8$ bits, but herein it leads us to compare codebooks with $N = 2^8 = 256$ constellation points with $M = 2n = 4$ real dimensions. All schemes have the same rate $R = 1024$ bits per OFDM symbol. The codebooks with $M = 4$ and $N = 256$ were designed in Sections 3.5, 4.4.2, and 4.4.3.

5.4.1 Performance comparison in terms of CER

In Figure 41, all precoded schemes as well as their UBs listed in Table 5 are compared. The schemes GLCP (16-QAM) [20], GLCP-

Figure 40 – CER/BER ratio versus SNR for the 8-dimensional codebooks.

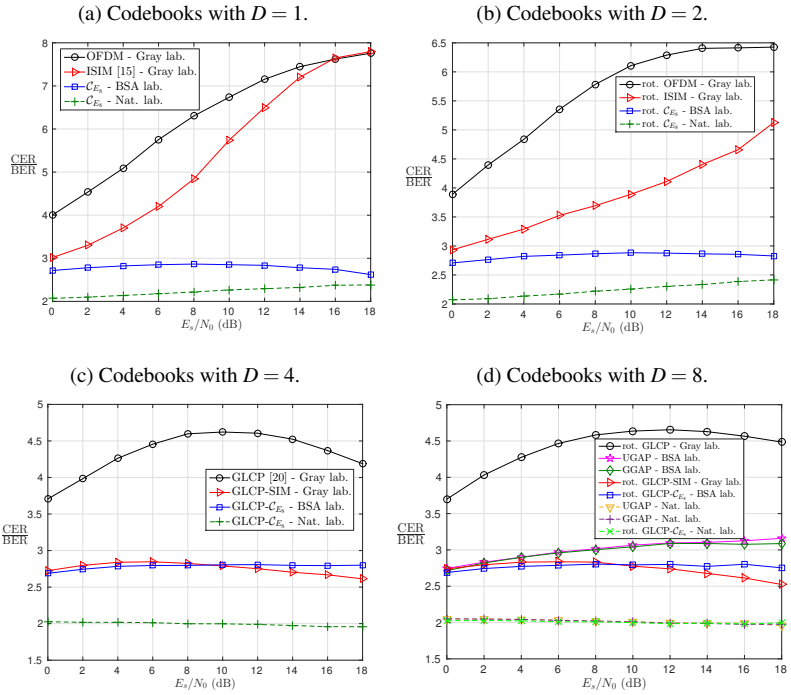

GIM, and GLCP-$\mathscr{C}_{D_4}$ behave similarly to the schemes in Figure 34. For an error probability of 10^{-3}, GLCP-GIM is ≈ 0.22 dB better than the GLCP (16-QAM) [20], while for the GLCP-$\mathscr{C}_{D_4}$ this gain is of ≈ 1 dB. The GLCP (16-APSK) presented a gain of ≈ 0.32 dB better than GLCP (16-QAM), which might seem surprising since, from Table 5, the SSD of the former is only $D = 1$. This behavior is due to the fact that only asymptotically the slope of the performance curve of a scheme will approach the SSD which, in this case, occurs for SNR > 45 dB, as presented in (3.43). This is also the reason why the GLCP (16-APSK) upper bound is not presented in Figure 41. It is outside the SNR range of interest of this work.

All fully-diverse codebooks for the second scenario are compared

Figure 41 – Constellation point error rates (simulated and theoretical UBs) of the precoded schemes GLCP (16-QAM) [20], GLCP (16-APSK), GLCP-GIM, and GLCP-$\mathscr{C}_{D_4}$, for $M = 4$ and $N = 256$.

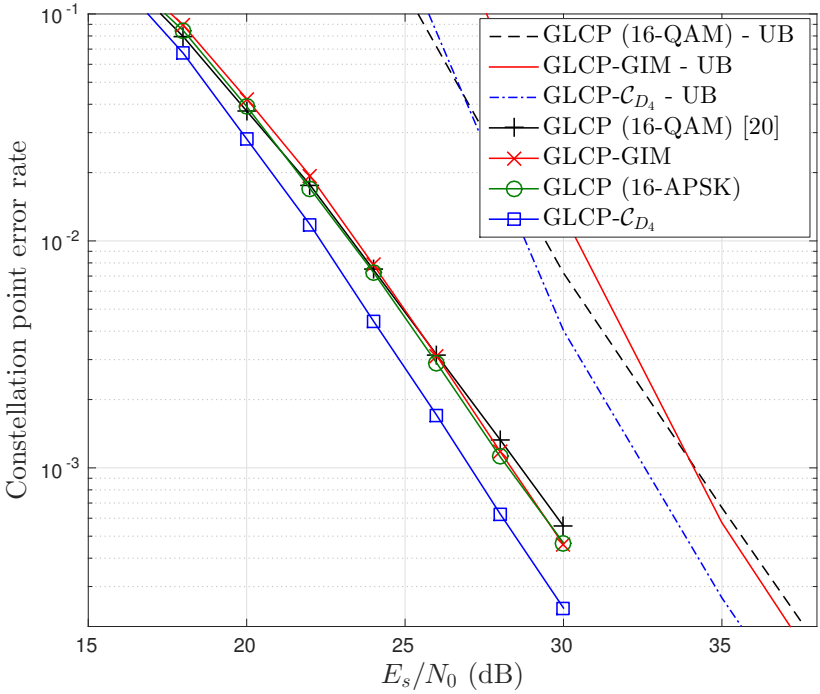

in Figure 42. To recall their parameters, see Tables 5 and 10. As can be seen, rot. GLCP-$\mathscr{C}_{D_4}$ and rot. GLCP, both proposed in the previous chapter, perform similarly and have the best performance in this scenario. They present a gain of ≈ 0.8 dB over the proposed GGAP and GGPI, and ≈ 1 dB compared to the proposed UGAP, for an error probability of 10^{-4}. Asymptotically, GGPI will exhibit a performance worst than UGAP, according to the UB. The proposed GGAP (and GGPI) and UGAP outperform rot. GLCP-GIM by 0.7 dB and 0.5 dB, respectively. The scheme rot. GLCP-GIM is better only than rot. GLCP (16-APSK), with a gain of 0.5 dB for the same error probability of 10^{-4}.

Figure 42 – Constellation point error rates (simulated and theoretical UBs) of the proposed fully-diverse codebooks for $M = 4$ and $N = 256$.

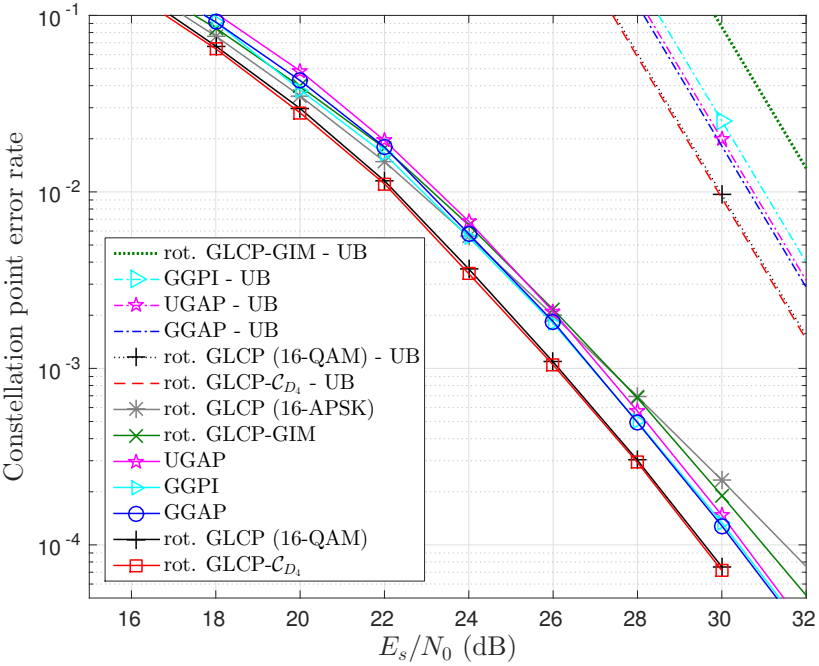

5.4.2 Performance comparison in terms of BER

Figure 43 presents the BER comparison of the precoded schemes for the second case of study. For an error probability of 10^{-1}, GLCP (16-QAM) [20] presents a gain of ≈ 1.25 dB and ≈ 2 dB compared to, respectively, GLCP-$\mathscr{C}_{D_4}$ and GLCP-GIM. In this same error probability, GLCP (16-APSK) presents pratically the same performance as GLCP-GIM, but from 22 dB on perform gets worse, which is in accordance with the behavior of the UBs (although the coding gain difference is larger). For SNR > 27 dB, GLCP-GIM outperforms GLCP (16-QAM) while the proposed GLCP-$\mathscr{C}_{D_4}$ can overcome GLCP (16-QAM), for SNR > 20 dB. For an error probability of 10^{-3}, GLCP-$\mathscr{C}_{D_4}$

presents a gain of 0.75 dB, 1.1, dB and 1.3 dB compared with GLCP (16-QAM), GLCP-GIM, and GLCP (16-APSK), respectively.

Figure 43 – Bit error rates (simulated and theoretical UBs) of the precoded schemes with SSD $D = 2$, for $M = 4$ and $N = 256$.

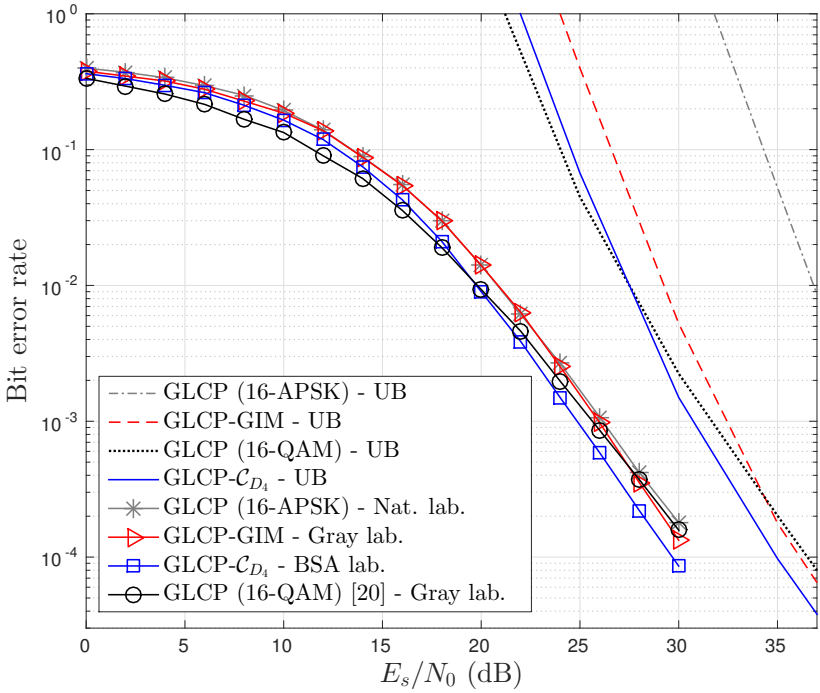

The proposed fully-diverse codebooks for the second scenario are presented in Figure 44. As can be seen, once again rot. GLCP (16-QAM) presents the best performance. The difference is that for this case rot. GLCP-$\mathscr{C}_{D_4}$ does not outperform rot. GLCP (16-QAM) as the SNR increases. Asymptotically, the performance of these two proposed schemes will be the same, according to the UBs. The gain of the rot. GLCP (16-QAM) is of ≈ 1.5 dB over rot. GLCP-$\mathscr{C}_{D_4}$ for an error probability of 10^{-1}, and this gain decreases as the SNR increases. For this same error probability, GGPI, UGAP, and GGAP present pratically the same performance and rot. GLCP-$\mathscr{C}_{D_4}$ outper-

forms these codebooks by ≈ 0.3 dB. These proposed codebooks based on the combinatorial approach outperform rot. GLCP-GIM and rot. GLCP (16-APSK) by ≈ 0.7 dB.

Figure 44 – Bit error rates (simulated and theoretical UBs) of the proposed fully-diverse schemes ($D = M$), for $M = 4$ and $N = 256$.

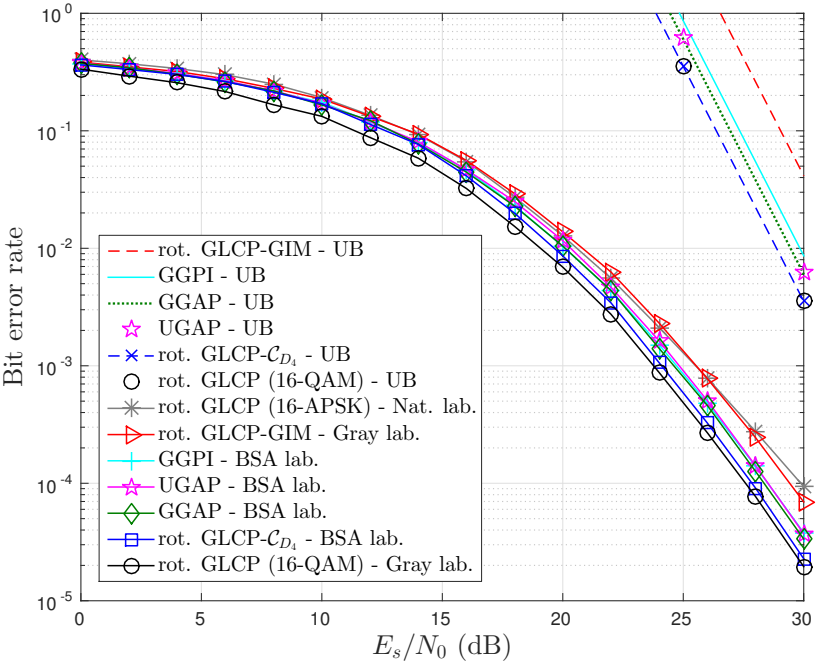

Similar to the Figure 39, Figure 45 presents the BER of the best codebooks, namely the proposed rot. GLCP (16-QAM) and GLCP (16-QAM), at low and medium SNR, for the second scenario. As can be seen, they perform similarly (a difference of about 0.08 dB for an error probability of 10^{-3}). This figure as well as Figure 39 show that the SSD is the most important parameter for Rayleigh channels, and as the SNR increases the performance gain also increases.

The CER/BER ratio is presented in Figure 46. As in the previous case, the QAM-based codebooks with Gray labeling present the best performance. Among the precoded codebooks (Figure 46a), the

Figure 45 – Bit error rates (simulated) of the best codebooks with $M = 4$ for each SSD and at low SNR regime.

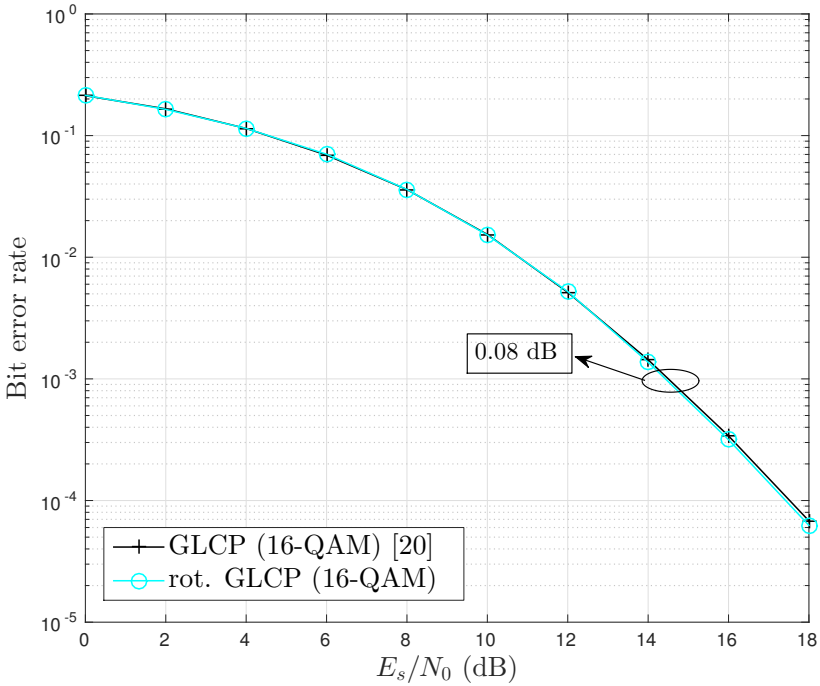

second best labeling is of GLCP-$\mathscr{C}_{D_4}$, followed by GLCP-GIM and GLCP (16-APSK). Among the proposed fully-diverse codebooks, from 5 dB on the second best labeling is of UGAP followed by GGAP, GGPI, rot. GLCP-$\mathscr{C}_{D_4}$, GLCP-GIM, and GLCP (16-APSK).

It is important to observe that, although the proposed codebooks GGAP and UGAP do not present the ultimate best performance, they have some advantages over their competitors that make them good candidates for practical systems. First, the performance of GGAP can be further improved by tunning the parameters $\boldsymbol{\sigma}$ and $\boldsymbol{\kappa}$, when designing the Gaussian grid. Second, both the codebook design (offline) complexity and the operational (online) complexity of the transmitter/receiver of the proposed codebooks are considerably smaller when compared to the benchmark codebooks, as explained in Section 4.5.

Figure 46 – CER/BER ratio versus SNR for the 4-dimensional codebooks.

(a) Codebooks with $D = 2$.

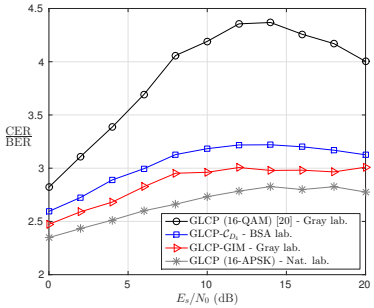

(b) Codebooks with $D = 4$.

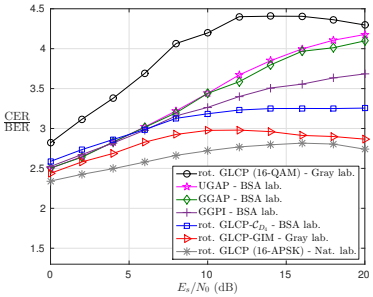

Based on BER simulation results, it is noted that as SSD increases, the SNR range in which labeling and distance spectrum have influence also increases. However, the proposed codebooks were not designed to meet these criteria, and all analysis in terms of BER and the attempt of improving the labeling through BSA were to understand and to explain the observed behavior: what was happening, why and the way to solve it. In terms of CER, all proposed codebooks performed as expected, according to the criteria of the previous chapter.

5.5 CHAPTER CONCLUSIONS

The simulation results presented in this chapter are in accordance with the theory presented in Chapters 3 and 4. The constellations with the best parameters present the best performance, except for the APSK-based codebooks, but for these cases the slope of the curve in high SNR tends to agree with the upper bounds. Exploiting the maximum modulation diversity provides improvements in all studied scenarios. The proposed lattice-based codebooks present the best performance in terms of CER for the whole SNR range and in terms of BER for medium to high SNR regime. For BER comparison at low and medium SNR, the proposed fully-diverse codebooks based on con-

ventional digital modulation perform better. The proposed codebooks based on the combinatorial approach are a better solution if compared with the SIM-based codebooks, and they presented potential and open issues for future works.

6 CONCLUSIONS

A general approach for OFDM with grouped subcarriers, which makes use of interleaving at the real dimension level, has been proposed. Performance analysis indicates design rules for designing codebooks that can achieve the maximum diversity gain. A construction of codebooks based on real lattices was also proposed. Constellation rotation and GLCP were also applied for obtaining large diversity gains. To test the proposed schemes, two cases study were considered. Conventional OFDM, ISIM, and GLCP, with the same system parameters, were used as reference schemes for comparison. Under all considered scenarios, the proposed codebooks following this approach have shown the best performance.

The second proposed approach is a simple and generalized methodology to design fully-diverse multidimensional codebooks for fading channels, without any rotation or precoding, i.e., in contrast with the literature. In this methodology, we prepare a grid with N distinct points, which is used in all dimensions. The points in the grid can follow a uniform or a Gaussian shape, and the M-dimensional codebook is obtained by performing $M-1$ permutations of the labels of the grid points.

An ensemble average performance over all possible fully-diverse codebooks is derived, both for the uniform and the Gaussian-shaped grids, which brings insight into the problem and reveals the difficulty in obtaining a good codebook with a random search.

Two algorithms were then proposed to design a good permutations set. The first algorithm, referred to as P-interleavers, optimizes each one of the $M-1$ interleavers (permutations) based on the minimum product distance criterion. The second algorithm proposed in this dissertation (Algebraic permutations algorithm) obtains permutations by a series of labels shifts, adhering to the condition that if in a given dimension the projections of two codebook points are neighbors, then in the other dimensions they are put further apart, guaranteeing a large product distance.

Some discussions are provided on the complexity and storage requirements of the proposed schemes. It has been shown that the proposed codebooks, designed with the second approach, can be designed with lesser efforts in comparison to previous approaches. Furthermore, the codebook can be implemented in the transmitter and the receiver with less memory.

Simulation results reveal that lattice-based codebooks presented the best performance in terms of CER and BER, in the latter case for high SNR. SIM-based codebooks, although claimed to be very promising in the literature, showed a poor performance compared to the proposed codebooks, not being a good alternative in any of the considered cases. APSK-based constellations also presented a poor performance. In terms of BER at low and medium SNR, the proposed codebook based on the combination of conventional digital modulation, rotation, and GLCP has the best performance. The proposed codebooks based on the second approach present a good performance in both scenarios. Although they do not present the ultimate best performance, they have some advantages as cited above.

Therefore, for all the reasons above, we believe that the proposed codebooks (and methodologies) are good candidates to be adopted in future communications systems. Furthermore, they have the potential to perform well in coded modulation, MIMO and multiuser schemes.

6.1 CONTRIBUTIONS

The major contributions and findings of this dissertation are the following:

- A performance analysis was developed for a grouped OFDM system with a single user, Rayleigh frequency-selective fading channel and single-antenna.

- A unified approach for designing fully-diverse multidimensional constellations for OFDM with grouped subcarriers is proposed, which encompasses schemes of the literature (conventional OFDM,

ISIM [15], and GLCP [20]) as particular cases. It has been shown that with low additional complexity the SSD of GLCP schemes can be doubled and a significant performance gain can be obtained. Some codebooks following this approach were proposed based on conventional digital modulation, SIM, and lattices constellations. The proposed codebook design criterion, the so-called mutiplicity-to-product distance ratio, produced better codebooks compared to the classical minimum product distance criterion and proved to be more appropriate for the scenarios considered.

- A simple and generalized methodology is proposed for designing fully-diverse multidimensional codebooks without making use of rotation or precoding. The number of dimensions and constellation points are totally flexible, without any restrictions.

- Two algorithms to find a good set of permutations (or interleavers) are also proposed. The first, called P-interleavers, optimizes each interleaver sequentially based on the minimum product distance criterion. The second algorithm is a simple algebraic method that is thought of to improve the so-called multiplicity-to-product distance ratio. The two algorithms have low complexity.

- An enumerative technique is introduced to obtain the average (squared) product distance spectrum of the ensemble of codebooks obtained with the uniform and Gaussian-shaped grids. This analysis yields an upper bound on the error performance of a good codebook, and sheds some light into the problem of designing a good codebook. In particular, it shows how difficult it is to obtain a good permutations set and how effectively our algorithms solve this problem.

- The problem of multidimensional codebook labeling for improving the performance in terms of BER at low and medium SNR has been discussed. It was found that new design criteria may be required. It constitutes a difficult problem yet to be solved. We observed that the second methodology for designing fully-diverse

multidimensional codebooks based on the Gaussian grid has soon for improvement (through the optimization of the parameters σ and κ in (4.18)). The BSA plays an important role and should be further elaborated on.

- The proposed codebooks based on the first approach present better error performance while the proposed codebooks following the second methodology are more general and flexible in terms of settings, have less complex design, and require less storage capacity.

- It is shown that SIM-based codebooks do not perform so well and the proposed codebooks are shown (both analytically and through simulations) to have very good performance. Thus, they are seen as a good alternative for future communication systems.

6.2 PUBLISHED PAPERS

The publications resulting from this dissertation were:

- J. C. Inácio, B. F. Uchôa-Filho and D. Le Ruyet. Grouped Linear Constellation-Precoding for Subcarrier Index Modulation OFDM. 2017 International Symposium on Wireless Communications Systems (ISWCS). Aug. 2017 [101].

- J. C. Inácio, B. F. Uchôa-Filho and D. Le Ruyet. Exploiting Signal Space Diversity in OFDM with Grouped Subcarriers: Going Beyond Subcarrier Index Modulation. IEEE Wireless Communications Letters. Feb. 2018 [102].

- J. C. Inácio, B. F. Uchôa-Filho and D. Le Ruyet. Diversidade de Espaço de Sinais em OFDM com Subportadoras Agrupadas: Resultados Adicionais. *Accepted for presentation in*: Simpósio Brasileiro de Telecomunicações. Sept. 2018.

- J. C. Inácio, B. F. Uchôa-Filho, D. Le Ruyet and S. Montejo-Sánchez. Fully-Diverse Multidimensional Codebook Design for

Fading Channels: a Combinatorial Approach. *Submitted for publication*.

6.3 FUTURE WORKS

Next, some open problems are suggested as future works.

- **An optimal solution for the labeling problem** – Although the BSA is widely used in literature to solve the labeling problem, in this work it has not presented a labeling good enough to overcome the proposed codebooks based on conventional constellations with Gray labeling. Thus, other labeling solutions can be investigated to try to solve this problem.

- **The design and analysis of less complex detectors for both coded and uncoded systems with the proposed codebooks** – Simpler detectors and coding are required in practical systems. The SSD was exploited in coded schemes in [9, 8, 39] and good results were obtained. Given the potencial of the proposed methodologies and codebooks in this dissertation, it would be interesting to investigate the performance of these schemes with these new blocks.

- **The extension to the MIMO scenario** – Multiples antennas are a basic requirement of current and future generation systems, and the proposed codebooks have the potencial to perform well in this scenario.

- **The extension to the multiuser scenario** – Codebook design is an important and open issue in SCMA systems. Some works, as for example [103, 104], use rotation in the optimization process. Then, it would be interesting to investigate the performance of the proposed constellations in SCMA scenarios. Another possibility of investigation is the multiuser scenario with massive MIMO, proposed in [88, 89]. Apart from the proposed constellations, the proposed algorithms (algebraic permutations and P-interleavers) can be applied to [96] as a simple and generalized solution to find

good permutations for constellations with $S > 8$ and $K > 2$. It may be required to modify the optimization criterion.

- **The impact of quantization** – It would be interesting to investigate the impact of quantization on the proposed codebooks and whether it would be necessary some change in the design of the constellations for this case.

- **Adaptations in the two proposed methodologies to compare them with other schemes** – It may be interesting to make some changes in relation to the optimization criteria in the proposed methodologies to make it possible the comparison with other schemes, as for example [9, 96, 10, 41].

BIBLIOGRAPHY

[1] BOUTROS, J.; VITERBO, E. Signal Space Diversity: A Power- and Bandwidth-Efficient Diversity Technique for the Rayleigh Fading Channel. *IEEE Trans. on Inform. Theory*, v. 44, n. 4, p. 1453–1467, Jul. 1998. 11, 35, 42, 49, 55, 58, 66, 74, 76, 77, 87, 88

[2] CONWAY, J.; SLOANE, N. *Sphere Packings, Lattices and Groups*. [S.l.]: Springer, Third Edition, 1999. 11, 35, 44, 58, 66, 69, 72

[3] BOUTROS, J. et al. Good Lattices Constellations for Both Rayleigh Fading and Gaussian Channels. *IEEE Trans. Inform. Theory*, v. 42, n. 2, p. 502–518, Mar. 1996. 11, 35, 38, 43, 44, 57, 66, 87

[4] BAYER-FLUCKIGER, E.; OGGIER, F.; VITERBO, E. New Algebraic Constructions of Rotated $\mathbb{Z}^n$-Lattice Constellations for the Rayleigh Fading Channel. *IEEE Trans. Inform. Theory*, v. 50, n. 4, p. 702–714, Apr. 2004. 11, 35, 43

[5] DIVSALAR, D.; SIMON, M. k. The Design of Trellis Coded MPSK for Fading Channels: Performance Criteria. *IEEE Trans. Commun.*, v. 36, n. 9, p. 1004–1012, Sept. 1998. 11, 35, 38, 43, 57, 62, 88

[6] LEE, H.; PAULRAJ, A. MIMO Systems Based on Modulation Diversity. *IEEE Trans. Commun.*, v. 58, n. 12, p. 3405–3409, Dec. 2010. 11, 35, 44

[7] AHMADZADEH, S. A.; MOTAHARI, S. A.; KHANDANI, A. K. Signal Space Cooperative Communication. *IEEE Trans. Wireless Commun.*, v. 9, n. 4, p. 1266–1271, Apr. 2010. 11, 35, 44

[8] XIE, Q. et al. Coded Modulation with Signal Space Diversity. *IEEE Trans. Wireless Commun.*, v. 10, n. 2, p. 660–669, Feb. 2011. 11, 35, 44, 137

[9] XIE, Q. et al. EXIT-Chart-Matching-Aided Near-Capacity Coded Modulation Design and a BICM-ID Design Example for Both Gaussian and Rayleigh Channels. *IEEE Trans. Veh. Technol.*, v. 63, n. 3, p. 1216–1227, Mar. 2013. 11, 35, 44, 74, 84, 137, 138

[10] HERATH, S. P.; TRAN, N. H.; Le-Ngoc, T. Rotated Multi-D Constellations in Rayleigh Fading: Mutual Information Improvement and Pragmatic Approach for Near-Capacity Performance in High-Rate Regions. *IEEE Trans. Commun.*, v. 60, n. 12, p. 3694–3704, Dec. 2012. 11, 35, 44, 138

[11] DIGITAL Video Broadcasting (DVB); frame structure, channel coding and modulation for a second generation digital terrestrial television broadcasting system (DVB-T2). 2008. 11, 35, 44

[12] GÓMEZ-BARQUERO, D. et al. DVB-NGH: The Next Generation of Digital Broadcast Services to Handheld Devices. *IEEE Trans. Broadcast.*, v. 60, n. 2, p. 246–257, Jun. 2014. 11, 35, 44

[13] BASAR, E. et al. Orthogonal Frequency Division Multiplexing with Index Modulation. *IEEE Trans. Signal Process.*, v. 61, n. 22, p. 5536–5549, Nov. 2013. 11, 36, 51, 52, 55, 57, 66, 67, 68

[14] MAO, T. et al. Dual-Mode Index Modulation Aided OFDM. *IEEE Access*, v. 5, p. 51 – 60, Feb. 2017. 12, 36

[15] AL., Y. X. et. OFDM with Interleaved Subcarrier-Index Modulation. *IEEE Commun. Letters*, v. 18, n. 8, p. 1447–1450, Aug. 2014. 12, 36, 53, 54, 57, 59, 67, 78, 85, 116, 118, 135

[16] BASAR, E. OFDM with Index Modulation Using Coordinate Interleaving. *IEEE Wireless Commun. Letters*, v. 4, n. 4, p. 381–384, Aug. 2015. 12, 36, 55, 57, 76

[17] MESLEH, R.; IKKI, S. S.; AGGOUNE, H. M. Quadrature Spatial Modulation. *IEEE Trans. Veh. Technol.*, v. 64, n. 6, p. 2738–2742, Jun. 2015. 12, 36

[18] FAN, R.; YU, Y. J.; GUAN, Y. L. Generalization of Orthogonal Frequency Division Multiplexing with Index Modulation. *IEEE Trans. Wireless Commun.*, v. 14, n. 10, p. 5350–5359, May 2015. 12, 36, 54, 57, 66, 68, 69

[19] AL., B. Z. et. Low-Complexity ML detector and Performance Analysis for OFDM with In-Phase/Quadrature Index Modulation. *IEEE Commun. Letters*, v. 19, n. 11, p. 1893–1896, Nov. 2015. 12, 36, 55

[20] LIU, Z.; XIN, Y.; GIANNAKIS, G. B. Linear Constellation-Precoding for OFDM with Maximum Multipath Diversity and Coding Gains. *IEEE Trans. on Commun.*, v. 51, n. 3, p. 416–427, Mar. 2003. 12, 36, 45, 46, 47, 51, 53, 57, 58, 66, 67, 74, 77, 78, 85, 88, 107, 116, 117, 120, 121, 123, 124, 126, 135

[21] WEN, M.; YE, B.; BASAR, E. Enhanced Orthogonal Frequency Division Multiplexing with Index Modulation. *IEEE Trans. Wireless Commun.*, v. 16, n. 7, p. 4786–4801, Jul. 2017. 12, 36, 55, 57

[22] HANZO, L. et al. *OFDM and MC-CDMA for Broadband Multi-user Communications, WLANs and Broadcasting*. [S.l.]: John Wiley & Sons, 2003. 41

[23] ROHLING, H. *OFDM Concepts for Future Communication Systems*. [S.l.]: Springer, 2011. 41

[24] CHO, Y. S. et al. *MIMO-OFDM Wireless Communications with MATLAB*. [S.l.]: John Wiley & Sons, 2010. 41

[25] PRASAD, R. *OFDM for Wireless Communication Systems*. [S.l.]: Arthec House Inc., 2004. 41

[26] GOLDSMITH, A. *Wireless Communications*. [S.l.]: Cambridge University Press, 2005. 41

[27] JELICIC, B. D.; ROY, S. Design of Trellis Coded QAM for Flat Fading and AWGN Channels. *IEEE Trans. Veh. Technol.*, v. 44, n. 1, p. 192 – 201, Feb. 1994. 43

[28] FORNEY, G. D. Coset Codes – Part I: Introduction and Geometrical Classification. *IEEE Trans. Inform. Theory*, v. 34, n. 5, p. 1123 – 1151, Sept. 1988. 43, 44

[29] FORNEY, G. D. Coset Codes – Part II: Binary Lattices and Related Codes. *IEEE Trans. Inform. Theory*, v. 34, n. 5, p. 1152–1187, Sept 1988. 43, 44

[30] VITERBO, E.; OGGIER, F. *Algebraic Number Theory and Code Design for Rayleigh Fading Channels*. [S.l.]: Now, 2004. 43, 44

[31] GIRAUD, X.; BOUTILLON, E.; BELFIORE, J. C. Algebraic Tools to Build Modulation Schemes for Fading Channels. *IEEE Trans. Inform. Theory*, v. 43, n. 3, p. 938–952, May 1997. 43

[32] CLARK, A.; TAYLOR, D. P. Lattice Codes and Generalized Minimum-Distance Decoding for OFDM Systems. *IEEE Trans. Commun.*, v. 55, n. 3, Mar. 2007. 44

[33] KURKOSKI, B. M. The E8 Lattice and Error Correction in Multi-Level Flash Memory. In: *IEEE Intern. Conf. Commun. (ICC)*. [S.l.: s.n.], 2011. p. 1 – 5. 44

[34] CARVAJAL, H. M.; OROZCO, N. G.; ALMEIDA, C. Signal Space Diversity in Single and Multiuser Scenarios Employing Sphere Decoder Detector. *IEEE Commun. Letters*, PP, n. 99, p. 1 – 1, Jan. 2018. 44

[35] LI, Y.; XIA, X.; WANG, G. Simple Iterative Methods to Exploit the Signal-Space Diversity. *IEEE Trans. Commun.*, v. 53, n. 1, p. 32 – 38, Jan. 2005. 44

[36] YIN, Y.; WEI, N.; ZHANG, Z. A Simple Transmit Scheme to Exploit Signal Space Diversity in V-BLAST System. In: *IEEE Intern. Conf. on Commun., Circuits and Syst.* [S.l.: s.n.], 2008. p. 190 – 194. 44

[37] LU, T.; YANG, Y.; GAO, Y. On Bit Error Performance of Full-Rate Signal Space Cooperative Communication over Nakagami-m Fading Channels. *IEEE Commun. Letters*, v. 16, n. 8, p. 1224–1227, Aug. 2012. 44

[38] AMIN, O. et al. Performance Analysis of Multiple-Relay Cooperative Systems with Signal Space Diversity. *IEEE Trans. Veh. Technol.*, v. 64, n. 8, p. 3414–3425, Aug. 2015. 44

[39] ABDMOULEH, A. et al. On Signal Space Diversity for Non Binary Coded Modulation Schemes. In: *23rd Intern. Conf. on Telecommunications (ICT)*. [S.l.: s.n.], 2016. p. 1 – 5. 44, 137

[40] GOZÁLEZ, D. et al. Rotated Constellations for Improved Time and Frequency Diversity in DVB-NGH. *IEEE Trans. Broadcast.*, v. 59, n. 2, p. 298–305, Jun. 2013. 44

[41] KARPUK, D. A.; HOLLANTI, C. Locally Diverse Constellations from the Special Orthogonal Group. *IEEE Trans. on Wireless Commun.*, v. 15, n. 6, p. 4426–4437, Jun. 2016. 44, 138

[42] WANG, Z.; GIANNAKIS, G. B. Linearly Precoded or Coded OFDM Against Wireless Channel Fades? In: *IEEE Worksh. Signal Process. Advanc. Wireless Commun.* [S.l.: s.n.], 2001. p. 267 – 270. 45

[43] ZOU, W.; WU, Y. COFDM: An Overview. *IEEE Trans. on Broadcast.*, v. 41, n. 1, p. 1–8, Mar. 1995. 45

[44] WANG, Z.; GIANNAKIS, G. B. Wireless Multicarrier Communications: Where Fourier Meets Shannon. *IEEE Signal Process. Mag.*, v. 17, n. 3, p. 29–48, May 2000. 45, 51

[45] XIN, Y.; WANG, Z.; GIANNAKIS, G. B. Space-Time Diversity Systems Based on Linear Constellation-Precoding. *IEEE Trans. Wireless Commun.*, v. 2, n. 2, p. 294–309, Mar. 2003. 46, 107

[46] AHMED, K. I.; TEPEDELENLIOGLU, C.; SPANIAS, A. Performance of Precoded OFDM with Channel Estimation Error Khawza. *IEEE Trans. Signal Process.*, v. 54, n. 3, p. 1165–1171, Mar. 2006. 47

[47] ZHU, X.; XUE, J. On the Correlation of Subcarriers in Grouped Linear Constellation Precoding OFDM Systems over Frequency Selective Fading. *IEEE Veh. Technol. Conf.*, v. 3, p. 1431 – 1435, May 2006. 47

[48] TOUTOUNCHIAN, M. A.; MUHAIDAT, S. Performance Evaluation of Linear Constellation Precoded OFDM with Linear Equalizers in Overestimated Channels. In: *Intern. Conf. on Inform. and Commun. Technol. Converg. (ICTC)*. [S.l.: s.n.], 2010. p. 120 – 124. 47

[49] TRAN, N. H.; NGUYEN, H. H.; LE-NGOC, T. Subcarrier Grouping for OFDM with Linear Constellation Precoding over Multipath Fading Channels. *IEEE Trans. Veh. Technol.*, v. 56, n. 6, p. 3607–3613, Nov. 2007. 48

[50] ATHAUDAGE, C. R. N.; WANG, J.; JAYALATH, A. D. S. An Efficient Framework to Exploit Frequency Diversity in OFDM: Precoding with Adaptive Subcarrier Selection. In: *IEEE Intern. Symp. on Personal, Indoor and Mobile Radio Commun.* [S.l.: s.n.], 2006. p. 1 – 5. 48

[51] UMASANKAR, B.; FERNANDO, X. OFDM Impairment Mitigation Technique. In: *Second Intern. Conf. on Access Networks & Worksh.* [S.l.: s.n.], 2007. p. 1 – 6. 48

[52] TRAN, N. H.; NGUYEN, H. H.; LE-NGOC, T. Bit-Interleaved Coded OFDM with Signal Space Diversity: Subcarrier Grouping and Rotation Matrix Design. *IEEE Trans. on Signal Process.*, v. 55, n. 3, p. 1137–1149, Mar. 2007. 48

[53] TRAN, N. H.; NGUYEN, H. H.; LE-NGOC, T. Multi-Dimensional Subcarrier Mapping for Bit-Interleaved Coded OFDM with Iterative Decoding. In: *IEEE Wireless Commun. and Networking Conf.* [S.l.: s.n.], 2007. p. 1350 – 1355. 48

[54] YANG, W.; CAI, Y. DMT Analysis and Optimization for OFDM-Based Relaying Systems with Linear Detector. In: *IEEE Global Commun. Conf.* [S.l.: s.n.], 2011. p. 1 – 5. 49

[55] PRASAD, N.; VENTURINO, L.; WANG, X. Diversity-Multiplexing Tradeoff Analysis for OFDM Systems with Subcarrier Grouping, Linear Precoding, and Linear Detection. *IEEE Trans. Inform. Theory*, v. 56, n. 12, p. 6078–6096, Dec. 2010. 49

[56] SEZGINER, S.; SARI, H. Analysis of Linear Precoding Techniques for OFDMA Systems. In: *IEEE Wireless Commun. and Networking Conf.* [S.l.: s.n.], 2007. 49

[57] YANG, W. et al. DMT analysis and optimization for cooperative multiuser OFDMA systems. In: *IEEE 22nd Intern. Symp. on Personal, Indoor and Mobile Radio Commun.* [S.l.: s.n.], 2011. p. 1585 – 1589. 49

[58] PRASAD, N.; VENTURINO, L.; WANG, X. Diversity Multiplexing Tradeoff Analysis of Coded OFDM Systems with Linear Precoding and Linear Receivers. In: *IEEE 11th Intern. Worksh. Signal Process. Advanc. Wireless Commun.* [S.l.: s.n.], 2010. p. 1 – 5. 49

[59] GUI, B.; QU, D. VBLAST-OFDM System with Linear Constellation Precoding. In: *IEEE 59th Veh. Technol. Conf.* [S.l.: s.n.], 2004. v. 2, p. 733 – 737. 49

[60] QU, D. et al. A Frequency Diversity Scheme Using Linear Constellation Precoding for V-BLAST OFDM System. In: . [S.l.: s.n.], 2004. v. 1, p. 274 – 278. 49

[61] CAO, M.; GE, H. GLCP OFDM Systems with I/Q Imbalance. *IEEE Commun. Letters*, v. 13, n. 4, p. 230–232, Apr. 2009. 49

[62] YAN, H.; NGUYEN, H. H.; SU, J. Distributed Precoding for OFDM in Two-Way Relaying Communications. *IEEE Trans. Veh. Technol.*, v. 64, n. 5, p. 1930–1941, May 2015. 49

[63] VO, B. T.; NGUYEN, H. H.; QUOC-TUAN, N. Spatial Modulation for OFDM with Linear Constellation Precoding. In: *Intern. Conf. Advanc. Technol. for Commun.* [S.l.: s.n.], 2015. p. 226 – 230. 49

[64] MESLEH, R. Y. et al. Spatial Modulation. *IEEE Trans. Veh. Technol.*, v. 57, n. 4, p. 2228–2241, Jul. 2008. 49, 55

[65] ABU-ALHIGA, R.; HAAS, H. Subcarrier-Index Modulation OFDM. In: *IEEE 20th Intern. Symp. on Personal, Indoor and Mobile Radio Commun.* [S.l.: s.n.], 2009. p. 177 – 181. 49, 50

[66] CHAU, Y.; YU, S.-H. Space Modulation on Wireless Fading Channels. In: *IEEE Veh. Technol. Conf.* [S.l.: s.n.], 2001. v. 3, p. 1668 – 1671. Atlantic City, NJ, USA. 49

[67] MESLEH, R. Y. et al. Spatial Modulation – A New Low Complexity Spectral Efficiency Enhancing Technique. In: *IEEE Intern. Conf. Commun. Networking*. [S.l.: s.n.], 2006. p. 1–5. Beijing, China. 49

[68] TSONEV, D.; SINANOVIC, S.; HAAS, H. Enhanced Subcarrier Index Modulation (SIM) OFDM. In: *IEEE Globecom Workshops*. [S.l.: s.n.], 2011. p. 728 – 732. 51

[69] ZHAO, L. et al. A High Energy Efficient Scheme with Selecting Subcarriers Modulation in OFDM System. In: *IEEE Intern. Conf. on Commun.* [S.l.: s.n.], 2012. p. 5711 – 5715. 51, 52

[70] LI, W. et al. Generalized Selecting Sub-carrier Modulation Scheme in OFDM System. In: *IEEE Intern. Conf. on Commun.* [S.l.: s.n.], 2014. p. 907 – 911. 52

[71] CHENG, X. et al. Index Modulated OFDM with Interleaved Grouping for V2X Communications. In: *IEEE 17th Intern. Conf. on Intelligent Transportation Syst.* [S.l.: s.n.], 2014. p. 1097 – 1104. 53, 59

[72] WEN, M.; CHENG, X.; YANG, L. Optimizing the Energy Efficiency of OFDM with Index Modulation. In: *Intern. Conf. on Commun. Syst.* [S.l.: s.n.], 2014. p. 31 – 35. 53

[73] AL, L. X. et. Performance Evaluation in PAPR and ICI for ISIM-OFDM Systems. In: *Intern. Worksh. on High Mobility Wireless Commun.* [S.l.: s.n.], 2014. p. 84 – 88. 54

[74] MA, Q. et al. Error Probability Analysis of OFDM-IM with Carrier Frequency Offset. *IEEE Commun. Letters*, v. 20, n. 12, p. 2434–2437, Dec. 2016. 54

[75] WEN, M. et al. On the Achievable Rate of OFDM with Index Modulation. *IEEE Trans. on Signal Process.*, v. 64, n. 8, p. 1919 – 1932, 2016. 54

[76] ISHIKAWA, N.; SUGIURA, S.; HANZO, L. Subcarrier-Index Modulation Aided OFDM - Will it Work? *IEEE Access*, v. 4, p. 2580–2593, May 2016. 54

[77] AL., Q. M. et. Subcarrier Allocation for OFDM with Index Modulation. *IEEE Commun. Letters*, v. 20, n. 7, p. 1469–1472, Jul. 2016. 54

[78] FAN, Y. J. Y. R.; GUAN, Y. L. Improved Orthogonal Frequency Division Multiplexing with Generalized Index Modulation. *IET Communications*, v. 10, n. 8, p. 969–974, 2016. 55

[79] WEN, M. et al. Equiprobable Subcarrier Activation Method for OFDM with Index Modulation. *IEEE Commun. Letters*, v. 20, n. 10, p. 2386 – 2389, 2016. 55

[80] BASAR, E. On Multiple-Input Multiple-Output OFDM with Index Modulation for Next Generation Wireless Networks. *IEEE Trans. Signal Process.*, v. 64, n. 15, p. 3868–3878, Aug. 2016. 55, 56

[81] WANG, S. et al. MIMO-OFDM with Interleaved Subcarrier-Index Modulation. In: *10th Intern. Conf. on Wireless Commun., Networking and Mobile Computing*. [S.l.: s.n.], 2014. p. 35 – 37. 55

[82] BASAR, E. Multiple-Input Multiple-Output OFDM with Index Modulation. *IEEE Signal Process. Letters*, v. 22, n. 12, p. 2259–2263, Dec. 2015. 55

[83] WANG, L. et al. Space-Frequency Coded Index Modulation with Linear-Complexity Maximum Likelihood Receiver in MIMO-OFDM System. *IEEE Signal Process. Letters*, v. 23, n. 10, p. 1439 – 1443, 2016. 55

[84] TSE, D.; .VISWANATH, P. *Fundamentals of Wireless Communcations*. [S.l.]: Cambridge University Press, 2005. 55, 66

[85] DATTA, T.; ESHWARAIAH, H. S.; CHOCKALINGAM, A. Generalized Space and Frequency Index Modulation. *IEEE Trans. Veh. Technol.*, v. 65, n. 7, p. 4911 – 4924, Sept. 2015. 55

[86] CHAKRAPANI, B.; NARASIMHAN, T. L.; CHOCKALINGAM, A. Generalized Space-Frequency Index Modulation: Low-Complexity Enconding and Detection. *IEEE Globecom Workshops*, p. 1 – 6, Dec. 2015. 55

[87] BASAR, E. Index Modulation Techniques for 5G Wireless Networks. *IEEE Commun. Mag.*, v. 54, n. 7, p. 168–175, Jul. 2016. 56

[88] ZHU, H. et al. Subcarrier Index Modulation OFDM for Multiuser MIMO Systems with Iterative Detection. In: *IEEE Intern. Symp. on Personal, Indoor and Mobile Radio Commun.* [S.l.: s.n.], 2016. p. 1 – 6. 56, 137

[89] ZHU, H. et al. Uplink Transceiver for Subcarrier Index Modulation OFDM in Massive MIMO Systems with Imperfect Channel State Information. In: *IEEE Intern. Conf. on Wireless Commun. & Signal Process.* [S.l.: s.n.], 2016. p. 1 – 6. 56, 137

[90] RANGAN, S. Generalized Approximate Message Passing for Estimation with Random Linear Mixing. In: *IEEE Intern. Symp. on Inform. Theory*. [S.l.: s.n.], 2011. p. 2168 – 2172. 56

[91] FORNEY, G. D. Trellis Shaping. *IEEE Trans. Inform. Theory*, v. 38, n. 2, p. 281–300, Mar 1992. 68, 97

[92] BOULLÉ, K.; BELFIORE, J. C. Modulation Scheme Designed for the Rayleigh Fading Channel. In: *Conf. on Inform. Scienc. and Syst. (CISS'92)*. [S.l.: s.n.], 1992. 76, 87

[93] ZEGER, K.; GERSHO, A. Pseudo-Gray Coding. *IEEE Trans. Commun.*, v. 38, n. 12, p. 2147–2158, Dec. 1990. 79

[94] SCHRECKENBACH, F. et al. Optimization of Symbol Mappings for Bit-Interleaved Coded Modulation with Iterative Decoding. *IEEE Commun. Letters*, v. 7, n. 12, p. 593–595, Dec. 2003. 80

[95] CAIRE, G.; TARICCO, G.; BIGLIERI, E. Bit-Interleaved Coded Modulation. *IEEE Trans. Inform. Theory*, v. 44, n. 3, p. 927–946, May 1998. 80

[96] BAO, J. et al. Bit-Interleaved Coded SCMA with Iterative Multiuser Detection: Multidimensional Constellations Design. *IEEE Trans. Commun.*, PP, n. 99, p. 1–1, Dec. 2017. 89, 90, 137, 138

[97] DOLINAR, S.; DIVSALAR, D. Weight Distributions for Turbo Codes Using Random and Nonrandom Permutations. In: *JPL, TDA Progress Report*. [S.l.: s.n.], 1995. v. 42–122, p. 56 – 65. 100

[98] RUYET, D. L.; THIEN, H. V. Design of Cycle Optimized Interleavers for Turbo Codes. In: *Int. Symp. on Turbo Codes and Related Topics*. [S.l.: s.n.], 2000. p. 335–338. 100

[99] CROZIER, S. New High-Spread High-Distance Interleavers for Turbo-Codes. In: *20th Biennial Symp. on Commun.* [S.l.: s.n.], 2000. p. 3–7. 100

[100] USER Equipment (UE) Radio Transmission and Reception. Partnership Project; Technical Specification Group Radio Access Network; Evolved Universal Terrestrial Radio Access (E-UTRA). 2017, Apr. p. 115

[101] Inácio, J. C.; Uchôa-Filho, B. F.; Le Ruyet, D. Grouped Linear Constellation-Precoding for Subcarrier Index Modulation OFDM. In: *Intern. Symp. on Wireless Commun. Syst.* [S.l.: s.n.], 2017. p. 308–313. 136

[102] Inácio, J. C.; Uchôa-Filho, B. F.; Le Ruyet, D. Exploiting Signal Space Diversity in OFDM with Grouped Subcarriers: Going Beyond Subcarrier Index Modulation. *IEEE Wireless Commun. Letters*, PP, n. 99, p. 1 – 1, Feb. 2018. 136

[103] CAI, D. et al. Multi-Dimensional SCMA Codebook Design Based on Constellation Rotation and Interleaving. In: *IEEE 83rd Veh. Techn. Conf. (VTC Spring)*. [S.l.: s.n.], 2016. p. 1 – 5. 137

[104] YAN, C.; KANG, G.; ZHANG, N. A Dimension Distance-Based SCMA Codebook Design. *IEEE Access*, v. 5, p. 5471 – 5479, Mar. 2017. 137